LA-UR-06-2494

Approved for public release; distribution is unlimited.

Title: ANALYSES OF SEQUENTIAL AQUIFER TESTS FROM THE GUAJE WELL FIELD

Author: Stephen G. McLin

Submitted to: Los Alamos National Laboratory
ENV-ERS Pathway Protection Program
April 2006

Los Alamos
NATIONAL LABORATORY
EST. 1943

Los Alamos National Laboratory, an affirmative action/equal opportunity employer, is operated by the University of California for the U.S. Department of Energy under contract W-7405-ENG-36. By acceptance of this article, the publisher recognizes that the U.S. Government retains a nonexclusive, royalty-free license to publish or reproduce the published form of this contribution, or to allow others to do so, for U.S. Government purposes. Los Alamos National Laboratory requests that the publisher identify this article as work performed under the auspices of the U.S. Department of Energy. Los Alamos National Laboratory strongly supports academic freedom and a researcher's right to publish; as an institution, however, the Laboratory does not endorse the viewpoint of a publication or guarantee its technical correctness.

14534

Table of Contents

I. INTRODUCTION 1
- Purpose and Scope 1
- Hydrogeologic Setting 2
- Aquifer Test Procedures 5
- Guaje Canyon Aquifer Configuration 7

II. METHODS OF DATA ANALYSES 12
- Background 12
- Data Preparation 12
- Methods of Test Analyses 13
- Specific Capacity Analyses of Guaje Well Field Data 14

III. ANALYSES OF G-2A TEST DATA 17
- Analyses of the 1998 Test Data at G-2a 17
- Analyses of the 2005 Test at G-2a 25

IV. ANALYSES OF G-3A TEST DATA 32

V. ANALYSES OF G-4A TEST DATA 36

VI. ANALYSES OF G-5A TEST DATA 40

VII. BARRIER BOUNDARY EFFECTS 44
- Background 44
- Boundary Effects in 1998 Aquifer Test at Well G-2a 46
- Boundary Effects in 2005 Aquifer Test at Well G-2a 47
- Boundary Effects in 1998 Aquifer Test at Well G-3a 49
- Boundary Effects in 1998 Aquifer Tests at Wells G-4a and G-5a 51

VIII. SUMMARY AND CONCLUSIONS 52

IX. ACKNOWLEDGEMENTS 54

X. REFERENCES 55

APPENDIX A. WELL COMPLETION DIAGRAMS AND LOCATION DATA 57

APPENDIX B. DESCRIPTION OF DATA FILES ON CD-ROM 69

APPENDIX C. GEOLOGIC MAP OF THE PUYE QUADRANGLE, LOS ALAMOS, RIO ARRIBA, SANDOVAL, AND SANTA FE COUNTIES 71

Analyses of Sequential Aquifer Tests from the Guaje Well Field

by
Stephen G. McLin

ABSTRACT

Four sequential aquifer tests were conducted in each of four new replacement wells in the Guaje well field shortly after they were completed in 1998. Each test consisted of a pumping phase that was about two days long and a recovery phase that was also about two days long. Adjacent wells were used to record both drawdown and recovery. One of these aquifer tests was repeated in 2005. Together, these data reveal horizontal propagation of drawdown in the regional aquifer for distances that vary from about 2500–4800 ft from each pumping well. Dynamic spinner logs from each of the four replacement wells reveal an effective aquifer thickness that ranges from about 435 ft at well G-2a in the east to about 325 ft at well G-5a in the west. Detailed analyses from two of these spinner logs suggest that the actual units yielding water to these wells are much thinner because zones of higher hydraulic conductivity are sandwiched together with lower conductivity units. In the east, most of these higher yielding zones are located above the Miocene basalt flows that separate medium-grained fluvial deposits from lower yielding fine-grained sands and silts that comprise the Tesuque Formation of the Santa Fe Group. In the west, these high-yielding units are interbedded with the basalts. The observed westward thinning of the regional aquifer reflects eastern and northern source areas for these piedmont-slope deposits. The spinner logs also reveal a complex, highly-stratified, aquifer system below Guaje Canyon that is considerably different from the regional aquifer in the central plateau area near wells PM-2 and PM-4.

The transmissivity of these high-yielding zones below Guaje Canyon varies from about 3700 ft^2/day near well G-2a, to about 1700 ft^2/day at well G-4a, and about 700 ft^2/day at well G-5a. The storage coefficient averages about 0.00097. In addition, complex barrier, or no-flow, boundary effects were also observed in the 1998 drawdown data recorded in most wells, including G-3 during both the G-2a and G-3a aquifer tests. Similar boundary effects were seen during the 2005 aquifer test at well G-2a using drawdown data in G-3 and G-3a. These boundary effects represent a complex response to pumping from an aquifer that dramatically thins toward the west. Furthermore, this aquifer may be simultaneously offset by several normal faults below Guaje Canyon. The first is located about 1200 ft east of well G-2a while a second is located between G-4a and G-5a. Fault orientations vary from north-south near well G-2a to northwest-southeast near G-5a, and tend to displace aquifer units downward toward the floor of the Rio Grande rift system. Surface expressions of faulting were previously mapped in the Puye Quadrangle by Dethier (2003) but have not been traced into the alluvial canyon drainage system.

Ultimately, these tests have yielded important new estimates for aquifer transmissivity and storage coefficient values. These parameters are significant because they provide experimental measurements of aquifer responses to controlled aquifer stresses. They also partially fulfill requirements for aquifer parameter identification that support model verification studies.

I. INTRODUCTION

Purpose and Scope

Four sequential aquifer tests were conducted in the Guaje well field shortly after four new replacement wells were installed in 1998. The original aquifer test at well G-2a was also repeated in January 2005 and clarified earlier test results. Each test consisted of pumping a single well at a constant discharge rate and observing water level changes in both the pumping and surrounding non-pumping supply and observation wells. During each test, a 2-day pumping interval was followed by a 2-day recovery period. The purpose of these tests was the experimental determination of regional aquifer parameters that characterize the saturated porous media below Guaje Canyon. Using an analogy between two-dimensional (2-D) heat and water flow, Charles Theis (1935) first developed an analytical solution to the governing partial differential equation that relates drawdown to aquifer transmissivity (T) and storage coefficient (S). Here T represents the rate of flow to a pumping well in gallons per minute through an imaginary, vertical cross-section of aquifer material one foot wide and extending the full saturated thickness of the aquifer that is subjected to a hydraulic gradient of one. Today T is commonly expressed in equivalent units of length squared per unit time. Hydraulic conductivity (K) is determined by dividing T by the aquifer thickness (b). Values for T and K are important because they define how the aquifer will respond to pumping, natural discharge, or recharge. In addition, S is defined as the volume of water yielded to a pumping well per unit area of saturated aquifer material per unit decline in water level. As such, S is dimensionless. Specific storage (S_s) is determined after dividing S by b, and has units of inverse length. Aquifer parameters like T and S were originally developed for confined aquifer conditions assuming radial, 2-D, horizontal flow. However, in complex, three-dimensional (3-D), stratified, groundwater representations, it is often best to use the parameters K and S_s because the influence of b has been removed. The primary objective of this report is to determine values for the aquifer parameters T, K, b, S, and S_s in the Guaje well field using test data obtained from both pumping and observation wells.

A secondary objective was to run each aquifer test long enough so that the cone of depression could expand radially outward to intersect any potential recharge or barrier boundaries that might be present. These boundary effects would typically be revealed by the differences between measured drawdown in an observation well and idealized drawdown predicted at the same time and location using an appropriate analytical aquifer model (e.g., the Theis confined aquifer model represented by the Theis type curve).

A third objective was to conduct step-drawdown tests at each new well so that optimal production rates could be determined. This objective was achieved using either a four or five step-test procedure where each step lasted at least 100 minutes (min).

These aquifer parameters are important because they provide experimental measurements of aquifer responses (i.e., drawdown and recovery) to controlled aquifer stresses (i.e., pumping). These aquifer parameters can then be used in numerical models to simulate aquifer behavior and test the validity of alternative conceptual models. Once verified, these models can be used to simulate complex aquifer behavior (e.g., transitional behavior suggested by changes in S or boundary influences) with confidence, or to test alternative geometric configurations in the model or physical-chemical processes affecting potential contaminant transport. They can also be used to identify data gaps where additional aquifer tests might be helpful, or to evaluate alternative aquifer monitoring configurations. Ultimately, these aquifer tests partially fulfill requirements for aquifer parameter identification that may be used for model verification studies.

Hydrogeologic Setting

The aging municipal water supply wells in the Guaje well field were replaced in 1998. Four new water supply wells were installed and most of the old wells were plugged and abandoned in accordance with State of New Mexico regulations. The lone exceptions were wells G-1a and G-3. Well G-1a was retained as a back-up production well. Well G-3 was converted to a permanent observation well after the pump was removed and the well house was demolished. The new replacement wells were originally identified as GR wells. However, when Los Alamos County assumed ownership of the Guaje well field in 1999, they renamed each well as seen in Table 1. These new names are used in this report and Table 1 serves as a cross-reference between the original and updated names. Additional well construction details can be found elsewhere (Shoemaker, 1999; Purtymun, 1995).

Table 1
Well-naming equivalency as used in this report correlated to historical names used in other investigations of the Guaje well field

Los Alamos County Well Name (this Report)	LANL Well Name (Historical Name)	Current Purpose of Well	Date Completed	Date Tested
G-1a	G-1a	Water Supply	October 1954	—
G-2a	GR-2	Water Supply	March 21, 1998	Feb-Mar 1998 Jan-Feb 2005
G-3	G-3	Observation Well	July 1951	—
G-3a	GR-3	Water Supply	May 9, 1998	Apr-May 1998
G-4a	GR-4	Water Supply	May 18, 1998	April 1998
G-5a	GR-1	Water Supply	June 20, 1998	July 1998

All of the wells in the Guaje well field are located in Guaje Canyon as seen in Figure 1. These wells are located on the northeastern flank of the Pajarito Plateau and penetrate into the regional aquifer. Historically, the highest yielding water supply wells have been located in the east-central plateau area and penetrate into relatively thick sequences of the Puye fanglomerate (Purtymun, 1984; Purtymun and Stoker, 1988) where axial deposits of ancestral Rio Grande gravels (i.e., the Totavi Lentil of Griggs) are commonly encountered. This east-central portion of the regional aquifer is the primary source of potable drinking water for Los Alamos County, Los Alamos National Laboratory, and Bandelier National Monument; it has been described by numerous authors (e.g., Collins et al., 2006; Broxton and Vaniman, 2005; Broxton and Reneau, 1996; Purtymun, 1995 and 1984; Purtymun and Stoker, 1988; Purtymun and Johansen, 1974; and Griggs, 1964). In contrast, the Guaje well field is less productive and shows more drawdown than other water supply wells located in the east-central plateau area (Koch and Rogers 2003). The Guaje Canyon area has been described by WoldeGabriel et al. (2006), Dethier (2003), Shomaker (1999); and Reneau and Dethier (1996).

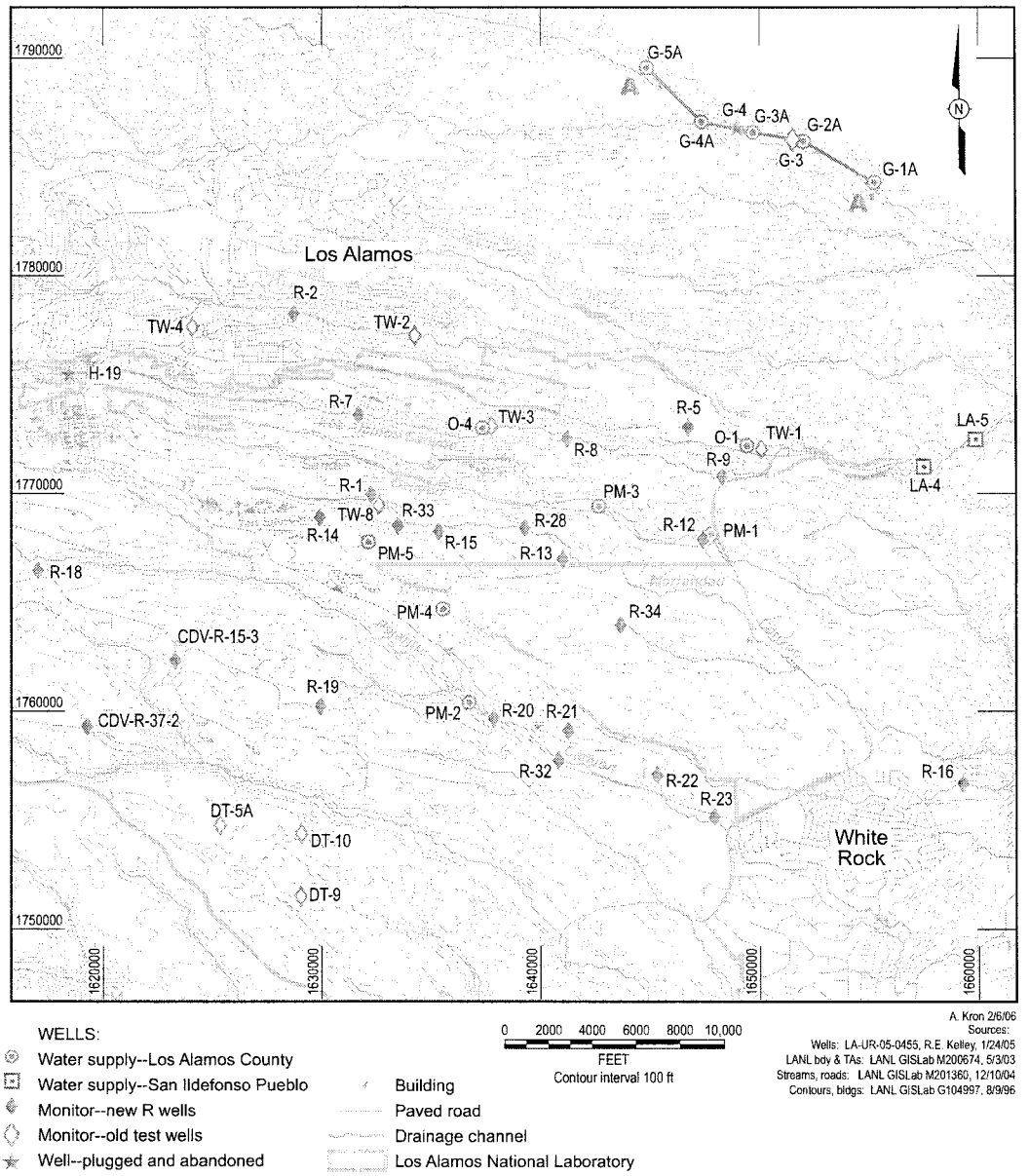

Figure 1. Location of wells on Pajarito Plateau. Note the location of geologic cross-section A-A'.

Figure 1 also shows the location of geologic cross-section A-A' that runs west-to-east through the Guaje well field. This geologic section is shown in Figure 2 and is based on recent work by WoldeGabriel et al. (2006) and Shomaker (1999). This cross-section shows a complex regional aquifer that includes eastward thickening, medium- to fine-grained, piedmont-slope deposits derived from distal sources on the east and north sides of the Española basin. This portion of the regional aquifer is overlain by unsaturated, coarse-grained, alluvial fans derived from the Jemez volcanic field. These unsaturated, volcanogenic materials thicken to the west and are not a significant source of water in Guaje Canyon wells (although they may be a recharge pathway). Because they are saturated farther to the south, these volcanogenic rocks comprise some of the most productive units in the regional aquifer located in the east-central plateau area. Historical information for the regional aquifer below Pajarito Plateau was previously described (McLin, 2005a, 2006; Cushman, 1965; Griggs, 1964; Conover et al. 1963; and Theis and Conover, 1962).

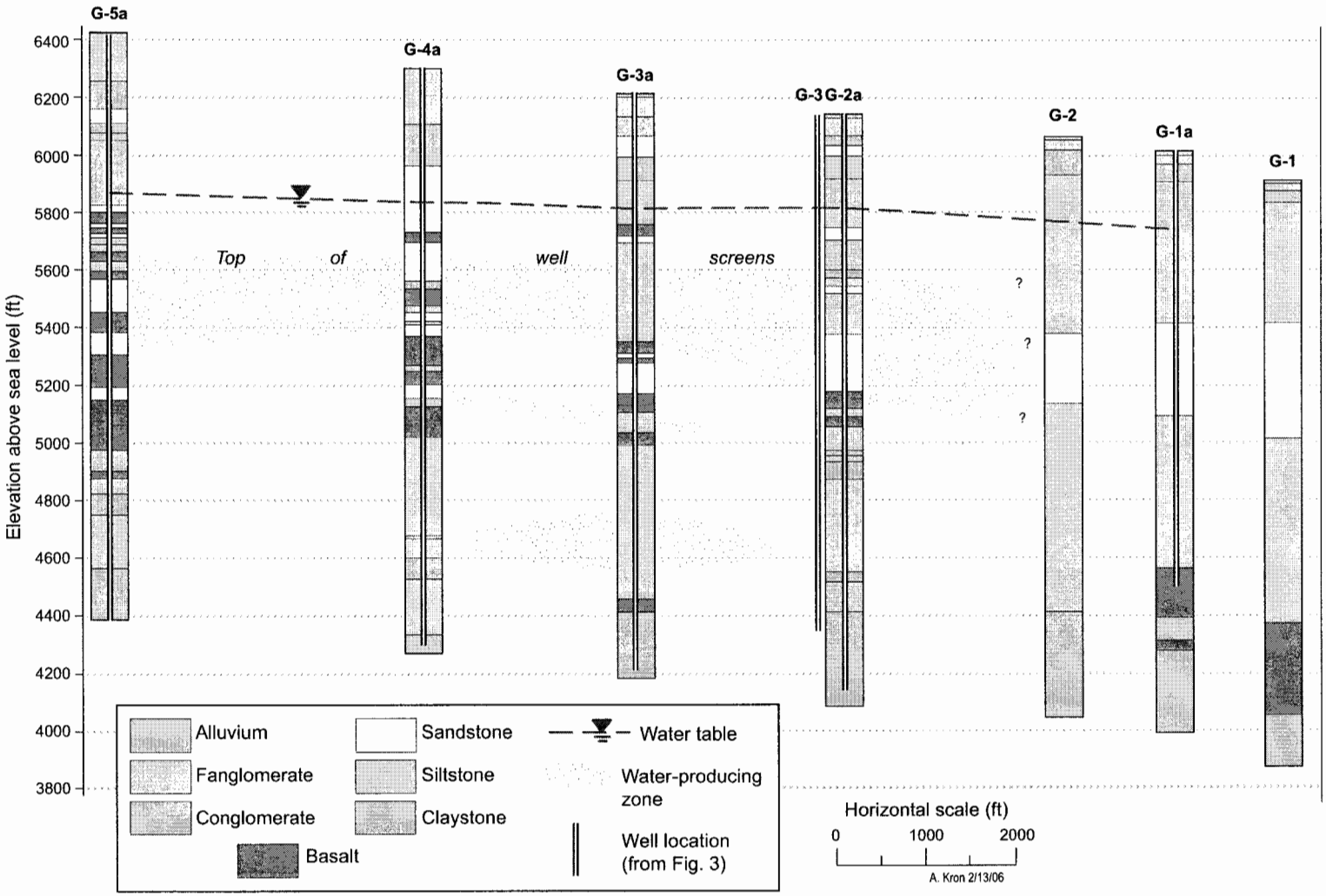

Figure 2. **Geological cross-section A-A' following Guaje Canyon (location of cross-section is shown in Figure 1, modified from WoldeGabriel et al., 2006)**

Aquifer Test Procedures

A conventional aquifer test procedure was followed in all tests described in this report (e.g., Kruseman and de Ridder, 1976). This procedure consisted of turning off all surrounding water supply wells and allowing hydrostatic conditions in the aquifer to reestablish prior to the start of actual test pumping. Then each new well in the Guaje well field was sequentially pumped for about two days and allowed to recover for about two days. The average pumping rate used in individual aquifer tests fluctuated less than about 3% throughout each test period. Data from the second recovery period were used to verify drawdown behavior recorded during the pumping phase of each individual aquifer test and to verify a return to near-hydrostatic conditions after pumping stopped.

The first non-pumping (or recovery) period occurred while the new replacement wells were being drilled (i.e., September 1997 to April 1998). This initial non-pumping period allowed for nearly complete water level recovery in all wells. However, once the sequential aquifer test procedure was initiated at well G-2a, the water level in the regional aquifer was disturbed and never fully recovered. Subsequent pump and recovery test cycles at other wells were conducted at intervals that ranged between about 19-78 days and minimized the effects of incomplete recovery. Furthermore, the order of testing maximized the distances between pumping wells. Thus, the first test was conducted at well G-2a and was followed by tests at wells G-4a, G-3a, and G-5a as seen in Table 1. Table 2 also indicates that hydrostatic conditions in well G-3 were lower in 1998 than when this well was first drilled in 1954. However, these long-term water level declines are widespread and will not significantly affect test results because the present regional piezometric surface is approximately parallel to, but lower than, the ancestral piezometric surface of 50 years ago (i.e., prior to any groundwater development). Finally, this incomplete recovery between tests did not prevent the successful analyses of test data. Ultimately, these tests represent the most comprehensive and reliable aquifer testing ever done in the Guaje well field.

Table 2
Water level measurements and elevations in wells used during the Guaje well field aquifer test. Individual water level elevations* were recorded on the dates indicated.

*All depths are in feet below ground surface (ft bgs)

Date	Well	Hydrostatic Water Level (ft bgs)	Remarks
Sept 1997 to July 1998	All	See below	G-1, G-1a, G-2, G-4, and G-5 shut off; G-6 used as drilling water source
1998	G-1a	Data not available	Static in 1951 was 250 ft bgs
February 1998	G-2a	5817.3 ft (or 322.7 ft bgs)	New well
February 1998	G-3	5817.8 ft (or 323.2 ft bgs)	Static in 1954 was 280 ft bgs
April 1998	G-3a	5815.2 ft (or 396.8 ft bgs)	New well
April 1998	G-4a	5837.6 ft (or 461.4 ft bgs)	New well
July 1998	G-5a	5864.1 ft (or 551.9 ft bgs)	New well
August 1998	All	Resume normal operations	Aquifer tests completed

As indicated above, individual aquifer tests were sequentially conducted in wells G-2a, G-4a, G-3a, and G-5a shortly after each well was completed in 1998. During these tests, usable drawdown and recovery data were recorded at 10-minute intervals in wells G-2a, G-3, G-3a, G-4, G-4a, and G-5a. A follow-up aquifer test was conducted in well G-2a in January 2005 using wells G-1a, G-3, G-3a, and G-4a as observation wells. During this follow-up test, water levels were recorded at 30-minute intervals. Appendix A contains well coordinate locations, elevations, and other important well construction data in Tables A-1 and A-2. Appendix A also includes detailed well-completion diagrams for each of these wells. All of the aquifer data files used in this report are contained on the CD-ROM attached to end of this report and are in ASC-II text format. Table B-1 in Appendix B describes the file naming convention used on the CD-ROM.

About 14.5 million gallons of water were produced during all of the aquifer tests conducted during 1998. These waters were discharged into Guaje Canyon in accordance with New Mexico Environment Department regulations. Another 3.1 million gallons of water were produced during the 2005 aquifer test at well G-2a. These waters were directed into the Los Alamos County water distribution system for normal consumptive use. Los Alamos County personnel with the Department of Public Utilities facilitated this latter arrangement. Except for an insufficient hydrostatic recovery period after each test, this procedure represented nearly ideal conditions for conventional aquifer testing.

A step-drawdown test was also conducted at each new Guaje replacement well during 1998. In a step-drawdown test, the pumping rate is sequentially increased in a series of steps during successive time periods, during which the discharge rate is held constant. One purpose of this type of test is to determine the energy-loss coefficients (i.e., B, C, and n) in the equation,

$$s = s_l + s_t = BQ + CQ^n \tag{1}$$

where s is the total head loss in the well, s_l is the laminar flow head-loss component, and s_t is the turbulent flow head-loss component (e.g., Driscoll, 1986, p. 555-559). In Equation (1), we can write $s_l = BQ$ and $s_t = CQ^n$, where B is a laminar-flow loss coefficient, C is a turbulent-flow loss coefficient, and n is an exponent related to the nonlinear nature of wellbore turbulence (typically $1.5 \le n \le 3.5$). Solution details can be found in Bouwer (1979, p. 83-85) or Bear (1979, p. 477-479). If we define R as a ratio of laminar flow head loss to total head loss, then $R = 100\ s_l/s$ and,

$$R = 100 \Big/ \left[1 + \left(\frac{C}{B} \right) Q^{n-1} \right] \tag{2}$$

Hence, if B, C, and n are found from a step-drawdown test, then R can be estimated as a function of Q. Note that in Equation (2), many authors assume $n = 2$. The ultimate objective in modern well design practice is to: (1) minimize turbulent head losses near the pumping well by optimizing the well screen openings and mean grain diameter in the filter pack so that energy losses are minimized (i.e., minimize C and/or n); and (2) design a well so that it does not produce excessive fine-grained sediments during routine use. In other words, the transition from laminar to turbulent flow is forced to occur at a relatively large Q value. A step-drawdown test simply gives an opportunity of selecting a production Q that minimizes turbulent flow near the wellbore once the well has been completed. The goal of this design objective is to minimize pumping costs during the life of the production well. One way to measure the transition from laminar to turbulent flow is to observe how s_t/Q changes during successive steps in the step-drawdown test. Ideally, this relationship is linear and the coefficients in Equation (1) are easily found. However, departures from linearity as seen on a graphical plot of Q versus s_t/Q may occur at

higher Q values because turbulent flow losses are starting to increase as Q increases. In these situations, we would determine the coefficients in Equation (1) using only the earlier step data with Q values below the identified transition. Ideally, we would then set the production Q below this transition point in order to minimize long-term pumping costs. Excellent discussions on this topic are presented in Rosco-Moss (1990, p. 97-107) and Driscoll (1986, p. 555-559). A related solution has also been suggested by ASTM (2004).

Guaje Canyon Aquifer Configuration

One of the best ways to determine exactly which zones within the screened interval yield water to a pumping well is with a dynamic spinner log. This log is really a downhole flow meter. Basically this elongated tool has an axial propeller that turns as the tool is raised or lowered past the screened portion of a well while the well is pumped. Each revolution of the propeller generates a pulse that is electronically recorded. More pulses are generated as the tool passes those portions of the screen where more water is entering the wellbore. Thus spinner rotation speed is related to fluid entrance velocity. Dynamic spinner logs for each new replacement well are shown in Appendix A (i.e., see Figures A-7 to A-10). These spinner logs were originally shown in Shomaker (1999), and are listed here as a convenience to the reader. These logs indicate that only a small portion of each well screen is yielding most of the water to each well. Collectively, these logs also reveal a water production zone that dramatically thins toward the west as shown in Figure 3. It is important to recognize that the upper boundary of this zone is defined by the tops of individual well screens and may actually extend vertically upward toward the water table. This restriction applies because a spinner log only yields meaningful results opposite a well screen and not blank casing. Figure 3 also shows a snapshot of the regional water table on January 28, 2005. Hence, this representation implies that the high-yielding zone in the regional aquifer may be somewhat thicker than indicated in Figure 3. When this water producing zone is superimposed onto the geologic cross-section shown in Figure 2, it reveals an effective saturated thickness that appears to be only partially related to specific geological units. Furthermore, it is not obvious in Figures 2 or 3 if the regional aquifer is under confined or phreatic (i.e., water table) aquifer conditions. Important dimensions for these water-bearing units are summarized in Table 3.

Table 3
Important Dimensions for Guaje Canyon Wells*

*Elevation is ft above mean sea level (msl); other dimensions are ft bgs or ft

Well	Elevation (ft above msl)	Top of Screen (ft bgs)	Bottom of Screen (ft bgs)	Effective Aquifer Top (ft bgs)	Effective Aquifer Bottom (ft bgs)	Screen Length (ft)	Effective Aquifer Thickness (ft)
G-1a	6014	272	1513	439	1002	563	563
G-2a	6140	565	1980	565	1000	1415	435
G-3	6139	695	1785	564	989	400	425
G-3a	6212	589	1980	589	850	1391	261
G-4a	6299	655	1980	655	900	1325	245
G-5a	6416	765	1980	765	1090	1215	325

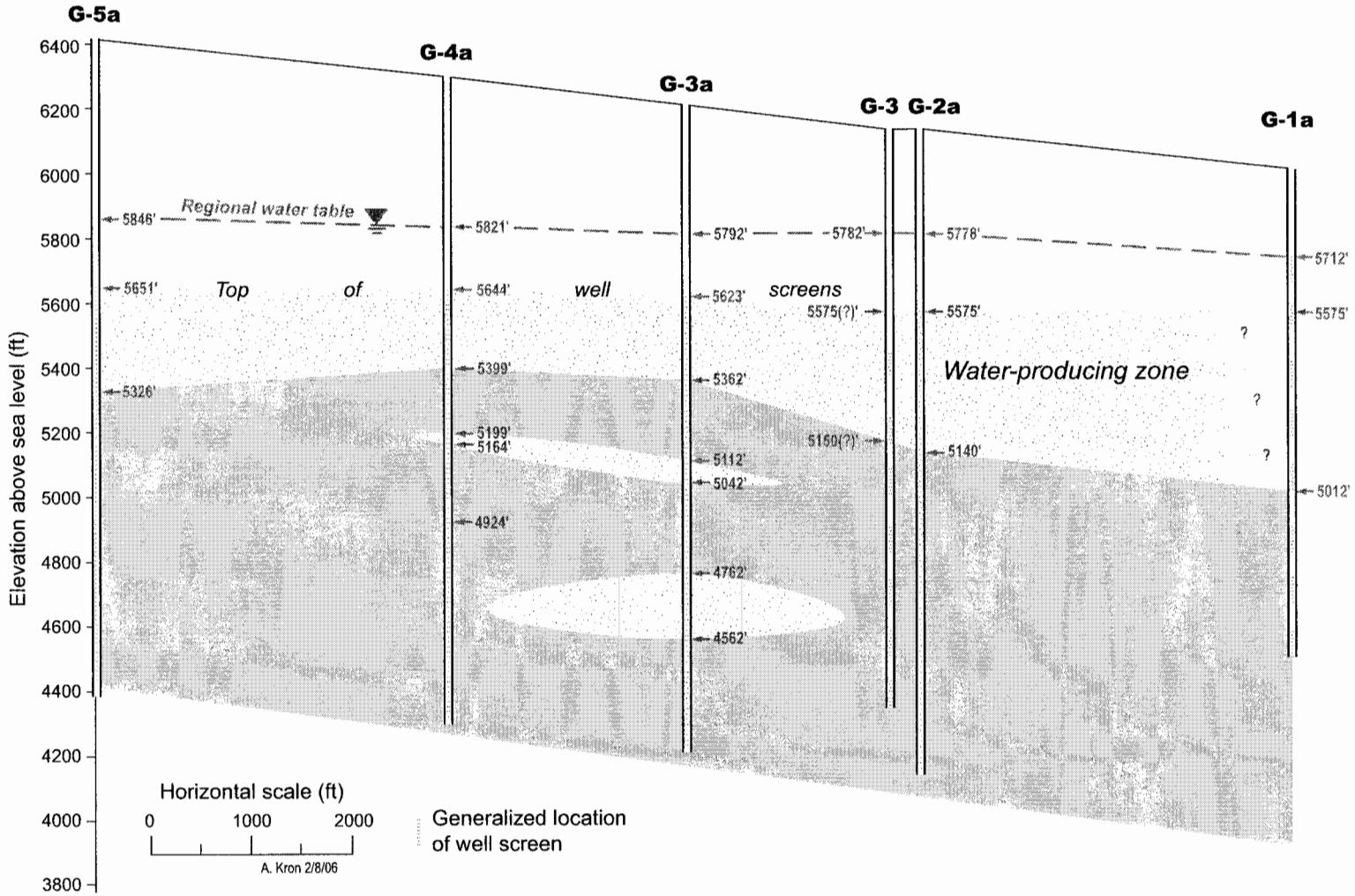

Figure 3. **Simplified representation of the regional aquifer along the geologic cross-section A-A' shown in Figure 2 using dynamic spinner logs to define important hydrostratigraphic contacts. Depths to water were recorded on January 28, 2005.**

Closer analyses of dynamic spinner logs at wells G-2a and G-4a reveal a clearer picture of important hydrostratigraphic units below Guaje Canyon. Figure 4 shows a detailed analysis of the G-2a log that was run in 1998 shortly after the well was completed. Table 4 summarizes the production characteristics from this log. Likewise, Figure 5 shows a detailed analysis of the G-4a log that was run shortly after that well was completed. Table 5 summarizes the production characteristics from this second log. Unfortunately, detailed analyses of the remaining spinner logs could not be performed because these data were not available for subsequent analyses.

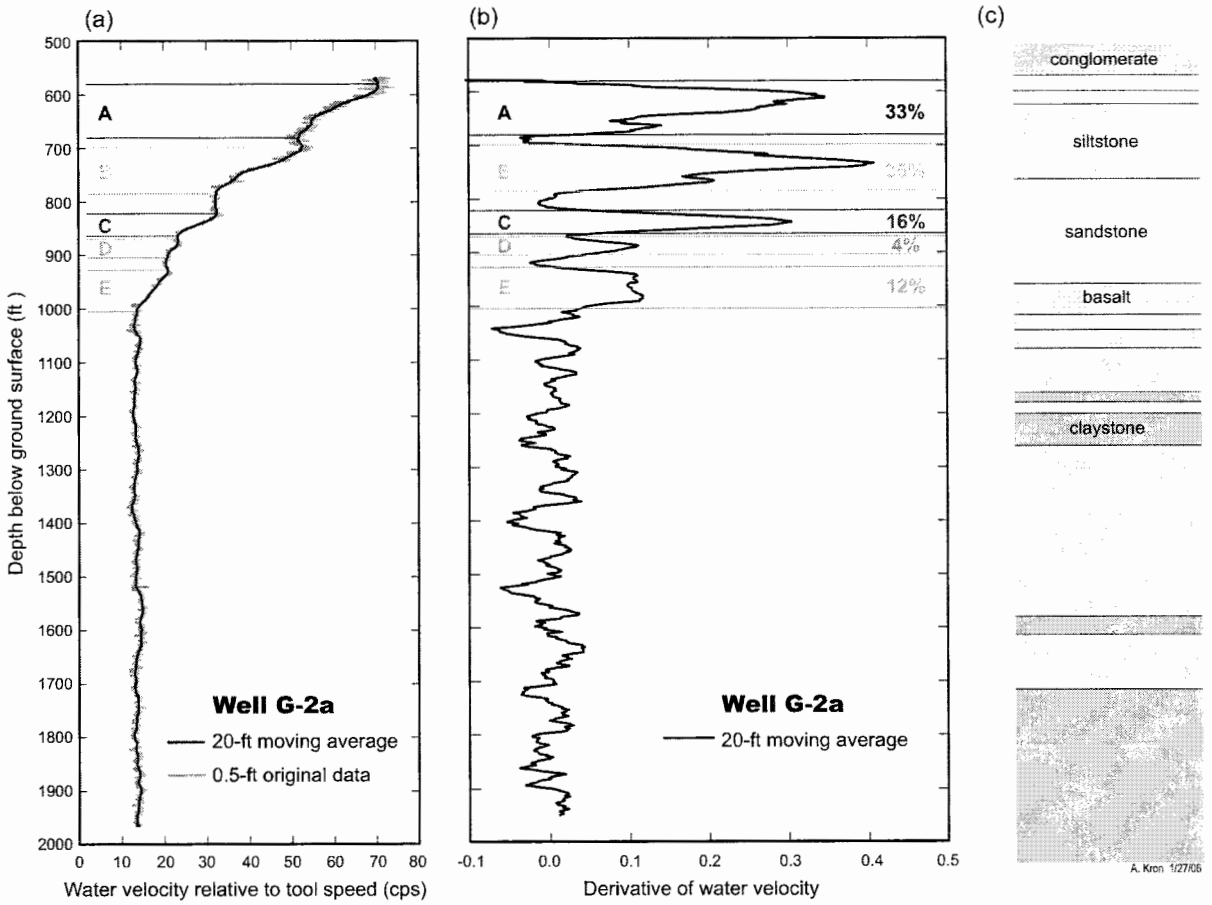

Figure 4. **Graphical results of (a) the dynamic spinner log at G-2a; (b) interpretative results showing the derivative of water velocity with respect to borehole depth; and (c) the geologic log opposite the G-2a well screen (from Figure A-2). Note that (b) shows percentage of total water production from each layer listed in Table 4.**

The results from the G-2a spinner log seen in Figure 4 clearly indicate that the Santa Fe Group sediments located immediately below the top of the well screen and down to about 1005 ft bgs yield almost all of the water produced at G-2a. In other words, five high-yielding zones (i.e., zones A, B, C, D, and E) total about 342 ft of saturated, sandy materials as shown in Table 4. According to the well completion diagram seen in Figure A-2 for well G-2a (see Appendix A), these five high-production zones are located in the 435 ft thick interval between about 570–1005 ft bgs, and are above the uppermost Miocene basalt layer. This detailed analysis suggests that high-yielding zones are sandwiched between thicker sequences of lower-yielding sediments. In addition, the high-yielding units are much thinner than the full screen length in the well.

Table 4
Summary of G-2a production zone characteristics
derived from the dynamic spinner log shown in Figure 4

	Producing Zones			Spinner Log Results			Summary	
Zone	Top Depth (ft bgs)	Bottom Depth (ft bgs)	Unit Thickness (ft)	Top (cps)	Bottom (cps)	Difference (cps)	Production Amount (%)	Geologic Unit
A	580	680	100	70.5	51.8	18.7	33	Santa Fe
B	698	785	87	52.4	32.2	20.2	35	Santa Fe
C	821	864	43	32.4	23.3	9.1	16	Santa Fe
D	870	905	35	23.3	20.7	2.5	4	Santa Fe
E	928	1005	77	21.0	13.7	7.3	12	Santa Fe

Similarly, results from the G-4a spinner log seen in Figure 5 also indicate that the Santa Fe Group sediments located between about 655-900 ft bgs (i.e., zones A, B, and C) yield most of the water produced at G-4a. These three zones total about 177 ft of saturated, sandy materials and are located above the uppermost Miocene basalt layer shown in Table 5. These units yield 80% of the total water production at G-4a. However, there are two additional zones located between 1105-1145 ft bgs and 1325-1370 ft bgs (i.e., zones D and E) that yield smaller amounts of water. Together, these five individual zones total about 272 ft of saturated materials. Note that the lower two zones (i.e., zones D and E) are located below the uppermost Miocene basalt layer according to the well completion diagram for G-4a that is shown in Figure A-5 (see Appendix A). Again, this detailed analysis tells us that high-yielding zones are sandwiched between thicker sequences of lower-yielding sediments. As in well G-2a, we see that the high-yielding units in well G-4a are also much thinner than the full screen length in the well. Finally, we note that the most productive zones are located above the Miocene basalt units.

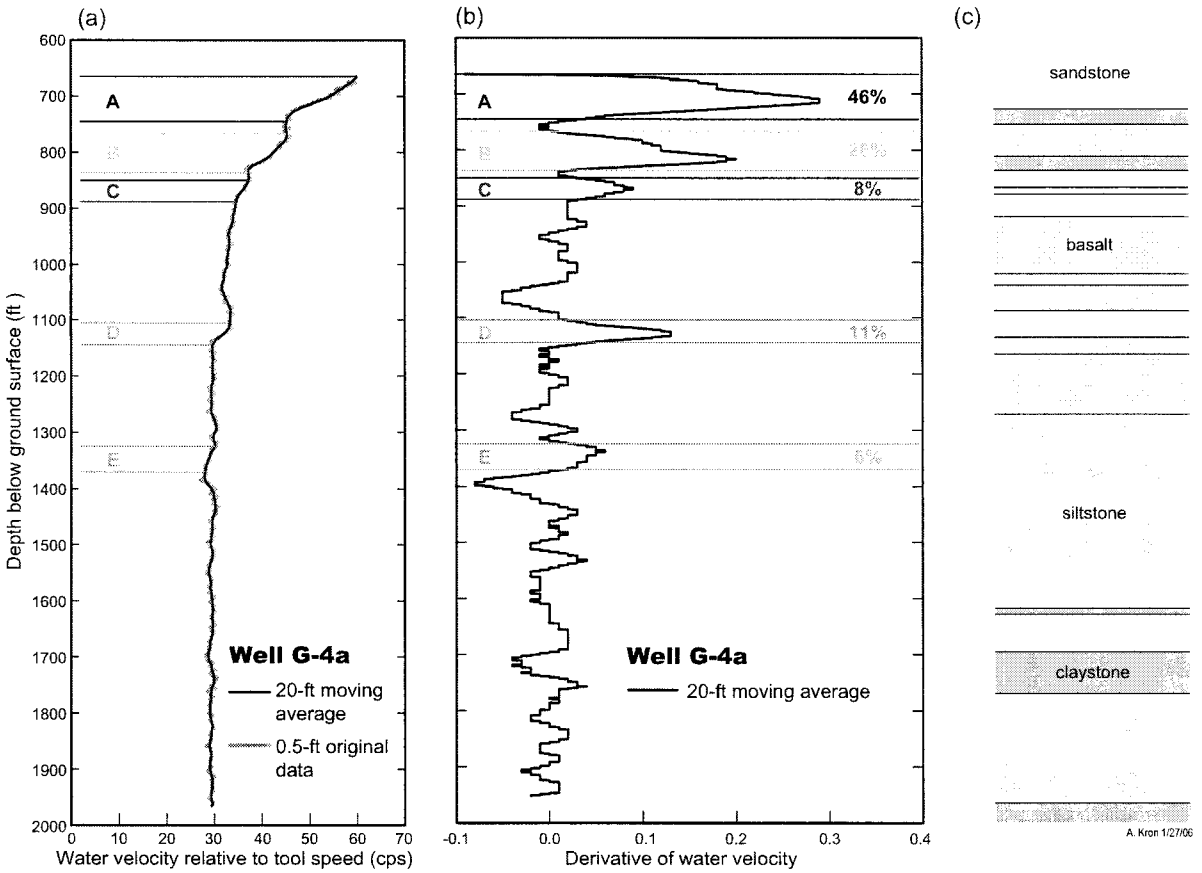

Figure 5. **Graphical results of (a) the dynamic spinner log at G-4a; (b) interpretative results showing the derivative of water velocity with respect to borehole depth; and (c) the geologic log opposite the G-4a well screen (from Figure A-4). Note that (b) shows percentage of total water production from each layer listed in Table 5.**

Table 5
Summary of G-4a production zone characteristics derived from the dynamic spinner log shown in Figure 5.

	Producing Zones			Spinner Log Results			Summary	
Zone	Top Depth (ft bgs)	Bottom Depth (ft bgs)	Unit Thickness (ft)	Top (cps)	Bottom (cps)	Difference (cps)	Production Amount (%)	Geologic Unit
A	675	745	70	59.8	45.2	14.6	46	Santa Fe
B	767	836	69	45.3	37.2	8.1	26	Santa Fe
C	850	888	38	37.2	34.6	2.6	8	Santa Fe
D	1105	1145	40	33.3	29.7	3.6	11	Santa Fe
E	1325	1370	45	30.1	28.1	2.0	6	Santa Fe

II. METHODS OF DATA ANALYSES

Background

Methods of drawdown analyses used in this report included several variations of Theis (1935), specific capacity, distance-drawdown, and step-drawdown procedures. In addition, Theis analyses were also performed using simultaneous drawdown values from both the pumping and observation wells if these data were available. For most of the analyses, commercially available aquifer testing software was used for a variety of reasons. These include public availability, program documentation, repeatability of analyses, and convenience. Except for the specific capacity, distance-drawdown, and step-drawdown methods, all test data were fitted to appropriate theoretical type-curve models using Aqtesolv™ for Windows (version 3.50, professional). These methods are briefly described below in a separate section.

The Aqtesolv™ software yields parameter estimates for transmissivity (T) and storage coefficient (S) using observed drawdown over time. This software package allows the anisotropy ratio (K_h/K_v) to vary for some methods of analysis but keeps it fixed at a value of one for other methods. However, none of the methods will provide a unique solution for both T and K_h/K_v at the same time. In other words, K_h/K_v must be fixed in order to find a unique value for T. This is a mathematical limitation of the method and not a shortcoming of the software. Hence, the traditional practice of fixing K_h/K_v at a value of one before solving for T is used here. This procedure was followed so that the results could be easily compared to those techniques where this ratio could not be adjusted. Aqtesolv™ also yields a storativity (S) value for any analysis by pumping-test methods as part of a solution. However, such a determination is only valid for multiple-well tests where both pumping and observation wells are used in the analysis. Therefore, results for this parameter are only listed in summary tables when this well combination is available. A brief discussion of data preparation and analysis is described below.

Data Preparation

Response to Pumping. Initially, static water levels are allowed to recover in all wells so that individual responses to pumping can be later determined. This initial recovery period varied for individual wells that are described here. For the aquifer tests that were conducted in 1998, these recovery periods varied from about 15 to 180 days; however, for the 2005 aquifer test it was about 80 days. Once pumping starts at time $t = 0$, a cone of depression propagates radially outward from the production well and intersects different observations wells at different times. That is, closer observation wells see drawdown first and these drawdown values are generally larger than observation wells located farther away. Here drawdown at a well is computed as the difference between the recorded water level at some time $t > 0$ and the initial static water level at $t \leq 0$. Likewise, when pumping stops, these water level declines start to rebound back toward initial static conditions. Hence, both drawdown and recovery data are collected over time for analyses by classical pumping techniques.

Simple Recovery. A procedure described by Driscoll (1986, p. 252-260) was employed to process recovery data collected after pumping ceased. In this method, a trend line was extended through the data collected from the latter portions of the pumping phase and into the recovery period, as illustrated in Figure 9.37 of Driscoll. Recovery was then computed as the difference between values on this trend line and the observed water levels for the same time. Results of this process are referred to simply as recovery data and the analysis is identical to that for pumping data. The advantage of using this type of recovery data is that the effects of partial penetration and anisotropy can be taken into consideration when using certain methods in Aqtesolv™.

Residual Recovery. Recovery was also determined by subtracting observed water levels after pumping ceased from the static equilibrium value established prior to pumping. Results of this operation are referred to as residual-recovery data. The advantage of this type of recovery data is that it is not potentially biased by a trend line fitted to the observed data as in the simple recovery method mentioned above. However, the disadvantage is that the effects of partial penetration and anisotropy are not taken into consideration when using certain methods in Aqtesolv™.

Data that were collected in 1998 from individual observation wells during the pumping and recovery intervals at wells G-2a, G-3a, G-4a, and G-5a were analyzed by various standard pumping-test methods. Observation wells for the tests at G-2a and G-3a included G-3; well G-4 served as an observation well for the G-4a test. During the 2005 aquifer test at well G-2a, observation wells included G-1a, G-3, G-3a, and G-4a. Test data collected at individual wells are analyzed by as many as five different methods for comparison, including Theis pumping, Theis recovery, Theis residual-recovery, distance-drawdown, and the specific capacity techniques. To avoid repetition in the text, parenthetical reference citations for the various methods (that is, the years of publication) are only given here.

Methods of Test Analyses

Theis Method (Theis 1935). Each aquifer test was initially analyzed by the Theis method. Analyses include both pumping and simple-recovery data (as defined above). In this classical method, a log-log plot of drawdown or recovery data versus time is fitted to a Theis type-curve. The method assumes that the well is fully penetrating, the hydraulic condition of the aquifer is confined, and application or relaxation of stress is by prolonged withdrawal or recovery of water. The method has been extended to include partial penetration effects in confined aquifers, and allows the anisotropy ratio (K_h/K_v) to vary. Theoretically, both pumping and recovery techniques should replicate one another in both the pumping and observation wells. However, when they do not, one might infer that wellbore clogging, turbulence, or other phenomena were present in the pumping well during some phase of the test. Differences can also occur when boundary effects are present or from incomplete recovery.

Theis-Residual Recovery Method (Theis 1935). Test data were also analyzed by the Theis-residual recovery method. This traditional method differs from the Theis analysis of recovery data described above in that it uses residual-recovery data. In practice, it is generally most applicable to recovery data from the pumping well where well bore turbulence or clogging may be a problem. In this method, a straight line is drawn through a semi-logarithmic plot of residual recovery data versus the dimensionless ratio of t/t'. Residual recovery is the difference between the original static water level and the depth of water at a given instant during recovery. In addition, t is the time since pumping started and t' is the time since pumping stopped. This method is probably more widely used than the simple Theis-recovery method mentioned above; however, corrections for partial penetration can not be made with this technique. Some readers may wonder why two different recovery methods were employed here. The answer is simple: when using the pumping well as the observation well, many hydrologists consider recovery data to be more reliable than pumping data because wellbore turbulence is minimized. As previously mentioned, all three approaches (i.e., Theis pumping, Theis simple recovery, and Theis residual recovery) should replicate one another exactly when the well is fully penetrating. When they do not, hydrologists simply have additional information to make inferences about dominant effects during certain phases of the test procedure. These differences can influence alternative interpretations by lending support to the method that is most reliable. However, when drawdown and recovery data are available from an observation well, the advantages of this method are probably over-shadowed by other techniques presented here.

Distance-Drawdown Method (Cooper and Jacob, 1946). This method is still another variation of the Theis method presented earlier; however, it is more restrictive since it requires multiple observation wells. When these additional wells are available, a very reliable estimate of T can usually be obtained for comparison to other techniques. Here drawdown recorded at a given time is plotted against radial distance from the pumping well. Details are discussed by Bouwer (1978, p. 92-93) or Fetter (1994, p. 227-229). The distance-drawdown formula is obtained from the Thiem (1906) steady-state solution, which says that,

$$T = \frac{Q\,\mathbf{ln}\left(r_2/r_1\right)}{2\pi\left(s_1 - s_2\right)} = \frac{2.303Q}{2\pi\Delta s} \tag{3}$$

where Q is the discharge rate in the pumping well, ln is the natural logarithmic function, r_1 and r_2 are the radial distances from the pumping well to observation wells 1 and 2, respectively, and where drawdown values s_1 and s_2 were recorded in observation wells 1 and 2 at the same time. If the logarithm of distance (r) is plotted against drawdown (s), then a linear fit through the data yields the second (or right-hand) relationship shown in Equation (3) where Δs is measured over one log cycle. When the best fitting straight line is extended to zero drawdown, a value for r_0 is found. Here r_0 defines an idealized (or average) radius of influence of the pumping well. Then S can be estimated from the relationship,

$$S = 2.25Tt/r_0^2 \tag{4}$$

Equation (4) is strictly valid only when $u \leq 0.05$, where $u = r^2\,S/4Tt$. Since the observation wells may be at large r values, this restriction may be violated. In addition, if the drawdown values have not stabilized for some relatively large t value, then T and r_0 may only be approximate. Equations (3) and (4) still provide estimates for T and S that can serve as a basis of comparison with other techniques because they often represent system-wide averages.

Specific Capacity Method (Theis, 1963). As an additional method of comparison, test data from the pumping well were also analyzed by the specific capacity method to determine T. This traditional technique was modified by McLin (2005b) from a procedure that was previously modified by Bradbury and Rothschild (1985). Here specific capacity is defined as discharge (Q) divided by drawdown or injection (s), and has units of gpm/ft. Strictly speaking, this method is only valid for confined aquifers and is typically used to estimate a minimum value for T when the well is assumed to be fully penetrating and 100% efficient. Ideally, this minimum T value becomes a constraint when applying the other methods presented above. In addition, K_h/K_v is also fixed at a value of one. As before, K is then obtained from the relationship $K = T/b$, where b is saturated thickness. Numerous authors (e.g., Walton, 1970) have demonstrated that T values from the specific capacity technique are somewhat insensitive to changes in S. However, since S must be estimated prior to finding T, there is also some uncertainty in this approach.

Specific Capacity Analyses of Guaje Well Field Data

Values for T and K were initially computed from historical data obtained from individual water supply wells using the specific capacity method described above. These values and supporting data are shown in Table 6 for historical Guaje wells, and in Table 7 for the new replacement Guaje wells. The T values shown in Table 6 are not representative because some data were affected by damaged wells or declining water production rates over time. Instead this information is presented for completeness and illustrates that T values should be used with caution. The information shown in Table 7 is more representative of the saturated aquifer materials below Guaje Canyon and can serve as a basis of comparison for aquifer test parameters presented below.

Table 6
Transmissivity[a] estimated from specific capacity data for historical Guaje wells

Parameter[b]	G-1[c]	G-1a[c]	G-2[c]	G-3[c]	G-4[c]	G-5[c]	G-6[c]
Year	1970	2001	1998	1974	1976	1987	1991
Q (gpm)	398	400	424	273	337	379	267
s (ft)	113	25	26	82	165	42	83
t (min)	480	480	480	480	480	480	480
L (ft)	490	563	435	425	360	400	810
d_c (in)	10	10	10	10	10	10	12
d_w (in)	12	12	12	12	12	12	22
S (dim)	0.00097	0.00097	0.00097	0.00097	0.00097	0.00097	0.00097
b (ft)	490	563	435	425	360	400	810
E (%)	100	100	100	100	100	100	100
T (ft^2/day)	815	4098	4182	767	454	2227	720
K (ft/day)	1.7	7.3	9.6	1.8	1.3	5.6	0.9

a Transmissivity from specific capacity; see McLin (2005b) for details.

b Parameter definitions are as follows:
Year = year that data were reported
Q = average well discharge (gpm)
s = quasi-steady state drawdown (ft)
t = estimated time of drawdown (min)
L = effective screen length (ft) from PM-4 spinner log or estimated value
d_c = screen or casing diameter (in.)
d_w = borehole diameter (in.)
S = average storage coefficient from Figure 7
b = total aquifer thickness (ft) estimated from well log
E = assumed well efficiency (%).
T = aquifer transmissivity estimated from specific capacity.
K = hydraulic conductivity computed from $K = T/b$

c Data summarized from Purtymun, 1995; and Koch and Rogers, 2003

Table 7
Transmissivity[a] estimated from specific capacity data for replacement Guaje wells

Parameter[b]	G-1a[c, d]	G-2a[c]	G-3a[c]	G-4a[c]	G-5a[c]
Year	2001	1998	1998	1998	1998
Q (gpm)	400	901	800	752	408
s (ft)	25	107	122	129	144
t (min)	480	2880	2880	2880	2880
L (ft)	563	435	261	245	325
d_c (in)	10	16	16	16	16
d_w (in)	12	26	26	26	26
S (dim)	0.00097	0.00097	0.00097	0.00097	0.00097
b (ft)	563	435	261	245	325
E (%)	100.0	100.0	100.0	100.0	100.0
T (ft^2/day)	4098	2186	1675	1478	685
K (ft/day)	7.3	5.0	6.4	6.0	2.1
Q/s (gpm/ft)	16.0	8.4	6.6	5.8	2.8

[a] Transmissivity from specific capacity; see McLin (2005b) for details.

[b] Parameter definitions are as follows:
Year = year that data were reported
Q = average well discharge (gpm)
s = quasi-steady state drawdown (ft)
t = estimated time of drawdown (min)
L = effective screen length (ft) from spinner log or estimated value
d_c = screen or casing diameter (in.)
d_w = borehole diameter (in.)
S = average storage coefficient from Figure 7
b = total aquifer thickness (ft)from spinner log or estimated from well log
E = assumed well efficiency (%).
T = aquifer transmissivity estimated from specific capacity.
K = hydraulic conductivity computed from $K = T/b$

[c] Data summarized from Purtymun, 1995; and Koch and Rogers, 2003; and this report

[d] Revised from Table 6 using an estimated value

III. ANALYSES OF G-2A TEST DATA

There were two separate aquifer tests and one step-drawdown test that were conducted in well G-2a. The first aquifer test was conducted in 1998 shortly after this well was completed. A step-drawdown test was also conducted at that time. A second aquifer test at well G-2a was conducted in January 2005. Analyses of each of these tests are presented below.

Analyses of the 1998 Test Data at G-2a

Constant Rate Aquifer Test. A two-day aquifer test was conducted at well G-2a from February 28 to March 2, 1998, at a constant discharge rate of 901 gallons per minute (gpm). This test was immediately followed by a two-day recovery period from March 2-3, 1998. Drawdown and recovery data were automatically recorded in wells G-2a and G-3 during the aquifer test. Observation well G-3 is located about 311 ft west of G-2a (see Figure 1 and Table A-1 in Appendix A). Analyses of the G-2a data are shown in Figure 6 using the aquifer configuration shown in Figure 3 and dimensions shown in Table 3. Theis analysis of drawdown is shown in Figure 6(a), while Theis analysis of recovery is shown in Figure 6(b). Figure 6(c) shows an analysis using the Theis residual-recovery method. All of the resulting T values compare favorably with the specific capacity value for T that was reported in Table 7 for this well. One advantage of these comparisons is that they demonstrate parameter variability generated in the curve-matching process using alternate methods of analyses. Note that in each of these analyses, the Theis type curve is fitted through the early-time data (i.e., before about 200 min). It is obvious that after this time, observed drawdown effects are larger than that predicted by the Theis model. In other words, the water level responses in G-2a are starting to sense the presence of a no-flow, or barrier, boundary. More will be said about these boundary effects later. Note that in Figure 6(c), this departure occurs at a dimensionless time of about $t/t' = 15$, and corresponds to about $t = 200$ min. Finally, we note that a phreatic analysis was not done for reasons discussed below. In this analysis, however, the aquifer thickness would be 638 ft according to Figure 3 and the well would be partially penetrating. We mention this because it is not obvious in Figures 2 and 3 (also see Figures A-2 and A-3 in Appendix A) if aquifer conditions are confined or phreatic. In fact, Figures 2–5 suggest a highly stratified, water-table aquifer lies below Guaje Canyon because no confining layer was identified in the drilling logs. In contrast, the analysis shown in Figure 7 suggests that the aquifer between wells G-2a and G-3 responds like a confined system according to the value obtained for S. Based on Figure 7, we also conclude that our estimated value for S used in Table 7 was reasonable. Finally, according to the T values shown in Figure 6 and $b = 435$ ft, we conclude that K varies between 6.6–6.9 ft/day, and averages about 6.7 ft/day.

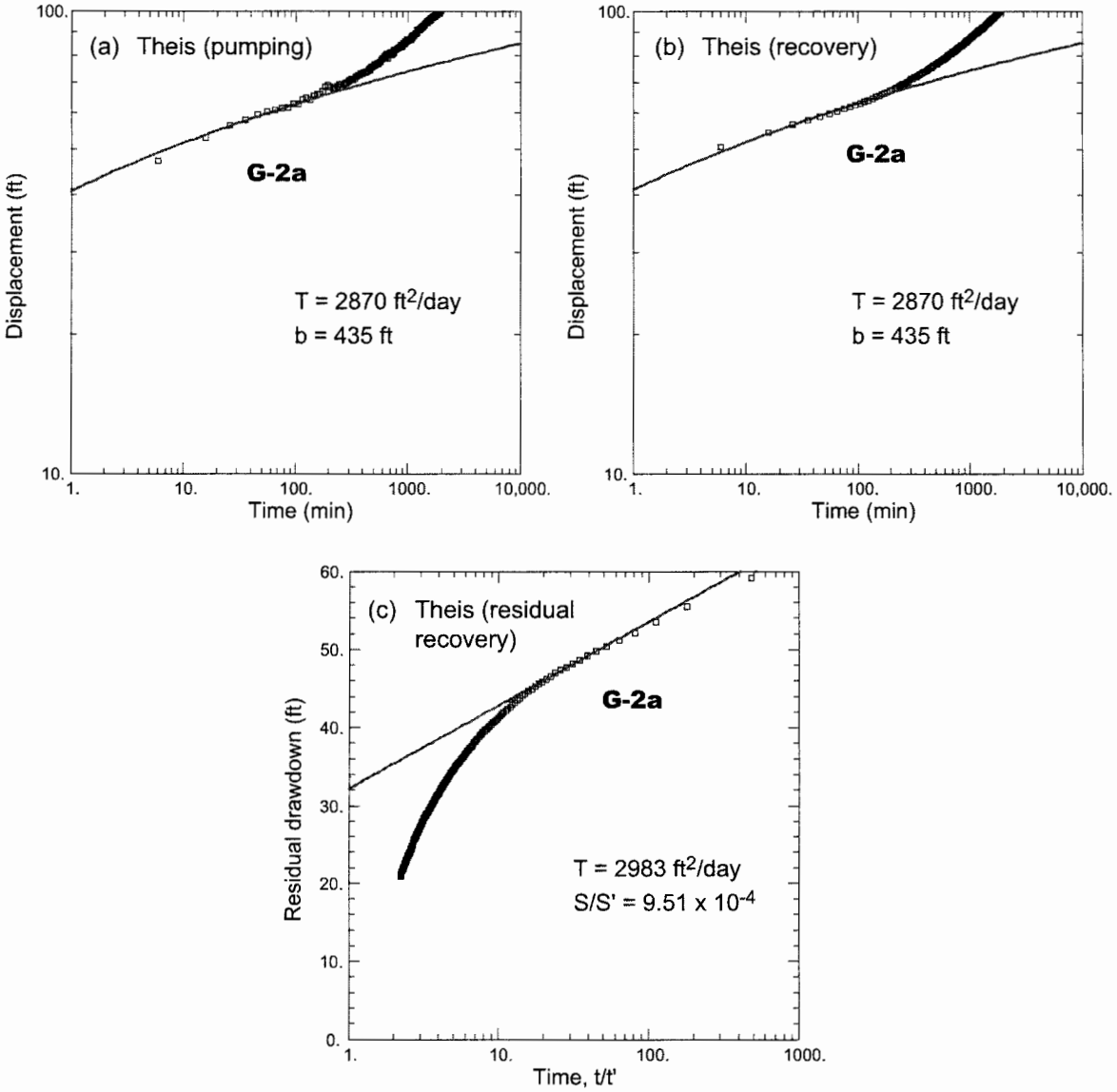

Figure 6. Theis confined aquifer analysis using the 1998 G-2a data from (a) drawdown, (b) recovery, and (c) residual recovery. Note that the anisotropy ratio is 1.

Similarly, analyses of the drawdown data from observation well G-3 are shown in Figure 7(a), while drawdown data from wells G-2a and G-3 are simultaneously analyzed in Figure 7(b). The *T* value from well G-3 is notably higher than other values shown in Figures 6 and 7 or Table 7, whereas, the *T* value shown in Figure 7(b) is similar to these other values. We conclude that boundary influences are affecting these *T* values in different ways. Other factors that influence *T* values are discussed in the next section. The 1998 analyses suggest that *K* varies from about 6.6-9.3 ft/day between wells G-2a and G-3. The real value of the data at well G-3 is that it provides an estimate for *S* that suggests the aquifer is confined. Unfortunately, this parameter estimate is only based on the first 100 min of drawdown data as seen in Figure 7(a).

The results shown in Table 7 and Figures 6 and 7 suggest that there are moderate differences between the specific capacity and Theis methods of analyses. The *T* estimates vary because of the particular analytical method used and differences in the curve-matching procedures. Another way to interpret these results is by comparing the ratio between the maximum and minimum *T* values from all of these analyses. Since this ratio is less than 2, we conclude that at a sufficiently large scale these results are essentially the same. These different comparisons can be reconciled by noting that as the expanding cone of depression continues to intersect a larger portion of the aquifer volume over time, the final answer is converging to some global average *T* value that is probably well-represented by the analysis shown in Figure 7(b).

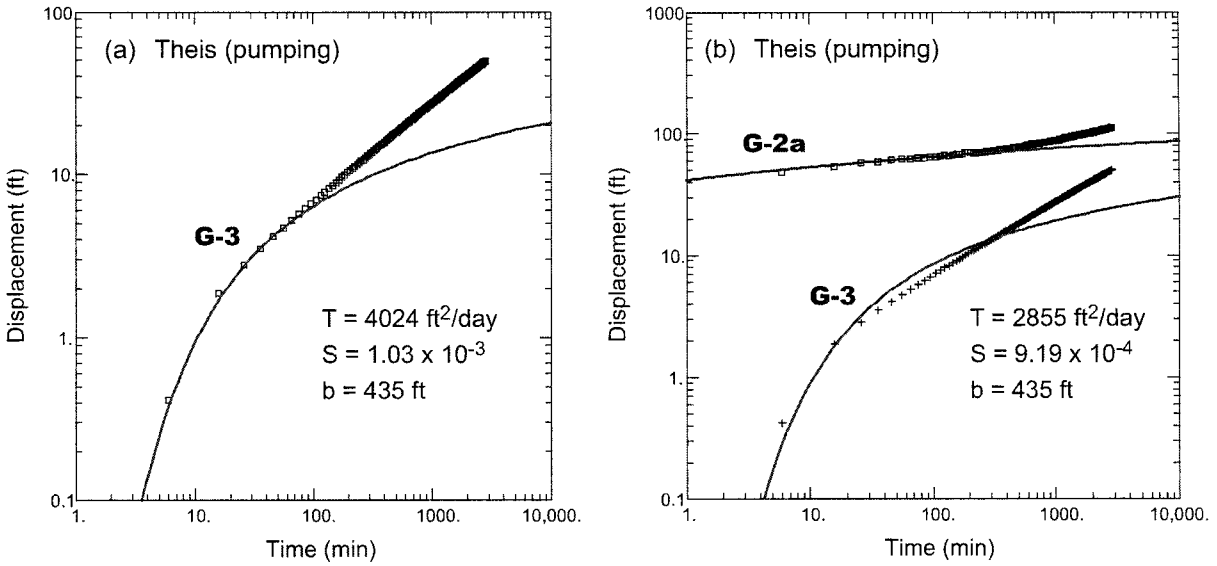

Figure 7. Theis confined aquifer analysis using the 1998 drawdown data from (a) G-3, and (b) both G-3 and G-2a simultaneously. Drawdown departures from Theis clearly suggest multiple barrier boundaries.

Boundary Effects. In addition to the analyses mentioned above, it is apparent that boundary influences are affecting drawdown values after about 100–200 min in Figures 6 and 7. These effects are addressed in a separate section near the end of this report.

Step-Drawdown Test. A step-drawdown test was also performed at well G-2a after the constant-rate aquifer test described above (i.e., on March 4-5, 1998). These data were recorded at one-minute intervals and are contained on the data CD-ROM attached to this report. The procedure for the step-drawdown test was also previously described. Figure 8(a) shows a plot of the raw test data recorded for each step in the test. Each step lasted 100 min at a constant discharge rate (Q). The important data from each step consists of quasi-steady state drawdown (s) and discharge (Q); these data are summarized in Table 8. The analyses of these data are shown in Figure 8(b). Finally, Figure 8(c) shows a plot of drawdown in well G-2a versus discharge that is predicted from Equation (1) and using the head loss parameters shown in Figure 8(b). In addition, Figure 8(c) also shows a plot of the ratio of laminar head loss (i.e., BQ) to total head loss (i.e., $BQ+CQ^n$) versus discharge that is predicted from Equation (2).

(a) G-2a Step-drawdown test

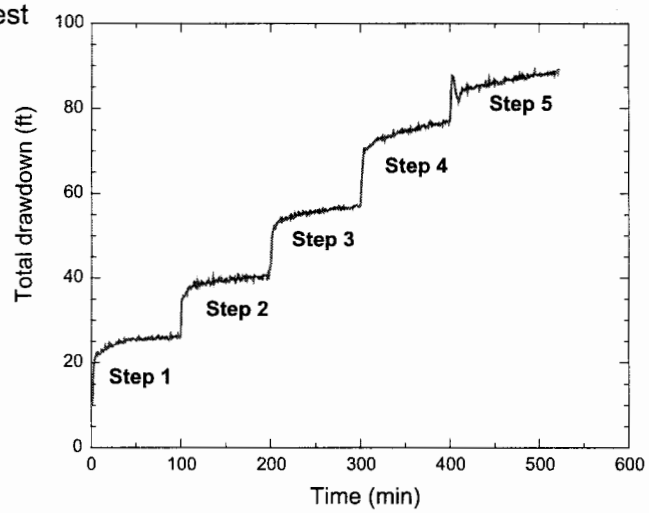

(b) Data analysis

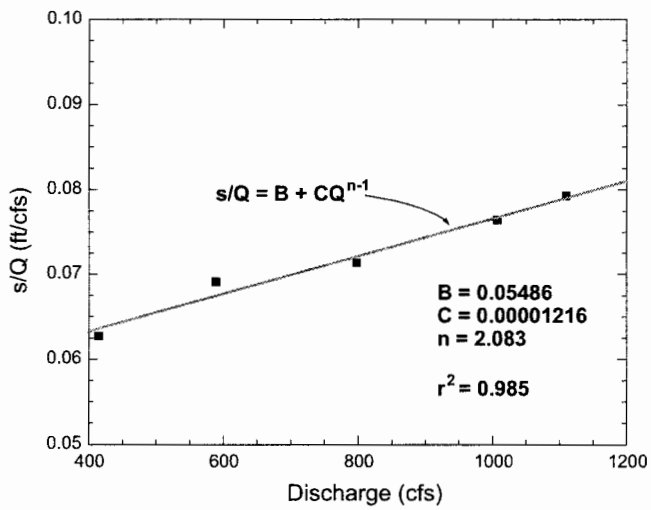

(c) Discharge vs total drawdown and laminar flow ratio

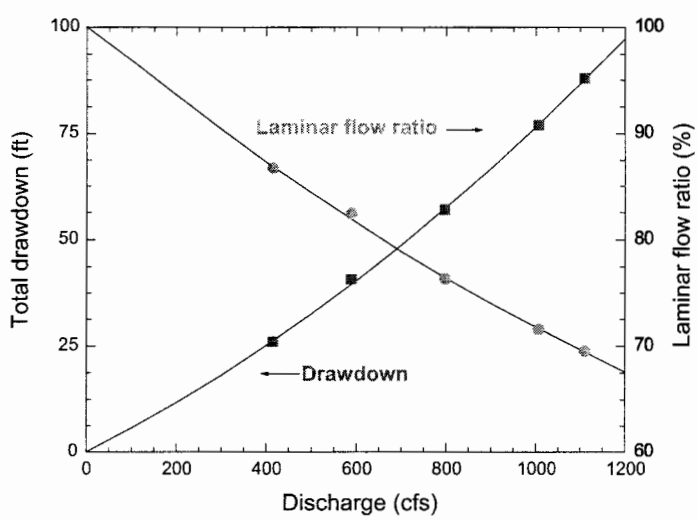

Figure 8. Step-drawdown test at G-2a

Results from the step-drawdown tests at all new replacement wells were used to derive optimal production rates that would minimize long-term energy costs associated with pumping these wells. These optimal rates are compared to routine production rates in Table 9.

Table 8
Step-Drawdown Data for the Test at Well G-2a

Step Number (j)	s_j (ft) at t_j = 100 min	Q_j (gpm)
1	26.03	415
2	40.70	589
3	56.93	798
4	76.96	1007
5	87.97	1110

Data obtained from Figure 8(a) for each step in the step-drawdown test.

Table 9
Recommended and Actual Production Rates in the Guaje Well Field

Well	Optimal Q (gpm)	Production Q (gpm)
G-1a	No step-test available	615
G-2a	~ 825	837
G-3a	~ 610	630
G-4a	~ 525	525
G-5a	~ 300	380

Discussion. The static water level obtained in well G-2a before the start of the 1998 aquifer test was not completely reestablished during the recovery period. This situation resulted for several reasons. First, an ideal aquifer test would have been longer (including a longer recovery period). Second, boundary influences caused additional drawdown compared to values predicted from a Theis analysis and longer recovery times are required. Alternately, we note that Q/s is smaller in the Guaje Canyon wells than similar values obtained for wells PM-2 and PM-4 (McLin, 2005a, 2006). Hence, the cone of depression caused by pumping in Guaje Canyon wells is deeper relative to Q but does not propagate radially outward as far. This deeper drawdown theoretically takes longer to recover than drawdown caused by pumping in the PM wells. In a practical sense, our aquifer test at well G-2a only lasted about 100-200 min before boundary effects began to dominate. So our estimates for T and S are from a very short test. In addition, the reported value for S is characteristic of a confined aquifer. Brief inspections of Figures 2-5 and the well completion diagram for G-2a shown in Appendix A (i.e., see Figures A-2) suggest that the aquifer is actually under stratified, water-table conditions. However, boundary effects were encountered before a theoretical transition from confined to leaky-confined and/or phreatic aquifer behavior occurred. In other words, we expect either leaky-confined or phreatic aquifer behavior to develop but this theoretical transition is apparently masked by barrier boundary effects. Alternately, one could argue that the aquifer responded like a confined aquifer and should be strictly viewed that way. We note that both arguments are reasonable and can not be resolved with the techniques used here.

In the confined aquifer analyses shown in Figures 6 and 7, wells G-2a and G-3 are considered to be fully penetrating. Hence, the tops of the respective well screens were used to define the top of the regional

aquifer and the spinner logs were used to define the bottom. These aquifer dimensions were shown in Table 3 and Figure 3. However, a phreatic analysis would be represented by a partially penetrating well because the well screen top is located about 200 ft below the static water level as seen in Figure 3. A Theis phreatic analysis was not performed because it is not strictly valid in this situation (i.e., the Jacob correction compensates for flow zone thinning effects that do not physically occur in the production zone). Alternative methods like Neuman (1974) or Moench (1997) are applicable but were not used because they yield similar results to those already shown. This raises an important question. Exactly how should we represent the regional aquifer (i.e., is it confined, phreatic, or somewhere in between these two conditions)? The results presented here imply that the aquifer is confined. However, the aquifer tests shown here are relatively short and may not have allowed for the transition from confined to leaky-confined or phreatic behavior. Furthermore, there is no single geologic unit that can be identified as a confining layer. Therefore, we prefer to characterize it as vertically stratified. This characterization is also supported by the spinner logs.

In addition to the slow static recovery problem, all of the Guaje Canyon wells contain alternating layers of high and low hydraulic conductivities that are sandwiched together into a single high-yielding zone. At well G-2a, these high-yielding units are located below the unsaturated Puye Fanglomerate and above the first significant Miocene basalt layer. This situation is analogous to that previously described by McLin (2005a, 2006) for the central portions of Pajarito Plateau near wells PM-2 and PM-4. However, the high-yielding units in Guaje Canyon contain finer grained materials and are thinner than on Pajarito Plateau. In addition, the basalt units are much older (WoldeGabriel et al., 2006). Finally, the barrier boundary effects observed in wells G-2a and G-3 are unique because they have never been observed before (probably because the old Guaje Canyon wells could not be used as observation wells due to transducer access limitations). These boundary effects may be related to aquifer thinning and normal faulting associated with the Rio Grande rift system. These effects are discussed in a separate section near the end of this report. Related information may also be found in WoldeGabriel et al. (2006) and Dethier (2003).

By now it is apparent that the regional aquifer below Guaje Canyon can be characterized as a high-yielding, heterogeneous zone that varies both laterally and vertically. Of course, this is not surprising. In addition, our conventional well analysis is idealized because it represents the real 3-D world as 2-D radial. According to the spinner logs presented earlier, the thickness of the high-yielding water-bearing unit varies between wells as seen in Figures 2 and 3. For example, b varies from a low of about 245 ft to a high of about 583 ft between wells G-4a and G-1a (see Table 3 and Figure 3). This causes T to change as individual cones of depression expand because b is thinning toward the west (also note that b appears to thicken slightly again between wells G-4a and G-5a). But even this representation is over-simplified because the actual units yielding water are much thinner than suggested by Figure 3. In fact, the individual, high-yielding units shown in Figures 4 and 5 suggest that each replacement well's vertical profile is highly variable. In addition, this variability extends horizontally between wells because each of these small, high-yielding zones can not be precisely correlated. In other words, we are representing b as a constant in each aquifer test analysis when we know it varies considerably from the values shown in Figure 3. This condition makes test analyses more difficult because there are no analytical methods that specifically apply to these complex test conditions. These conditions are further complicated because there are multiple barrier boundaries present and these boundary locations can not be precisely determined with only one observation well. In addition, long-term aquifer tests are often impractical because of water production requirements.

Another important point to recognize is that all of the analytical models used here assume horizontal (radial) flow toward the pumping well. Departures from this assumption may result because both b and K_h/K_v change in unpredictable ways. Characterization of some of this variability can be achieved by using

multiple techniques to analyze drawdown and recovery data in the pumping well. As reported in the earlier PM-2 aquifer test (McLin 2005a), uncertainty in T has also been associated with varying the anisotropy ratio. These earlier analyses suggest that T increases only about 7% as the K_h/K_v ratio increases from 1 to 1,000 in the Theis analysis. Hence, the influence of anisotropy was not explored here because uncertainty associated with the Theis curve matching method is probably larger that this amount. Ultimately, these analyses are only approximate because the aquifer test was relatively short before boundary effects appeared. Regardless, important new estimates for aquifer parameters were made and these results are significant. More importantly, however, these tests provide a reliable estimate for S that was previously unavailable.

Finally, we mention the theoretical duration of casing storage can be calculated from the following equation (Schafer 1979),

$$t_c = \frac{0.6\left(D^2 - d^2\right)}{Q/s} \tag{5}$$

where t_c is the duration of casing storage (min), D is the inside diameter of the well casing (15.375 in. here), d is the outside diameter of column pipe (8.625 in. for the G-2a production tubing and pump bowls), Q discharge rate (gpm), and s is drawdown at time t_c. The data from the G-2a aquifer test and Equation (5) produced a theoretical casing storage duration of less than 10 min. Hence, the pumping and recovery data should each describe a steep curve for about 10 min. This curve should gradually transition to the correct theoretical slope after these effects have dissipated. This formula usually produces a conservative t_c estimate. In many tests, the observed effects of casing storage can be as little as half the theoretical value because the asymptotic approach of the data to the theoretical drawdown curve has been largely achieved by then. The effects of casing storage dissipated quickly because the sampling interval was 10 min. Hence, these effects were not significant during the G-2a aquifer test.

Which analytical method gives the most representative hydraulic properties for the formation opposite the screen in G-2a? This is not an easy question to answer. Some would favor an analysis that emphasized the very early time data (i.e., < 50 min) and that tend to yield higher T values. If we look only at the 1998 test results, we favor those analyses that are based on all of the data not affected by boundary effects (i.e., < 100 min) and that are based on both production and observation well data. These analyses tend to yield somewhat lower T and S values as seen in Figure 7(b). However, the results from the 2005 test at G-2a are more representative as explained in the next section. Finally, the spinner log at G-2a provides the best available representation of aquifer thickness. Some might argue that a partially penetrating, phreatic aquifer analysis is appropriate with b = 638 ft; however, this procedure yields similar results to those already presented in Figure 6. All of these values are summarized in Table 10.

Table 10
Summary of Aquifer Parameters from 1998 Guaje Well Field Aquifer Tests

Well	Method	Figure	r (ft)	*T* (ft^2/day)	*b* (ft)	*K* (ft/day)	*S*	B[a]	C[a]	n[a]
G-2a	Theis pumping	6-a	—	2870	435	6.6	9.73E-04			
G-2a	Theis recovery	6-b	—	2870	435	6.6	9.07E-04			
G-2a	Theis residual recovery	6-c	—	2983	435	6.9	—			
G-2a	Specific capacity	—	—	2186	435	5.0	9.70E-04			
G-3	Theis pumping	7-a	311	4024	425	9.5	1.03E-03			
G-2a & G-3	Theis pumping	7-b	—	2855	435	6.6	9.19E-04			
G-2a	Step drawdown	8	—	—	—		—	5.486E-02	1.216E-05	2.083
G-3a	Theis pumping	12-a	—	2123	261	8.1	1.46E-05			
G-3a	Theis recovery	12-b	—	2000	261	7.7	1.69E-04			
G-3a	Theis residual recovery	12-c	—	1946	261	7.5	—			
G-3a	Specific capacity	—	—	1675	261	6.4	9.70E-04			
G-3	Theis pumping	13-a	2050	1647	261	6.3	7.73E-04			
G-3a & G-3	Theis pumping	13-b	—	1588	261	6.1	7.69E-04			
G-3a	Step drawdown	14	—	—	—		—	9.801E-02	3.031E-05	2.000
G-4a	Theis pumping	15-a	—	1676	245	6.8	5.11E-04			
G-4a	Theis recovery	15-b	—	1632	245	6.7	5.74E-04			
G-4a	Theis residual recovery	15-c	—	1604	245	6.5	—			
G-4a	Specific capacity	—	—	1478	245	6.0	9.70E-04			
G-4	Theis pumping	16-a	3610	1650	245	6.7	1.05E-04			
G-4a & G-4	Theis pumping	16-b	—	1847	245	7.5	1.06E-04			
G-4a	Step drawdown	17	—	—	—		—	9.265E-02	5.419E-05	2.000
G-5a	Theis pumping	18-a	—	717	325	2.2	2.55E-04			
G-5a	Theis recovery	18-b	—	717	325	2.2	3.15E-04			
G-5a	Theis residual recovery	18-c	—	565	325	1.7	—			
G-5a	Specific capacity	—	—	685	325	2.1	9.70E-04			
G-5a	Step drawdown	19	—	—	—		—	2.565E-01	1.673E-04	2.000

[a] See Equation (1) for step-drawdown test description.

Analyses of the 2005 Test at G-2a

Constant Rate Aquifer Test. A second aquifer test was conducted at well G-2a from January 28-February 3, 2005, using a similar test procedure to that previously described. The initial non-pumping recovery period was about 80 days from November 10, 2004 to January 28, 2005, and included no pumping from wells G-1a, G-2a, G-3a, and G-4a. Then well G-2a was pumped for three days at a constant discharge rate of 837 gpm. This pumping interval was immediately followed by three days of recovery from January 31-February 3, 2005. Water levels were automatically recorded in wells G-1a, G-2a, G-3, G-3a, and G-4a. Drawdown and recovery data were obtained at G-2a, G-3, and G-3a; however, no analyzable drawdown values were observed at wells G-1a or G-4a during this test. The usable data can be evaluated for aquifer transmitting properties as seen in Figure 9 using the aquifer configuration shown in Figure 3 and aquifer dimensions shown in Table 3. Theis analysis of G-2a drawdown is shown in Figure 9(a), while Theis analysis of the G-2a residual recovery is shown in Figure 9(b). Figure 9(c) shows a Theis analysis of the G-3 drawdown data, while Figure 9(d) shows a Theis analysis of the G-3a drawdown data. Finally, according to the T values shown in Figure 9 with $b = 435$ ft, we conclude that K averages about 8.3 ft/day. These results suggest that the 2005 aquifer test at well G-2a produced larger K values compared to those previously obtained in the 1998 test; these previous results were shown in Figures 6 and 7. More will be said about this in the discussion.

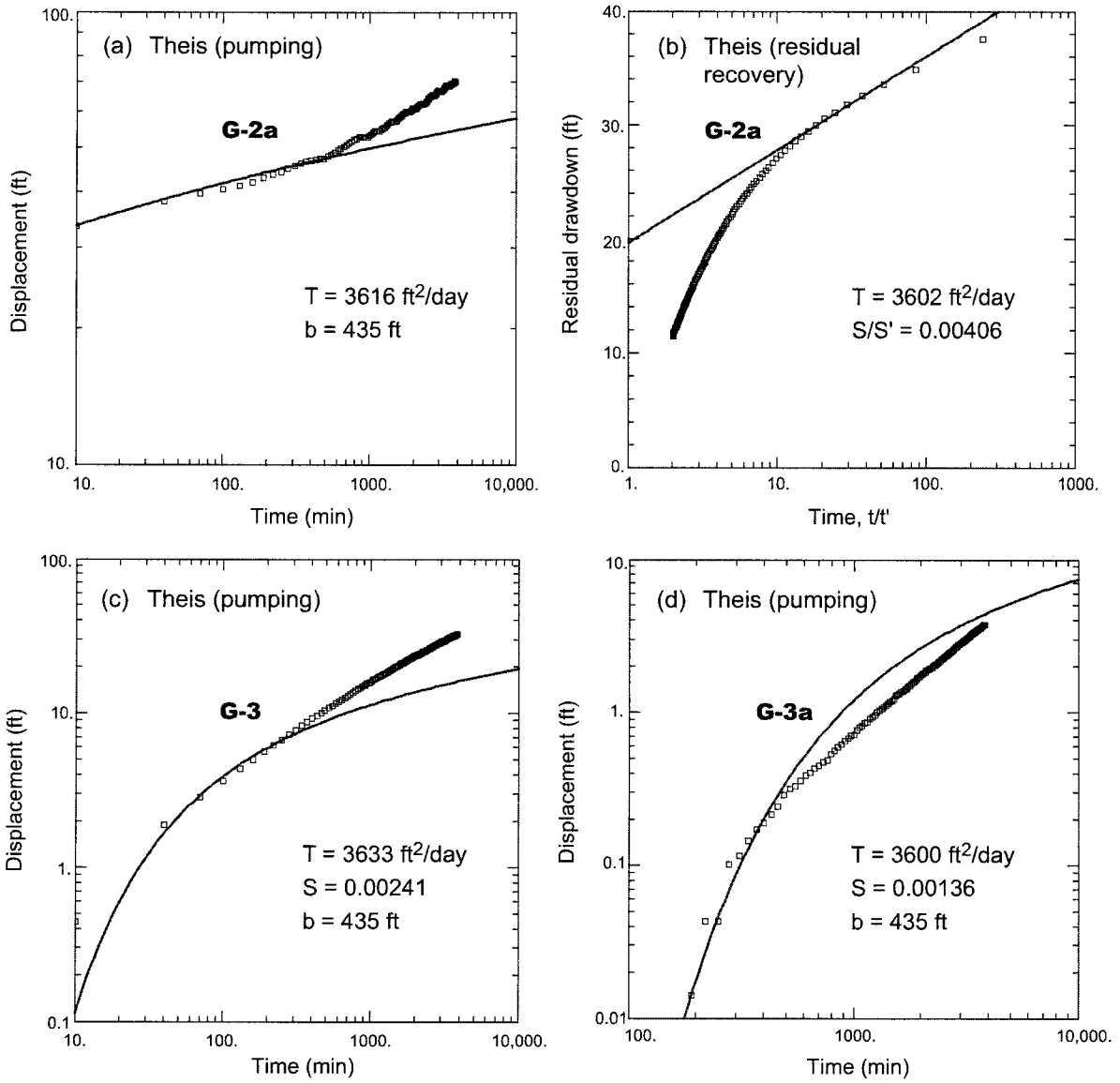

Figure 9. Theis confined aquifer analyses using the 2005 G-2a data from (a) drawdown and (b) residual recovery. Theis confined aquifer analyses using drawdown data from (c) well G-3 and (d) well G-3a. Note that the anisotropy ratio is 1.

The 2005 data from the G-2a test are also analyzed in Figure 10 by simultaneously using combinations of data from multiple observation wells. Hence, Figure 10(a) shows a distance-drawdown analysis using data from all three wells, while Figure 10(b) shows a combined Theis analysis for drawdown data from wells G-2a and G-3. Figure 10(c) shows a combined Theis analysis for drawdown data from wells G-3 and G-3a, while Figure 10(d) shows a combined Theis analysis for all three wells. According to the T values shown in Figure 10 with $b = 435$ ft, we conclude that K varies between 8.4–9.2 ft/day, and averages about 8.9 ft/day. Results from the 2005 test at G-2a, G-3, and G-3a are also summarized in Table 11.

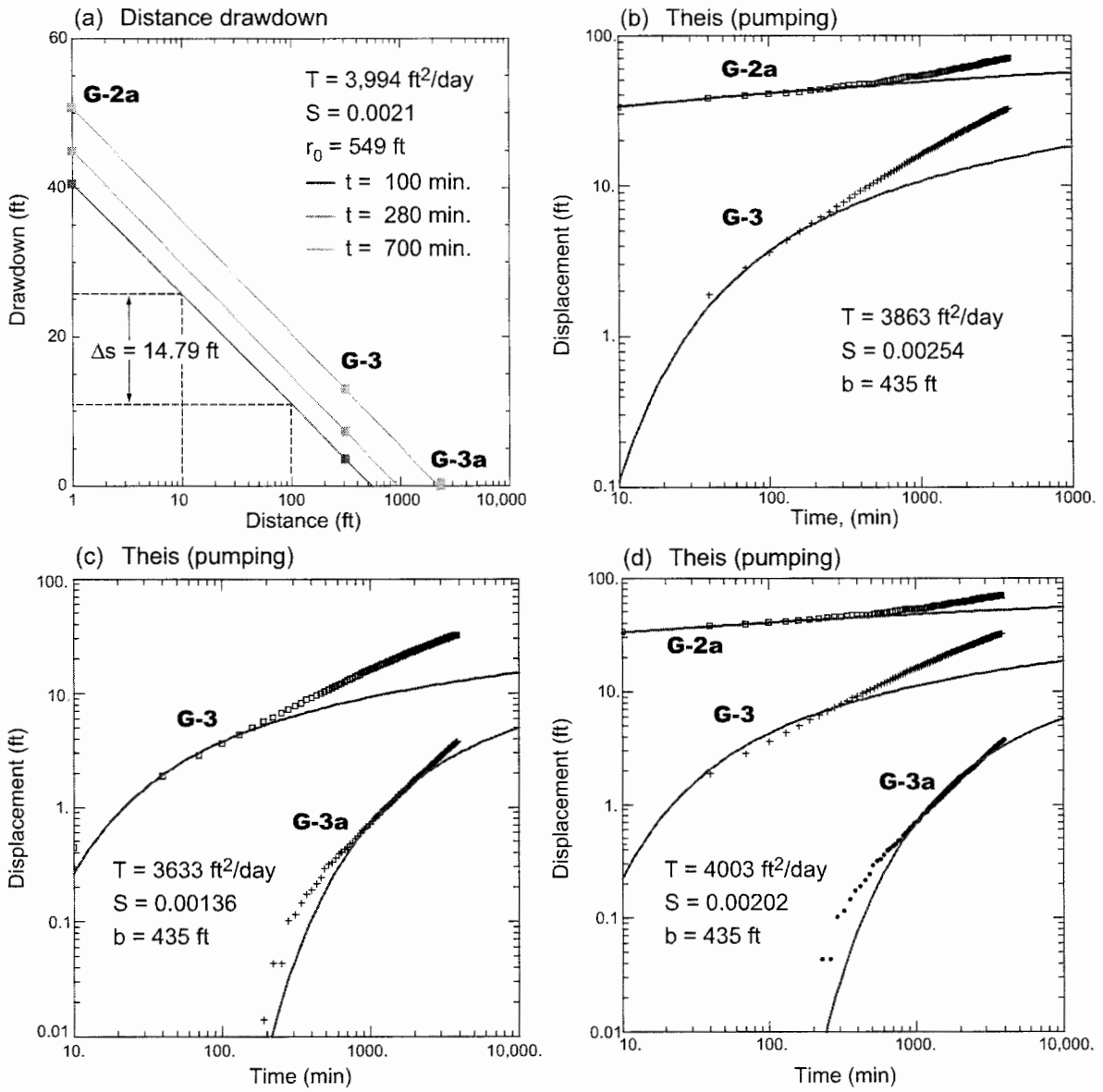

Figure 10. **Multiple well results using 2005 drawdown data for (a) distance-drawdown analysis, (b) G-2a and G-3 combined Theis analysis, (c) G-3 and G-3a combined Theis analysis, and (d) G-2a, G-3, and G-3a combined Theis analysis. Note that the anisotropy ratio is 1.**

Table 10
Summary of Aquifer Parameters from 1998 Guaje Well Field Aquifer Tests

Well	Method	Figure	r (ft)	*T* (ft^2/day)	*b* (ft)	*K* (ft/day)	*S*
G-2a	Theis pumping	9-a	1	3616	435	8.3	4.37E-03
G-2a	Theis residual recovery	9-b	1	3602	435	8.3	—
G-3	Theis pumping	9-c	311	3633	435	8.4	2.41E-03
G-3a	Theis pumping	9-d	2359	3600	435	8.3	1.36E-03
G-2a	Specific capacity	—	—	2186	435	5.0	9.70E-04
G-2a, G-3, & G-3a	Distance-drawdown	10-a	1, 311, & 2359	3994	435	9.2	2.10E-03
G-2a & G-3	Theis pumping	10-b	1 & 311	3863	435	8.9	2.54E-03
G-3 & G-3a	Theis pumping	10-c	311 & 2359	3633	435	8.4	1.36E-03
G-2a, G-3, & G-3a	Theis pumping	10-d	1, 311, & 2359	4003	435	9.2	2.02E-03

Boundary Effects. It is also apparent in Figures 9 and 10 that barrier boundary effects were present in the 2005 aquifer test at well G-2a. These effects are addressed in a separate section near the end of this report.

Discussion. Results from the 2005 aquifer test yield higher T and S values compared to those previously obtained in 1998. For example, Figures 9 and 10 show an average T of 3,743 ft^2/day whereas Figures 6 and 7 yield an average T of 3,120 ft^2/day. There are also other similarities and differences between the 1998 and 2005 tests as seen in Figure 11. These data suggest that both tests produced similar drawdown curves at wells G-2a and G-3 as seen in Figures 11(a) and 11(b), respectively. Here we see a remarkable similarity in the linear boundary effect in both wells. But a closer examination of these data suggests some important differences too. For example, Figure 11(c) suggests that specific capacity (Q/s) changed between each successive test. Hence, Q/s values from the 1998 data appear to decline (i.e., from about 14.5 to 13.5 at 901 gpm) between the constant rate test (conducted first) and the step-drawdown test (conducted second). Furthermore, Q/s increased in the 2005 test to about 21 after 100 min of pumping. On first thought, it appears that the well has continued to develop while it was in routine service between 1998 and 2005. This change seems large and some would argue that it can not be explained by continued well development alone. In addition, note that the ratio in respective constant rate discharges is about 1.08 (i.e., 901/837). According to the Theis model used in the parameter analysis, the respective drawdown values should also have this same ratio but they do not. For example, at t = 100 min, we see that the drawdown ratio is about 1.55 in well G-2a (i.e., 62.95/40.51) and about 1.81 in well G-3 (i.e., 6.61/3.65). Likewise, the ratio of average T values is 1.20 (i.e., 3743/3120) using T values from Figures 9 and 10 versus Figures 6 and 7. This is significant because we expect the T values to be similar but they are not.

These data suggest that an error may have occurred while measuring the respective discharges or drawdown values in either the 1998 or 2005 tests. All of the 1998 discharge measurements were made using an 8-in by 6-in orifice plate and manometer arrangement (see Shomaker, 1999). The 2005 constant rate discharge measurements were made with a flow meter and stop watch. The 2005 discharge data were independently verified by a discharge value obtained from the G-2a pump rating curve (i.e., using the total head difference between the water level in the well and in the storage tank receiving the G-2a discharge). Both the 1998 and 2005 data sets fluctuated less than 3% about their respective mean flow rates. Both sets of drawdown data were made from recording transducers with calibration errors of about 0.03 ft between measurements. We were unable to discover any obvious anomalies regarding measurement of pumping rate and drawdown and we are at a loss to explain the G-3 response differences shown in Figure 11(b).

The data summarized in Table 12 show that Q/s has changed in all wells over time. These data compare discharges and drawdown values recorded at similar times in the same well and further demonstrate how Q/s values have changed. According to Table 12, Q/s values have increased in both G-2a and G-3a but they have decreased in wells G-4a and G-5s. This behavior is common in newly developed wells with about half showing a Q/s improvement, and half showing a decline. The individual Q/s change is largest in well G-2a and is smaller in all of the remaining wells. These results also imply that the aquifer parameters estimated from the 1998 test at G-2a are underestimated (e.g., compare T values from the 1998 test to those from 2005 test as described above). Alternatively, we could make the same point by comparing Figures 6 and 7(a). Figure 6 shows a T value of about 2900 ft^2/day for G-2a, while it is over 4000 ft^2/day at well G-3 according to Figure 7(a). This difference resulted because of incomplete well development at G-2a shortly before the 1998 aquifer test. Aquifer parameters from the 2005 test were shown in Figures 9 and 10 and compare favorably to the Figure 7(a) value. Hence, the 2005 T values are more representative than the 1998 values for well G-2a. Table 12 also implies that similar estimates from the G-3a test may also be underestimated but by a smaller amount than the G-2a test values because the Q/s changes are smaller. Using the same argument, Table 12 also suggests that aquifer parameters from wells G-4a and G-5a are somewhat overestimated but that these differences are also smaller than the G-2a differences.

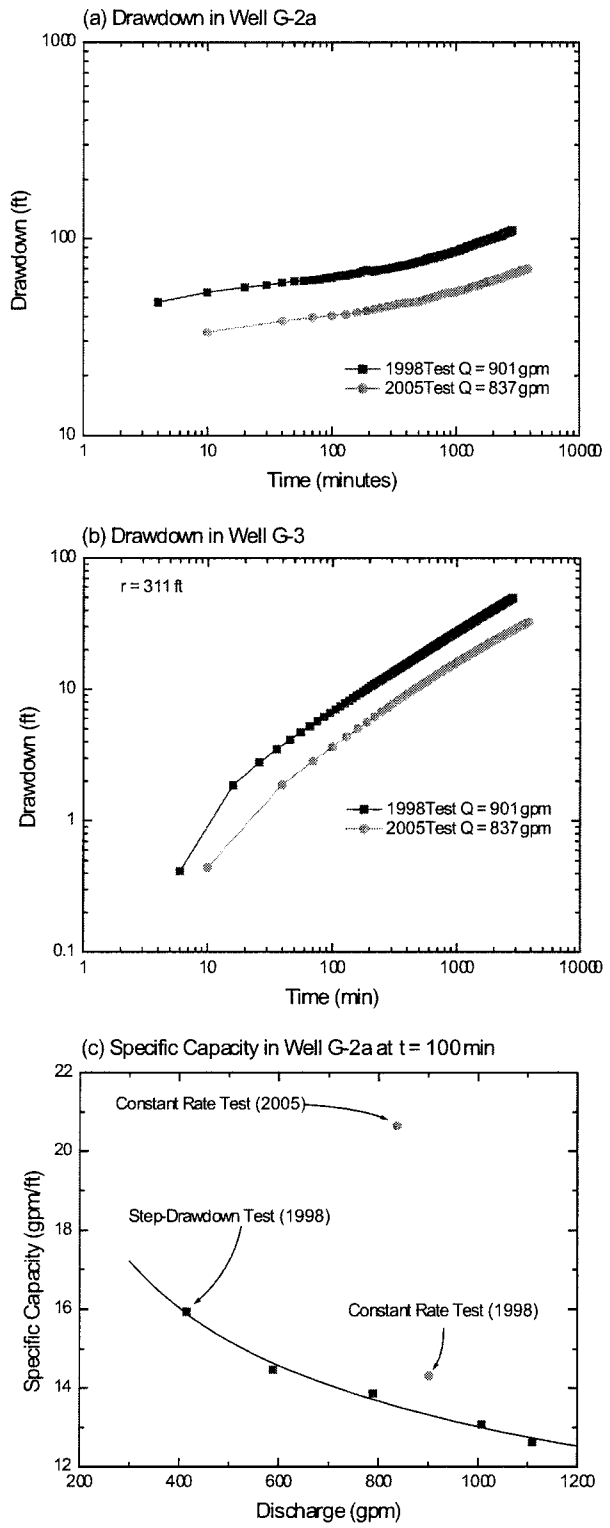

Figure 11. **Drawdown responses to a constant G-2a pumping rate at (a) well G-2a; and (b) well G-3. (c) Apparent changes in specific capacity at well G-2a over time. See text for discussion.**

Table 12
Summary of Specific Capacity Changes Over Time in Various Wells

Well	Date	*Q* (gpm)	s (ft)	t[a] (min)	*Q/s* (gpm/ft)	Change[b] in *Q/s* (gpm/ft)	Remarks
G-2a	02/28/98	901	68.26	186	13.2		*Q/s* has substantially increased for comparable times between 1998 to 2005
	02/29/98	901	94.11	1446	9.6		
	01/28/05	837	42.76	190	19.6	6.4	
	01/29/05	837	57.47	1450	14.6	5.0	
G-3a	05/28/98	800	114.89	905	7.0		*Q/s* has increased somewhat from 1998 to 2005
	05/29/98	800	118.02	1445	6.8		
	09/07/05	630	70.86	900	8.9	1.9	
G-4a	04/08/98	780	114.23	600	6.8		*Q/s* has decreased somewhat from 1998 to 2005
	04/09/98	780	123.79	1440	6.3		
	02/03/05	525	99.06	600	5.3	-1.5	
G-5a	07/21/98	408	131.10	405	3.1		*Q/s* has decreased slightly from 1998 to 2005
	07/22/98	408	147.52	1445	2.8		
	05/28/04	380	143.61	420	2.6	-0.5	

[a] Time in min after pumping starts and when drawdown (s) is recorded.
[b] Change in *Q/s* values computed at similar t values (e.g., 19.6 - 13.2 = 6.4).

Figure 12 shows additional water level records that were recorded by the Los Alamos County Department of Public Utilities during 2004–2005. These data show numerous pumping and non-pumping water production cycles in well G-2a over a two year period. Individual cycles typically show a water level change of 45–50 ft over a 4–6 hr pumping interval as seen in Figure 12(a). However, a strong seasonal pattern is also apparent. For example, during the winter months (e.g., between 25-125 days), non-pumping water levels are about 150–160 ft above the pump bowls. However, during the spring and early summer months (e.g., between 150–250 days), the non-pumping levels are only about 90 ft above the bowls. These observations are significant for several reasons. First, the change in water levels during a given pumping to non-pumping cycle is about the same over both winter and summer seasons. Second, after about 80 days of continuous recovery (i.e., between 325–400 days), the G-2a aquifer test started (i.e., after about 400 days). The change in water levels during this test was about 70 ft. These data demonstrate that water level changes are directly related to the duration of the recovery period immediately preceding a test. Similar differences in recovery in other Guaje wells are not as dramatic as at well G-2a.

Figure 12(b) shows the 80 day recovery period that preceded the G-2a aquifer test in greater detail. Obviously, water levels recorded in well G-2a responded the most with about 113 ft of recovery. This was followed by about 70 ft of drawdown after 3 days of continuous pumping. Likewise, well G-3a showed almost 48 ft of recovery and < 4 ft of drawdown in the same period. Finally, well G-4a showed almost 46 ft of recovery and < 1 ft of drawdown. These effects can not usually be observed during routine production use because of incomplete recovery between pumping cycles as seen in Figure 12(a), or from simultaneous pumping at multiple wells. The data from G-2a and G-3a were presented in Figures 9 and 10. However, the data from G-4a were not analyzed because drawdown effects were small. These observations are significant, however, because they suggest a continuation of the poor hydraulic connection between wells G-2a and G-3a. They also support the argument that the boundary effects

already noted in these wells are probably associated with aquifer thinning rather than a buried fault between wells G-2a and G-4a. Alternately, one could argue that both a leaky barrier boundary and aquifer thinning are present. More importantly, they demonstrate that aquifer responses depend on both the duration of the recovery period preceding a aquifer test and the length of pumping during the test.

The observations in Figure 12 also imply that any future tests in the Guaje well field should be preceded by a long non-pumping recovery period of about 75-90 days. Many hydrologists recommend that an initial recovery period should only be about 3-5 times longer than the planned pumping time. According to this view, a 3-day aquifer test should be preceded by about 9-15 days of recovery. Clearly that recommendation would not allow for sufficient recovery in the Guaje wells. Finally, we note that many of the previous comments that were made for the 1998 test at well G-2a also apply here and are not repeated. Perhaps the most significant observation from both the 1998 and 2005 G-2a tests was the identification of multiple barrier boundaries. The first barrier boundary appears to be associated with aquifer thinning west of well G-2a, while the second barrier boundary is probably associated with a buried fault located about 1,200 ft east of G-2a. The location of this buried fault corresponds to an extension of a surface mapped feature shown in Dethier (2003). Two additional buried faults may also be located in the subsurface between wells G-3 and G-3a, and between wells G-4a and G-5a. These boundary effects are discussed in a separate section near the end of this report.

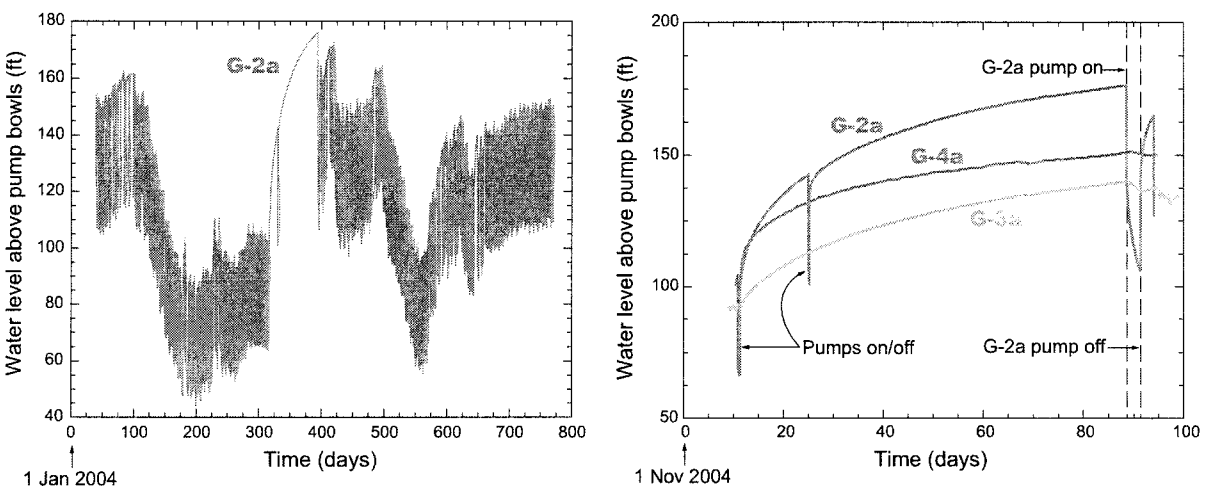

Figure 12. (a) Well G-2a pumping responses during 2004 and 2005. (b) Static recovery in wells G-2a, G-3a, and G-4a preceding the 2005 aquifer test in G-2a. See text for discussion.

IV. ANALYSES OF G-3A TEST DATA

Constant Rate Aquifer Test. A two-day aquifer test was conducted at well G-3a from April 28-30, 1998, at a constant discharge rate of 800 gpm. This test was immediately followed by a two-day recovery period from April 30-May 2, 1998. Drawdown and recovery data were automatically recorded in wells G-3a and G-3 during the aquifer test. Observation well G-3 is located about 2,050 ft east of G-3a (see Figure 1 and Table A-1 in Appendix A). Analyses of the G-3a data are shown in Figure 13 using the aquifer configuration shown in Figure 3 and aquifer dimensions shown in Table 3. Theis analysis of drawdown is

shown in Figure 13(a), while Theis analysis of recovery is shown in Figure 13(b). Figure 13(c) shows an analysis using the Theis residual-recovery method. All of the *T* values are larger than the specific capacity value for *T* that was reported in Table 7 for this well. Again, these comparisons demonstrate parameter variability generated in the curve-matching process using alternate methods. Note that in each of these analyses, barrier boundary effects are apparent. As previously noted for well G-2a, it is not obvious if aquifer conditions are actually confined or controlled by a highly stratified, water-table aquifer (see Figure A-4 in Appendix A). However, we have not included a phreatic aquifer analysis as previously explained. Furthermore, the analysis shown in Figure 14 suggests that the aquifer between wells G-3a and G-3 responds like a confined aquifer according to the value obtained for *S*. Finally, according to the *T* values shown in Figure 13 and $b = 261$ ft, we conclude that *K* varies between 7.5-8.1 ft/day, and averages about 7.8 ft/day.

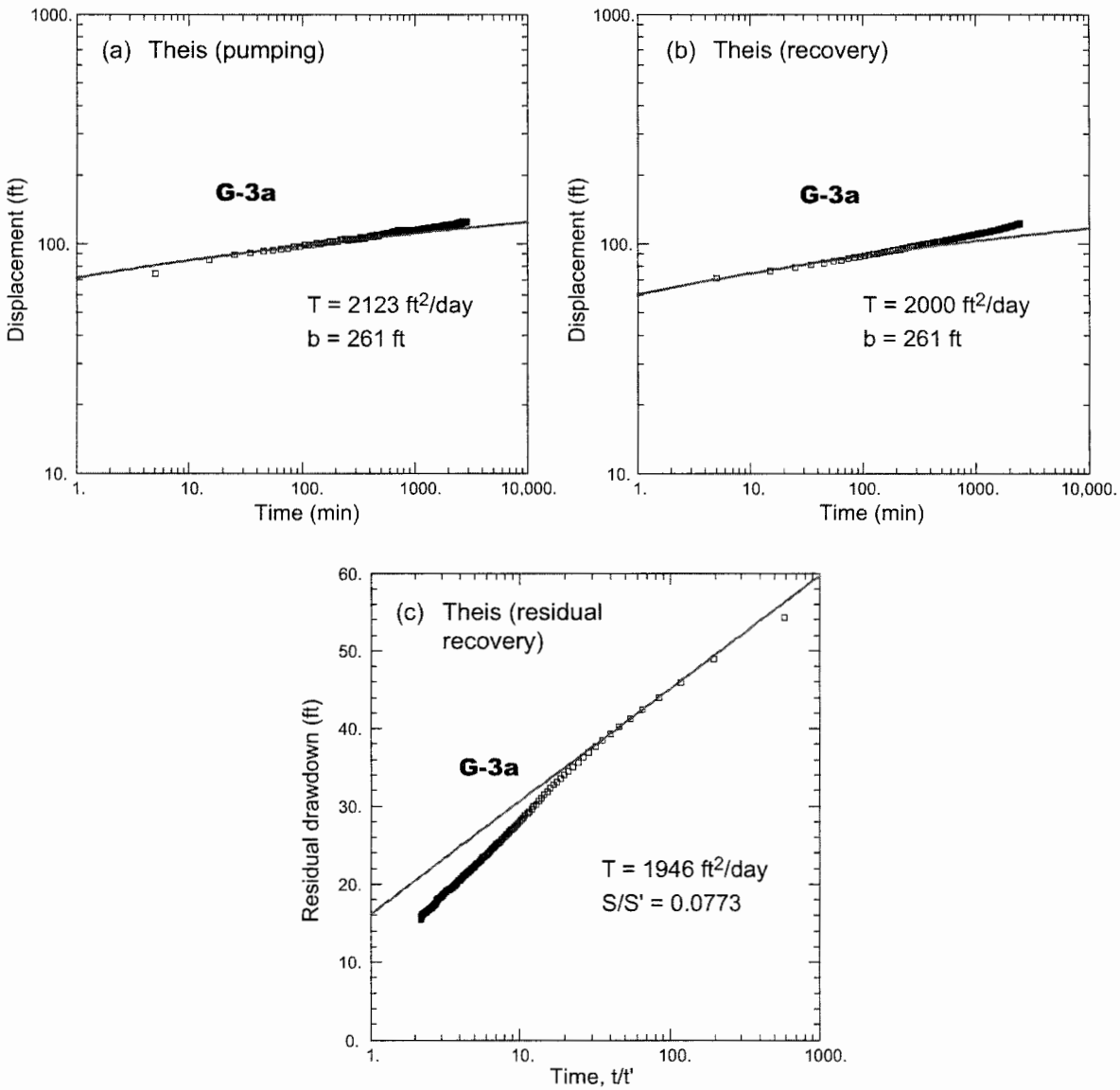

Figure 13. Theis confined aquifer analysis using the 1998 G-3a data from (a) drawdown, (b) recovery, and (c) residual recovery. Note that the anisotropy ratio is 1.

Similarly, analyses of the drawdown data from observation well G-3 data are shown in Figure 14(a), while drawdown data from wells G-3a and G-3 are simultaneously analyzed in Figure 14(b). These results are supported by the lower-bounding value for *T* presented in Table 7. In addition, these analyses suggest that *K* averages about 6.2 ft/day between wells G-3a and G-3. The real value of this test is that it provides an estimate for *S* that suggests the aquifer is confined. This parameter estimate is based on the first 350 min of drawdown data as seen in Figure 14(a) so this estimate is from a relatively short test. Recall that the data shown in Figures 2-5 suggest a highly stratified, water-table aquifer.

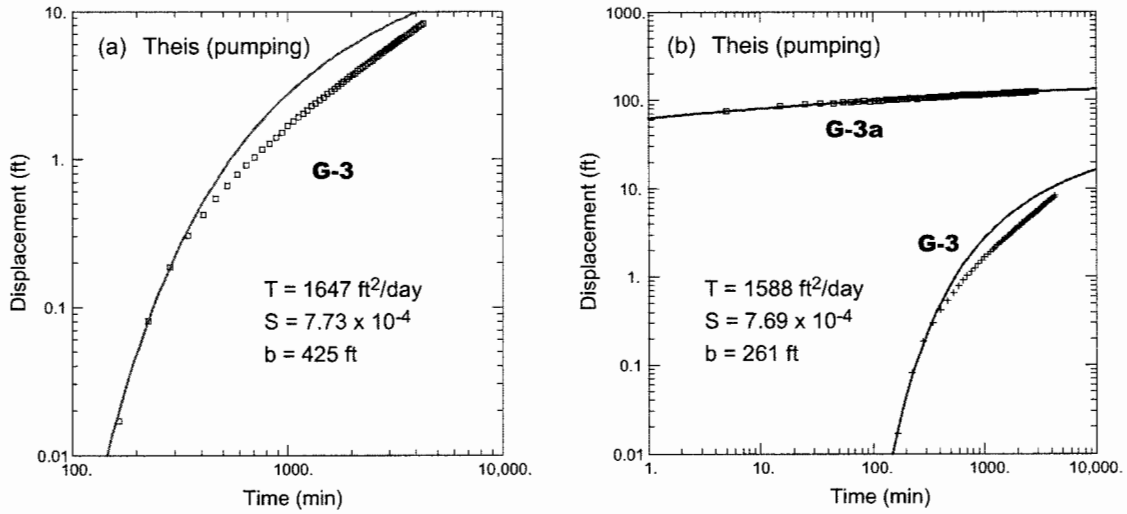

Figure 14. Theis confined aquifer analysis using the 1998 drawdown data from (a) G-3, and (b) both G-3 and G-3a simultaneously. A no-flow boundary is clearly apparent in G-3.

As before, the results shown in Table 7 and Figures 13 and 14 suggest that there are some differences between the specific capacity and Theis methods of analyses. Hence, by using the specific capacity *T* value as a lower bound, we were able to constrain the first appearances of barrier boundary departures from the Theis type-curve matches seen in Figures 13 and 14. These effects first appear after about 200 min and correspond to $t/t' = 15$ in Figure 13(c). Although there seems to be a bias toward overestimated *T* values relative to those estimated from specific capacity, these differences are not excessive and are required to maintain consistent boundary departure times in each analysis. The Theis analyses seen in Figure 13 actually yield reasonably good curve matches before barrier boundary effects first appear.

Boundary Effects. It is apparent that barrier boundary influences were present in the G-3a aquifer test. These influences are discussed in a separate section near the end of this report.

Step-Drawdown Test. On May 2–3, 1998, a step-drawdown test was also performed at well G-3a after the constant-rate aquifer test described above. These data were recorded at one-minute intervals and are contained on the data CD-ROM attached to this report. The procedure for the step-drawdown test was also previously described. Figure 15(a) shows a plot of the raw test data recorded for each step in the test. Each step lasted 100 min at a constant discharge rate (Q). The important data from each step consists of drawdown (s_j) and discharge (Q); these data are summarized in Table 13. The analyses of these data are shown in Figure 15(b). Finally, Figure 15(c) shows a plot of drawdown in well G-3a versus discharge predicted from Equation (1) and using the head loss parameters shown in Figure 15(b). In addition, Figure 15(c) also shows a plot of the ratio of laminar head loss to total head loss versus discharge that is predicted from Equation (2).

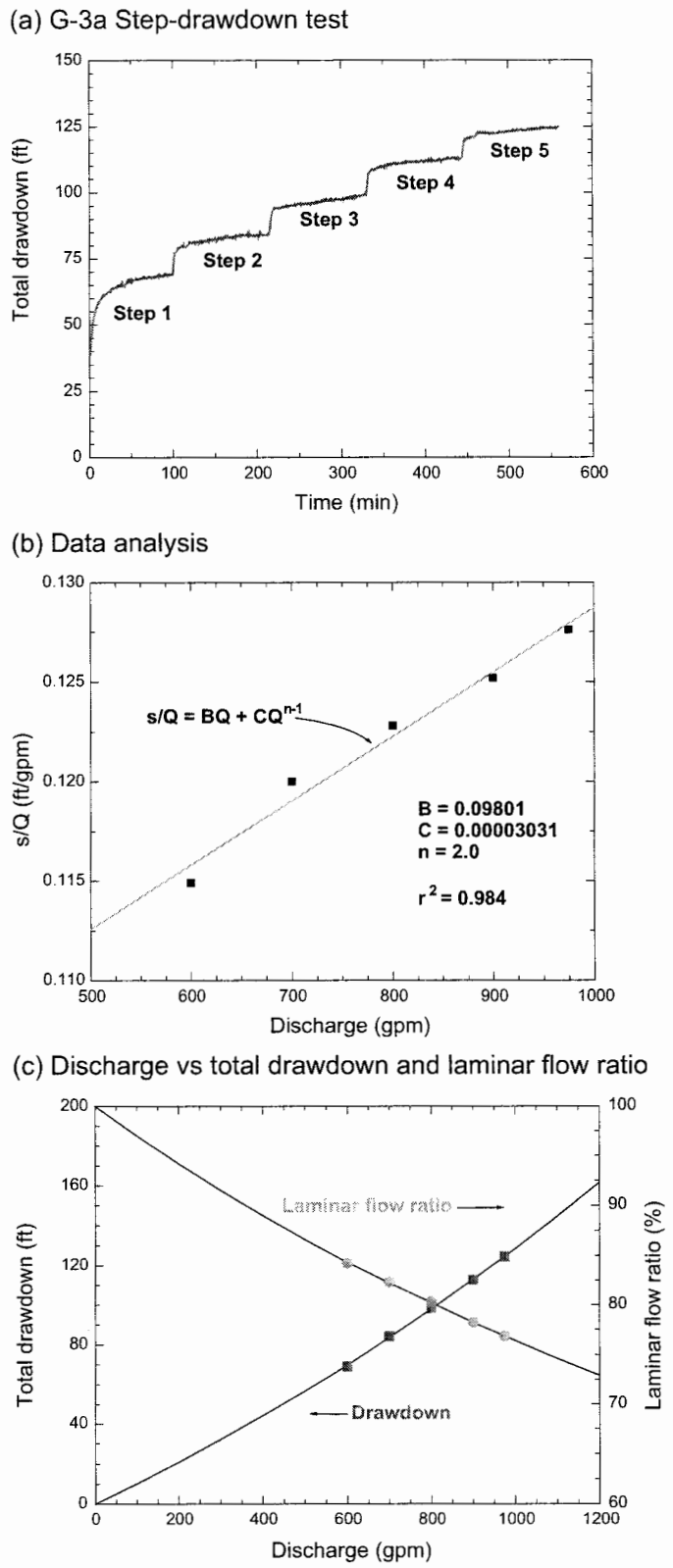

Figure 15. Step-Drawdown Test at G-3a

Table 13
Step-Drawdown *Data for the Test at Well G-3a

Step Number (j)	s_j (ft) at t_j = 100 min	Q_j (gpm)
1	68.96	600
2	84.00	700
3	98.23	800
4	112.66	900
5	124.38	975

*Data obtained from Figure 15(a) for each step in the step-drawdown test.

Discussion. Most of the discussion points presented earlier for G-2a also apply here but are not repeated. In addition, barrier boundary effects were also observed in well G-3 during the G-3a aquifer test. These effects appear after about 200 min in all wells. In addition, there is a noticeable decline in T values between tests at G-2a and G-3a. This decline is probably due to aquifer thinning to the west. Furthermore, there is poor hydraulic communication between G-2a and G-3a because observed drawdown values in G-3a are smaller than predicted by Theis. This poor communication is further proof that either aquifer thinning or a barrier discontinuity exists between these wells. We think these boundary effects result from aquifer thinning because pumping influences extend from wells G-2a to G-4a according to Figure 12(b). However, other contributing factors might include thin discontinuous, high-yielding zones between these wells or the presence of a fault that only partially off-sets these same units. Another very interesting comparison can be made between Figures 7(a) and 14(a). This comparison suggests that water levels in well G-3 respond differently to pumping influences at G-2a and G-3a even though similar boundary effects are encountered. These effects are discussed in a separate section near the end of this report.

As previously noted, variations in the K_h/K_v ratio were not explored in this test. The reasons for these variations were previously noted for well G-2a and are not repeated here. In addition, the effects of casing storage dissipated in less than 10 min. Hence, these effects were not significant because the sampling interval was 10 min and the pumping duration was more than 2 days. Furthermore, since well G-3 was used as an observation well, no casing storage effects were computed because these effects are equal to or less than similar effects in the pumping well.

V. ANALYSES OF G-4A TEST DATA

Constant Rate Aquifer Test. A two-day aquifer test was conducted at well G-4a from April 8-10, 1998, at a constant discharge rate of 780 gpm. This test was immediately followed by a two-day recovery period from April 10-11, 1998. Drawdown and recovery data were automatically recorded in wells G-4a and G-4 during the aquifer test. Observation well G-4 is located about 1,743 ft east of G-4a (see Figure 1 and Table A-1 in Appendix A). Analyses of the G-4a data are shown in Figure 16 using the aquifer configuration shown in Figure 3 and aquifer dimensions shown in Table 3. Theis analysis of drawdown is shown in Figure 16(a), while Theis analysis of recovery is shown in Figure 16(b). Figure 16(c) shows an analysis using the Theis residual-recovery method. All of these T values compare favorably with that obtained from the specific capacity technique reported in Table 7 for this well. Again, these comparisons demonstrate parameter variability generated in the curve-matching process using alternate methods. Note that in each of these analyses, a barrier boundary effect is apparent after about 100 min. Furthermore, the analyses in Figure 17 suggest that the aquifer between wells G-4a and G-4 responds like a confined aquifer according to the value obtained for S. Finally, according to the T values shown in Figure 16 and b = 245 ft, we conclude that K averages about 6.7 ft/day.

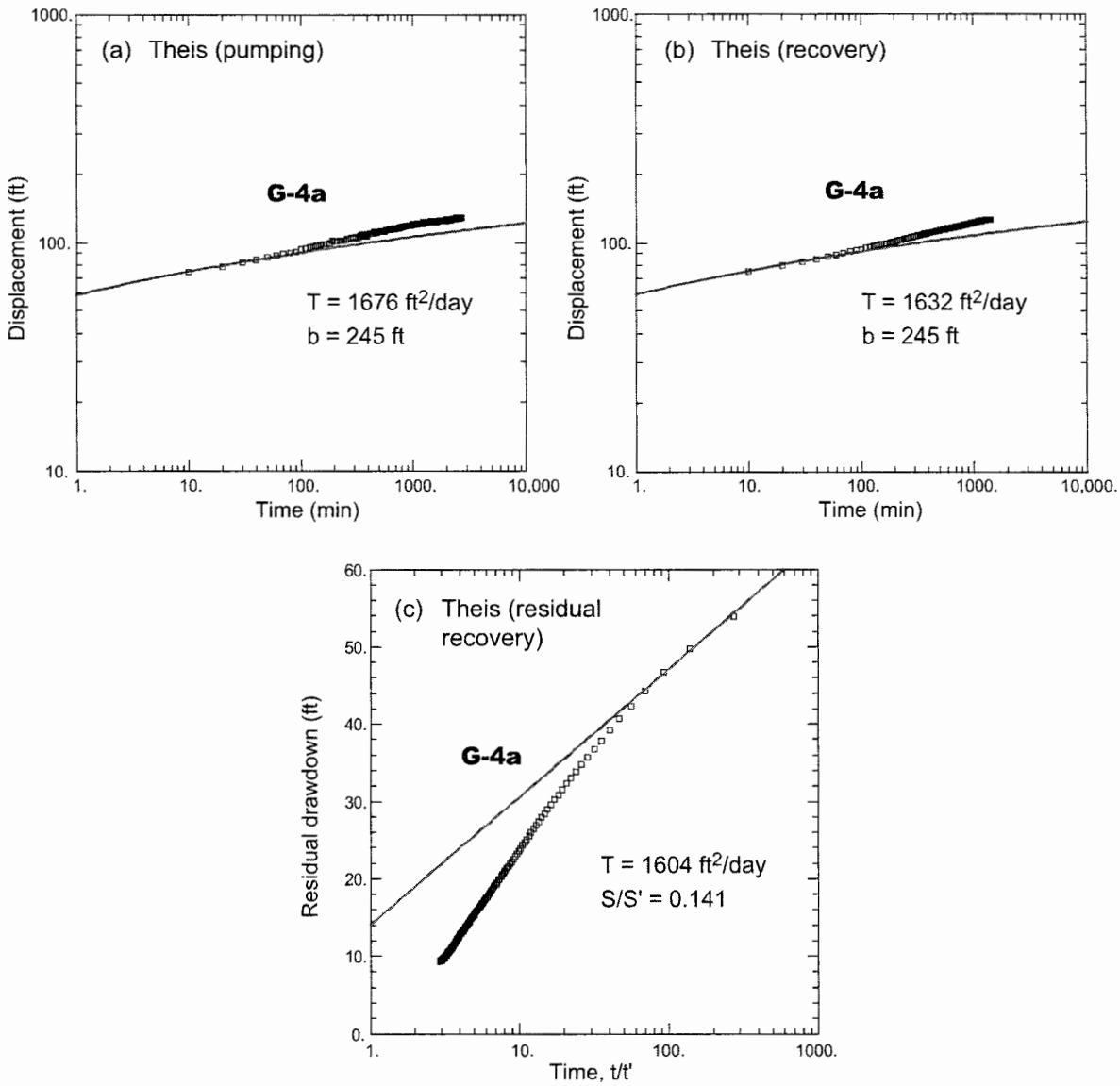

Figure 16. **Theis confined aquifer analysis using G-4a data from (a) drawdown, (b) recovery, and (c) residual recovery. A barrier boundary effect is apparent after about 200 min.**

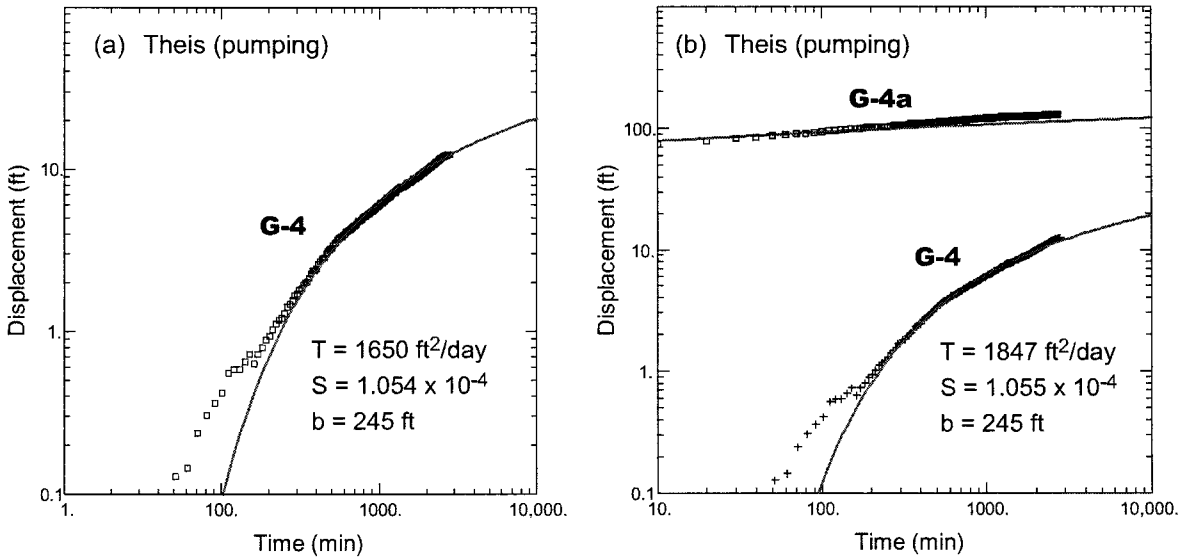

Figure 17. Theis confined aquifer analysis using drawdown data from (a) G-4, and (b) both G-4 and G-4a simultaneously. A boundary influence is apparent in both wells G-4 and G-4a.

Figure 17(a) shows the Theis analysis of drawdown at well G-4 in response to pumping at G-4a, while Figure 17(b) shows a similar analysis for both G-4 and G-4a simultaneously. Hence, using the T values shown in Figure 17 with $b = 245$ ft, we conclude that K averages about 7.1 ft/day. It is also obvious that barrier boundary effects are present in well G-4a but not in well G-4. Hence, these effects appear after about 400 min in well G-4a according to Figure 17(b). However, they are not evident in G-4 according to Figure 17(a). If the aquifer were homogeneous, we would expect boundary effects to appear at similar times in these respective analyses.

In the first analysis, no barrier boundary effects are obvious in G-4. However, Figure 17(b) suggests that a small barrier boundary effect is present in well G-4a so it is consistent with the analyses shown in Figure 16. Obviously, this boundary effect is smaller than that previously reported in wells G-2a or G-3a. This effect also continues the trend toward a declining barrier boundary influence as we move toward the west. This declining influence also coincides with westward aquifer thinning that was noted previously. Again, both of these observations are consistent with declining T values associated with this thinning.

Boundary Effects. As mentioned above, it is apparent that barrier boundary effects are present in well G-4a but not G-4. These effects are addressed in a separate section near the end of this report.

Step-Drawdown Test. A step-drawdown test was also performed at well G-4a after the constant-rate aquifer test described above (i.e. on April 11, 1998). These data were recorded at one-minute intervals and are contained on the data CD-ROM attached to this report. The procedure for the step-drawdown test was also previously described. Figure 18(a) shows a plot of the raw test data recorded for each step in the test. Each step lasted 100 min at a constant discharge rate (Q). The important data from each step consists of drawdown (s_j) and discharge (Q); these data are summarized in Table 14. The analyses of these data are shown in Figure 18(b). Finally, Figure 18(c) shows a plot of drawdown in well G-4a versus discharge predicted from Equation (1) and using the head loss parameters shown in Figure 18(b). In addition, Figure 18(c) also shows a plot of the ratio of laminar head loss to total head loss versus discharge that is predicted from Equation (2).

(a) G-4a Step-drawdown test

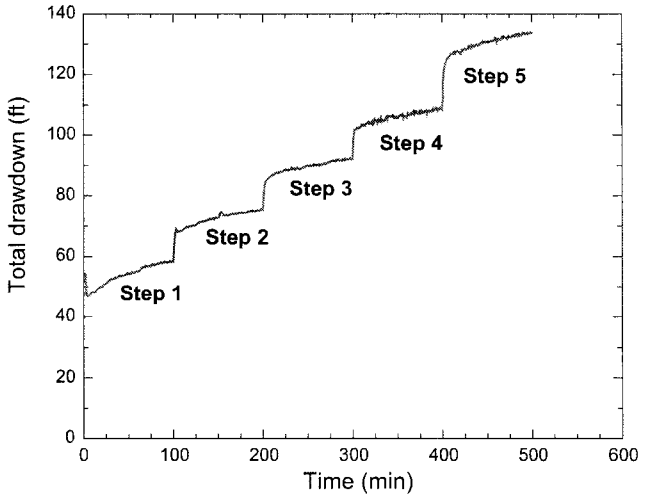

(b) Data analysis

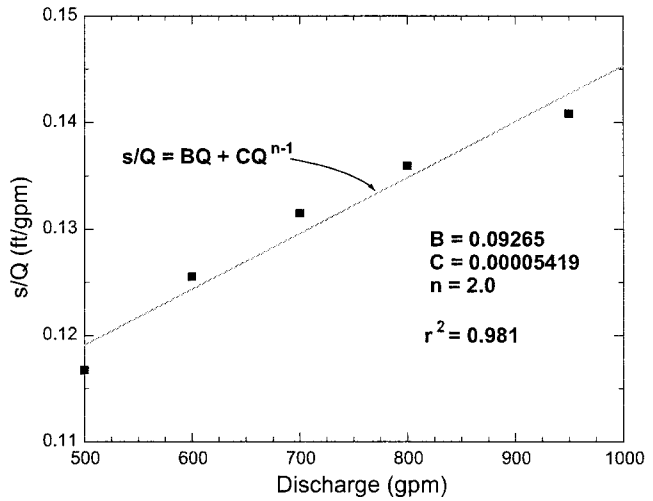

(c) Discharge vs total drawdown and laminar flow ratio

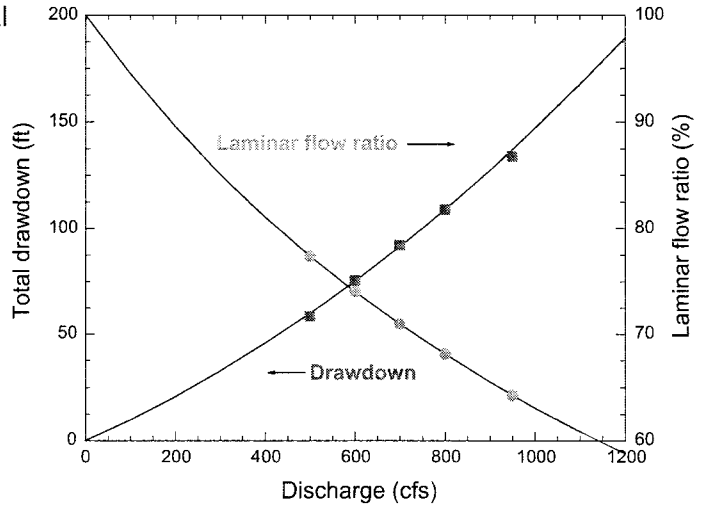

Figure 18. Step-Drawdown Test at G-4a

Discussion. Most of the discussion points presented earlier for G-2a and G-3a also apply here but are not repeated. In addition, barrier boundary effects were observed in well G-4a but were not obvious in well G-4 during the G-4a aquifer test. The most significant observation from this test is that T values are lower than at wells G-2a and G-3a. As reported in Table 10, it is apparent that K values are remaining about the same but the aquifer is thinning toward the west. This westward thinning also appears to be affecting the magnitude of the barrier boundary effects because they are causing less boundary-related drawdown in wells located farther to the west.

Table 14
Step-Drawdown Data* for the Test at Well G-4a

Step Number (j)	s_j (ft) at t_j = 100 min	Q_j (gpm)
1	58.75	500
2	75.10	600
3	92.38	700
4	108.80	800
5	133.77	950

*Data obtained from Figure 18(a) for each step in the step-drawdown test

As previously noted, variations in the K_h/K_v ratio were not explored in this test. The reasons for these variations were previously noted for well G-2a and are not repeated here. In addition, the effects of casing storage dissipated in less than 10 min. Hence, these effects were not significant because the sampling interval was 10 min and the pumping duration was almost two days. Furthermore, since well G-4 was used as an observation well, no casing storage effects were computed because these effects are similar to those in the pumping well. These results and the recommended values for aquifer parameters are summarized in Table 10.

VI. ANALYSES OF G-5A TEST DATA

Constant Rate Aquifer Test. From July 21-23, 1998, a two-day aquifer test was conducted at well G-5a at a constant discharge rate of 408 gpm. This test was immediately followed by a four-day recovery period from July 23-27, 1998. Drawdown and recovery were automatically recorded in well G-5a during this aquifer test. Since no drawdown data were recorded in any adjacent observation wells, we used only G-5a data to estimate aquifer transmitting properties.

These analyses are shown in Figure 19 using the aquifer configuration shown in Figure 3 and aquifer dimensions shown in Table 3. Hence, Theis analysis of drawdown is shown in Figure 19(a), while Theis analysis of recovery is shown in Figure 19(b). Figure 19(c) shows an analysis using the Theis residual-recovery method. All of the T values are comparable to the specific capacity value for T that was reported in Table 7 for this well. Again, these comparisons demonstrate parameter variability generated in the curve-matching process using alternate methods. Note that in each of these analyses, there are small but discernable boundary effects that are apparent. These are discussed below. Previous analyses from the other Guaje wells suggest that the aquifer should respond like a confined aquifer even though it is highly stratified. Finally, according to the T values shown in Figure 19 and b = 325 ft, we conclude that K varies between 1.7–2.2 ft/day, and averages about 2.1 ft/day.

Boundary Effects. In addition to the analyses mentioned above, it is apparent that boundary influences are affecting drawdown values as seen in Figure 19. These effects are addressed in a separate section near the end of this report.

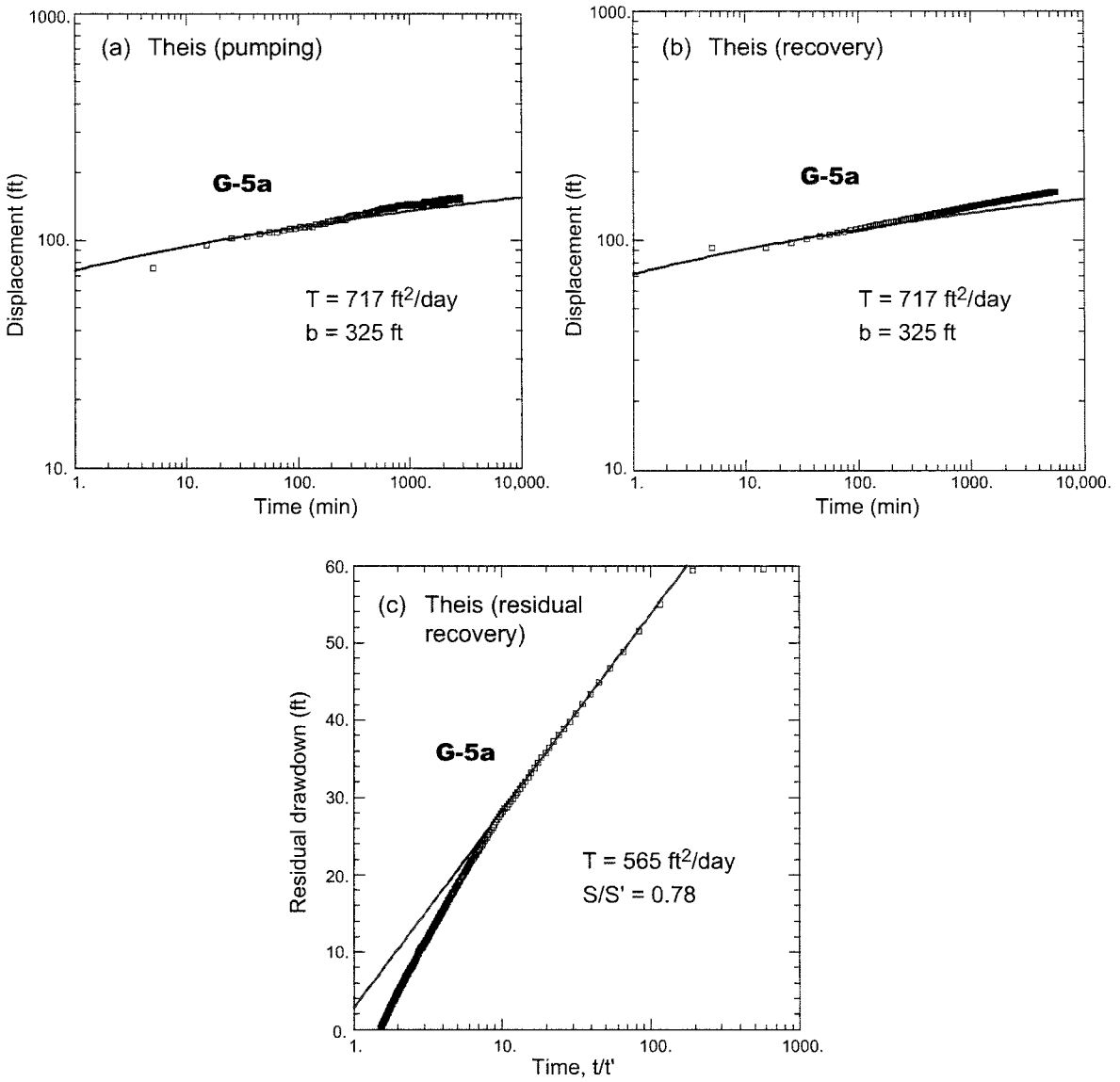

Figure 19. Theis confined aquifer analysis using G-5a data from (a) drawdown, (b) recovery, and (c) residual recovery. Note that the anisotropy ratio is 1.

Step-Drawdown Test. A step-drawdown test was also performed at well G-5a after the constant-rate aquifer test described above (i.e., on July 27, 1998). These data were recorded at one-minute intervals and are contained on the data CD-ROM attached to this report. The procedure for the step-drawdown test was also previously described. Figure 20(a) shows a plot of the raw test data recorded for each step in the test. Each step lasted 100 min at a constant discharge rate (Q). The important data from each step consists of drawdown (s_j) and discharge (Q); these data are summarized in Table 15. The analyses of these data are shown in Figure 20(b). Finally, Figure 20(c) shows a plot of drawdown in well G-5a versus discharge predicted from Equation (1) and using the head loss parameters shown in Figure 20(b). In addition, Figure 20(c) also shows a plot of the ratio of laminar head loss to total head loss versus discharge that is predicted from Equation (2).

Table 15
Step-Drawdown Data* for the Test at Well G-5a

Step Number (j)	s_j (ft) at t_j = 100 min	Q_j (gpm)
1	64.49	220
2	105.61	335
4	131.66	400
5	160.10	500

*Data obtained from Figure 20(a) for each step in the step-drawdown test.

Discussion. Most of the discussion points presented earlier for G-2a, G-3a, and G-4a apply here but are not repeated. Furthermore, since the aquifer test at well G-5a had no observation well, no reliable estimates for S were obtained. In addition, barrier boundary effects were also apparent during the G-5a aquifer test.

The most significant observation from the G-5a aquifer test is the relatively low K values that were obtained. Since b actually increases slightly between wells G-4a and G-5a, this reduction is even more dramatic. This decrease in K values is perhaps the most compelling evidence that suggests a buried fault is located between wells G-4a and G-5a. These boundary effects are discussed in the next section. Alternately, one might argue that the high-K zone near well G-5a is actually located above the screened interval but below the water table.

As previously noted, variations in the K_h/K_v ratio were not explored in this test. The reasons for these variations were previously noted for other wells and are not repeated here. In addition, the effects of casing storage dissipated in less than about 10 min. Hence, these effects were not significant because the sampling interval was 10 min and the pumping duration was more than 2 days.

(a) G-5a Step-drawdown test

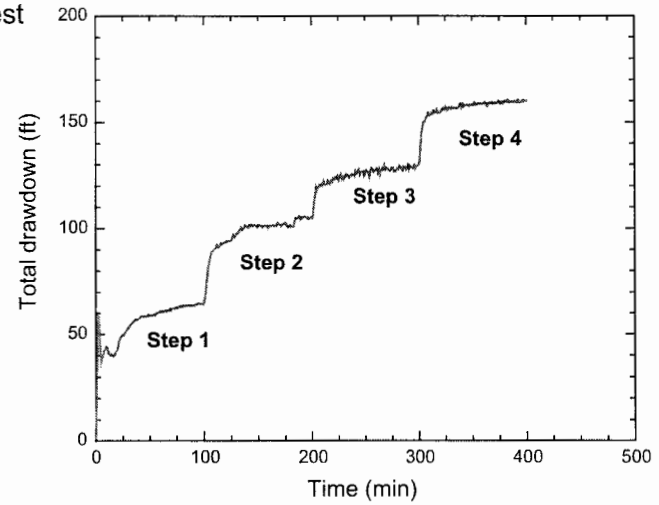

(b) Data analysis

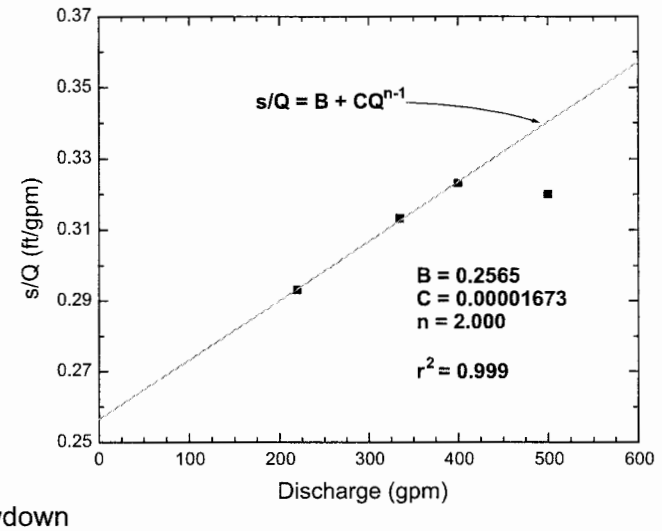

(c) Discharge vs total drawdown and laminar flow ratio

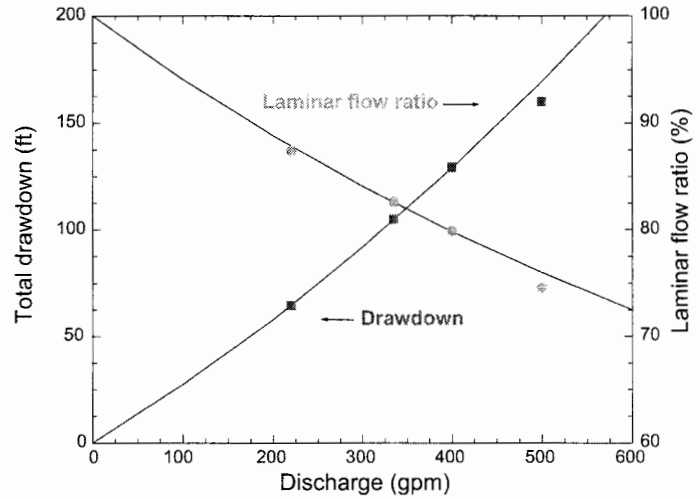

Figure 20. Step-drawdown test at G-5a

VII. BARRIER BOUNDARY EFFECTS

Background

Most of the wells in the preceding sections showed barrier boundary effects during portions of the various aquifer tests summarized in this report. All of these boundaries can be classified as barriers to flow because observed drawdown rises above Theis-predicted values at some given time. In this report, we refer to these times as departure times because they represent time after pumping started when boundary effects first appear (or time after recovery starts). Table 16 summarizes these important departure times.

Table 16
Summary of Barrier Boundary Effects in Different Aquifer Tests

Test	Well	Year	Figure	First Appearance of Boundary (min)[a]
G-2a	G-2a	1998	6a	200
	G-2a	1998	6b	200
	G-2a	1998	6c	$t/t' = 15$ (205 min)
	G-3	1998	7a	100
	G-2a	1998	7b	400
	G-3	1998	7b	25
G-2a	G-2a	2005	9a	500
	G-2a	2005	9b	$t/t' = 10$ (500 min)
	G-3	2005	9c	300
	G-3a	2005	9d	400
	G-2a	2005	10b	500
	G-3	2005	10b	200
	G-3	2005	10c	150
	G-3a	2005	10c	2500
	G-2a	2005	10d	500
	G-3	2005	10d	300
	G-3a	2005	10d	3000
G-3a	G-3a	1998	13a	400
	G-3a	1998	13b	300
	G-3a	1998	13c	$t/t' = 15$ (t = 205 min)
	G-3	1998	14a	350
	G-3a	1998	14b	none
	G-3	1998	14b	350
G-4a	G-4a	1998	16a	100
	G-4a	1998	16b	100
	G-4a	1998	16c	$t/t' = 40$ (t = 80 min)
	G-4	1998	17a	none
	G-4a	1998	17b	400
	G-4	1998	17b	3000
G-5a	G-5a	1998	19a	400
	G-5a	1998	19b	400
	G-5a	1998	19c	$t/t' = 8$ (t = 400 min)

[a] Time after pumping started or time of recovery (min)

These barrier boundary effects can be analyzed using traditional image well theory (e.g., Walton, 1970, p. 157-160). According to this theory, water levels in the observation well will only decline under the influence of the production well until the barrier boundary is encountered by the expanding cone of depression. Then additional drawdown will occur in the observation well in response to the barrier boundary. This additional drawdown occurs because the cone of depression can not theoretically expand beyond the boundary so extra water is removed from aquifer storage near the observation well. We can mimic this additional drawdown by assuming an imaginary (or image) well starts to pump at the same time as the real well. However, since it is located farther away from the observation well than the real pumping well, its imaginary cone of depression takes longer to arrive. Hence, this 'extra' pumping causes additional drawdown in the observation well that is delayed with respect to drawdown from the real pumping well. If we locate the barrier boundary midway between the pumping well and the image well, we can simulate the observed drawdown using superposition. The problem, however, is that we do not know where the boundary is located. In practice, we work this problem in reverse (i.e., an inverse problem) because we know the drawdown and want to find the boundary location.

We can visualize this general problem by representing it as shown in Figure 21 where only one barrier boundary is shown for simplicity. Figure 21 is constructed by randomly locating an image well. Then we draw the boundary along the perpendicular bisector of the line connecting the real and image pumping wells. Notice that in Figure 21, the boundary cannot pass between the pumping and observation wells (otherwise there would be no drawdown in the observation well). This means that the real well must be located closer to the observation well than the image well (i.e., $r_i > r_p$.) Thus, drawdown from the real well will reach the observation well before drawdown from the image well. This condition is apparent in both Figures 6 and 7 because the drawdown response in both wells clearly follows the Theis type-curve until the boundary starts to influence drawdown. Once the location of the image well has been assumed in Figure 21, we can remove the boundary and analyze the resultant drawdown in the observation well as if it was produced by an equivalent system with two pumping wells (i.e., one real well and one imaginary well). In other words, we can express drawdown as

$$s = \frac{Q}{4\pi T}\left[W(u_p) + W(u_i)\right] \text{ where } u_p = \frac{r_p^2 S}{4Tt} \text{ and } u_i = \frac{r_i^2 S}{4Tt} \tag{6}$$

where Q is discharge, T is transmissivity, $W(u)$ is the Theis well function, r_p is the radial distance between the pumping and observation wells, r_i is the radial distance between the image and observation wells, S is the storage coefficient, and t is time since pumping started. The ultimate objective of this exercise is to determine the unknown distance between the observation well and the image well representing the barrier boundary (r_i). When the cone of depression from the image well first reaches the observation well, the time-rate of drawdown will increase because both the real and image wells are now affecting drawdown and the curve will deflect upward. For example, the drawdown shown in Figure 7(a) initially follows a Theis type-curve because only the effects from the pumping well have arrived at the observation well. We have already used this information to estimate T and S in Figures 6 and 7. When the delayed effect of the boundary arrives at the observation well, the observed drawdown suddenly increases and the curve departs from the Theis curve. We can use this information to calculate r_i as follows. First, we select a random point on Figure 7(a) before any boundary effect is apparent and record the drawdown s_p. Then we find the point on Figure 7(a) where incremental drawdown caused by the real and image wells are equal. This second point will be located at some time after the boundary effect is apparent and where $s_i = s_p$, where s_i is the drawdown in well G-3 caused by the image well, and s_p is the drawdown in G-3 caused by the real well (i.e., G-2a). Since $s_i = s_p$, then $W(u_i) = W(u_p)$ and $u_i = u_p$. Thus,

$$\frac{r_i^2}{t_i} = \frac{r_p^2}{t_p} \text{ and } r_i = r_p\sqrt{\frac{t_i}{t_p}} \tag{7}$$

We can use Equation (7) to find r_i because we know r_p and can determine t_i and t_p from Figure 7(a), as illustrated in the next section.

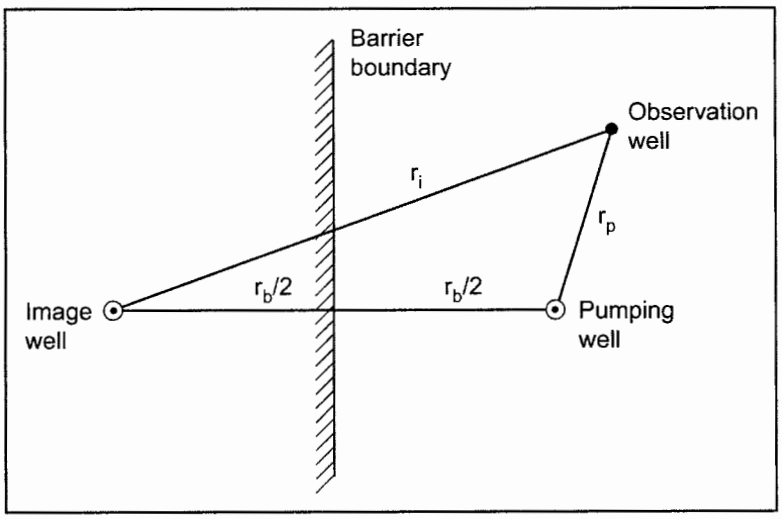

Figure 21. Idealized diagram showing both real and imaginary pumping wells in relation to some unknown boundary

Boundary Effects in 1998 Aquifer Test at Well G-2a

According to Figures 6(a) and 6(b), it is apparent that boundary influences are affecting drawdown values in wells G-2a during the aquifer test because we can see an upward deflection in drawdown after 100–200 min. As a result, the observed drawdown is higher than the Theis type-curve after these times, suggesting a no-flow (or barrier) boundary. In addition, the initial pumping effect from well G-2a dominates the drawdown in G-3 for the first 100 min as shown in Figure 7(a). Then the influence of the barrier boundary slowly increases until it completely dominates the time-drawdown curve. If we look closely at Figure 7(a), we are struck by the almost linear appearance of the boundary effect (i.e., the drawdown appears like a straight line after 100 min). If only one boundary were present, we would expect that the drawdown departures from the Theis curve would decrease as time increased. In other words, we would expect the drawdown behavior to deviate above the Theis curve and still be non-linear after 100 min. Since it is not, we conclude that more than one boundary is affecting drawdown at well G-3. This same linear effect is also visible in well G-2a as seen in Figure 6. Undoubtedly, the presence of multiple boundaries makes the analysis more difficult.

As seen above, boundary effects in the production well begin after about 100-200 min. However, according to Figure 7(b), these effects first appear after about 25 min in G-3. These timing differences are significant and may shed insight on the aquifer between these wells. On first thought, these timing differences suggest that the first of several boundaries is located closer to well G-3 than to G-2a. On closer examination, however, other explanations seem more reasonable. First, the expanding cone of depression should radiate from the production well close to the speed of sound in a saturated medium. Hence, timing differences marking the first appearance of a boundary should be similar in all wells. Second, the duel analysis shown in Figure 7(b) assumes a homogeneous aquifer between wells G-2a and G-3. So this analysis may actually represent evidence that this assumption has been violated (i.e., the medium is actually heterogeneous). Finally, the Theis curve fits to the drawdown data contain some uncertainties, and these uncertainties translate into different boundary departure times (i.e., slightly different Theis curves can be fit to the data and these different fits give different times when boundary effects first appear). In other words, these timing differences can not be reliably translated into a known location for the boundary. Additional uncertainty is also present because there is only one observation well. Regardless, these data still imply that there are multiple barrier boundaries present and that these

boundaries are acting in combination with one other. These combination effects may be the result of aquifer thinning to the west (i.e., see Figures 2 and 3) and buried faults between wells as reported in WoldeGabriel et al. (2006). Additional information will be presented later since the aquifer test at G-2a was repeated in 2005 using multiple observation wells.

We can approximately analyze the effect of the first of several boundaries by starting with the *T* and *S* values shown in Figure 7(a). We arbitrarily select $s_p = 1.0$ ft at $t_p = 10.7$ min (i.e., select any convenient (s_p, t_p) coordinate pair before the drawdown in well G-3 is affected by the first barrier boundary). In practice, we select any convenient s_p and then compute t_p from Equation (6) because we know *Q*, *T*, *S*, and r_p (noting that $W(u_i) \to 0$ for $t < 100$ min). Once the barrier boundary influence starts affecting drawdown in G-3 (i.e., at some $t \geq 100$ min), we find a second coordinate point (s_i, t_i) where $s_i = 1.0$ ft (i.e., look for this incremental s_i value between the Theis curve and the observed data and record t_i). Thus at $s_i = 1.0$ ft, we find that $t_i = 165$ min. Using Equation (7), we find that $r_i = 1,223$ ft since $r_p = 311$ ft (see Table A-1 in Appendix A for all distances between wells). These analyses are summarized on Figure 22(a). It should come as no surprise that our analysis contains some uncertainty. In other words, the image well representing the first boundary is approximately located somewhere on a circle of radius $r_i > 1,200$ ft away from well G-3. With only this information, it is apparent that we can not precisely locate the image well (and thus the first boundary). However, this information may be helpful when we analyze the independent data from the 2005 test, including data from wells G-3 and G-3a.

Ideally, we can locate additional boundaries that are affecting drawdown at G-3 by fitting additional Theis curves to the observed data at times greater than 100 min. As seen in Figure 22(a), two additional Theis curve matches are shown to illustrate this point. However, it quickly becomes apparent that a large number of different Theis curves can be fitted to the data (supporting the argument that a large number of boundaries are present). But our attempt to locate a second barrier boundary simply contains too much uncertainty. We conclude that we can not uniquely locate additional boundaries with available data. Again, this information may be helpful when we analyze the independent data from the 2005 test.

Boundary Effects in 2005 Aquifer Test at Well G-2a

It is also apparent in Figures 9 and 10 that barrier boundary effects were present in the 2005 aquifer test at well G-2a. For example, the observed drawdown values plot above the Theis predicted drawdown in Figures 9(a) and 9(c). In other words, as the cone of depression expands laterally away from well G-2a, it eventually encounters one or more barrier boundaries. We know these boundaries are barriers to flow because the cone of depression cannot theoretically continue to expand past the boundary. Since *Q* is held constant, this restriction in the expanding cone of depression causes additional water to be extracted from aquifer storage near the observation well. Hence, we see additional drawdown compared to the Theis aquifer model (which has no restrictive boundary). This behavior is very similar to that previously described in Figures 6 and 7.

We can analyze the boundary effects as previously described using Equation (7). Hence, from Figure 9(c), we select $s_p = 1.0$ ft at $t_p = 27.1$ min from the first type curve. Once the barrier boundary influence starts affecting drawdown in G-3 (i.e., at some $t \geq 300$ min), we find a second coordinate point (s_i, t_i) where $s_i = 1.0$ ft at $t_i = 403$ min. Using Equation (7), we find that $r_i = 1,199$ ft since $r_p = 311$ ft. These analyses are shown in Figure 22(b). While we can not precisely locate this first image well, we can say that it is approximately located somewhere on a circle of radius $r_i \approx 1200$ ft away from well G-3. Recall that we previously estimated a similar value using the 1998 data. This information is used below.

(a) Barrier boundary analysis using Figure 7(a) data.

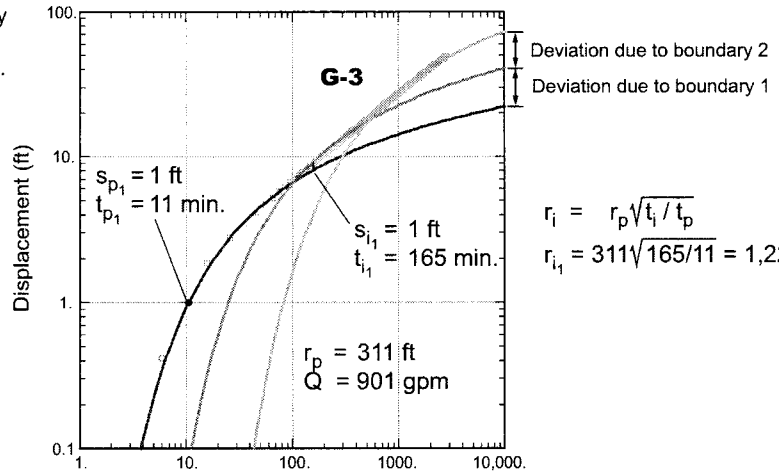

$r_i = r_p\sqrt{t_i / t_p}$

$r_{i_1} = 311\sqrt{165/11} = 1{,}223$ ft

(b) Barrier boundary analysis using Figure 9(c) data.

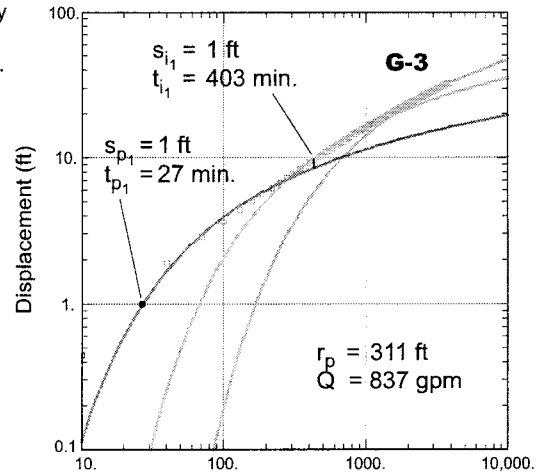

$r_{i_1} = 311\sqrt{403/27} = 1{,}199$ ft

(c) Barrier boundary analysis using Figure 14(a) data.

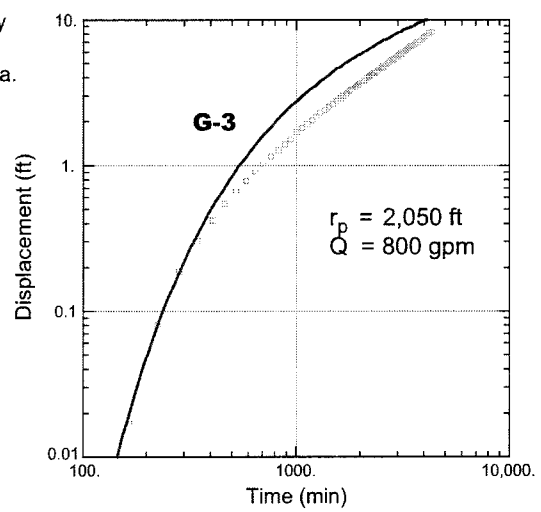

No analysis attempted.

Figure 22. **G-2a aquifer tests showing barrier boundary effects that are revealed in well G-3 drawdown data during: (a) the 1998 test and (b) the 2005 test. The 1998 G-3a aquifer test also revealed boundary effects at well G-3 as seen in (c). Multiple boundaries are apparent in all tests. See text for discussion.**

The linear nature of the G-3 boundary effect is apparent in both the 1998 and 2005 aquifer tests as seen in Figures 7(a) and 9(c), or in Figures 22(a) and 22(b). And like before, we conclude that more than one boundary is present. But we still can not uniquely locate additional image wells (and thus additional boundaries). Hence, Figure 22(b) shows several additional Theis matches to the data but many different curves are possible. Again, this argument implies that more than two boundaries are affecting water levels in G-3 when well G-2a is pumped.

Boundary effects were also apparent in well G-3a when G-2a was pumped as seen in Figure 9(d). However, the data quality is much poorer than at G-3 because the Theis curve fit is poorer. According to Figure 9(d), the linear boundary effect begins after about 450 min and falls below the Theis curve. This response is unusual and suggests that there is poor hydraulic communication between wells G-2a and G-3a. Hence, we can not uniquely locate this image well either (and thus the third boundary). Again, this information will be helpful in the next section.

Boundary Effects in 1998 Aquifer Test at Well G-3a

According to Figures 13 and 14, it is again obvious that one or more barrier boundary influences were present at well G-3 when G-3a was pumped. Theoretically, the effect at G-3 can be analyzed using the same image well theory described earlier. As seen in Figure 22(c), however, the Theis curve rises above the field curve and suggests poor communication between wells G-3a and G-3. Hence, these data were not evaluated. A similar behavior was noted at well G-3a during the 2005 test at G-2a as seen in Figure 9(d). Hence, the field data plot below the Theis type-curve after about 350 min. This response is unusual but its linear appearance resembles that shown in Figures 22(a) and 22(b) when well G-2a was pumped. We conclude that the water levels in G-3 respond linearly to the boundary effect when G-2a is pumped on the east or when G-3a is pumped on the west. However, the nature of this response to the Theis relationship is different in each case and suggests a more complex heterogeneous aquifer.

Figure 23 shows the location of the Guaje well field in relation to previously mapped faults in the Puye quadrangle (Dethier 2003). A copy of the Dethier map is shown in Appendix C as a convenience to the reader. Figure 23 shows a circle with an average radius defined by the values from Figures 22(a) and 22(b). This radius represents the distance between well G-3 and image wells from the 1998 and 2005 aquifer tests. Since these radii were almost identical, we think they represent the same unknown boundary. We can use this information to locate these and other unknown boundaries (recall that there are several boundaries). Hence, the first image well lies somewhere on a circle defined by $r_i \approx 1200$ ft from G-3 as seen in Figure 23. This representation implies that other boundaries are located at $r > 1200$ ft (although they remain unknown).

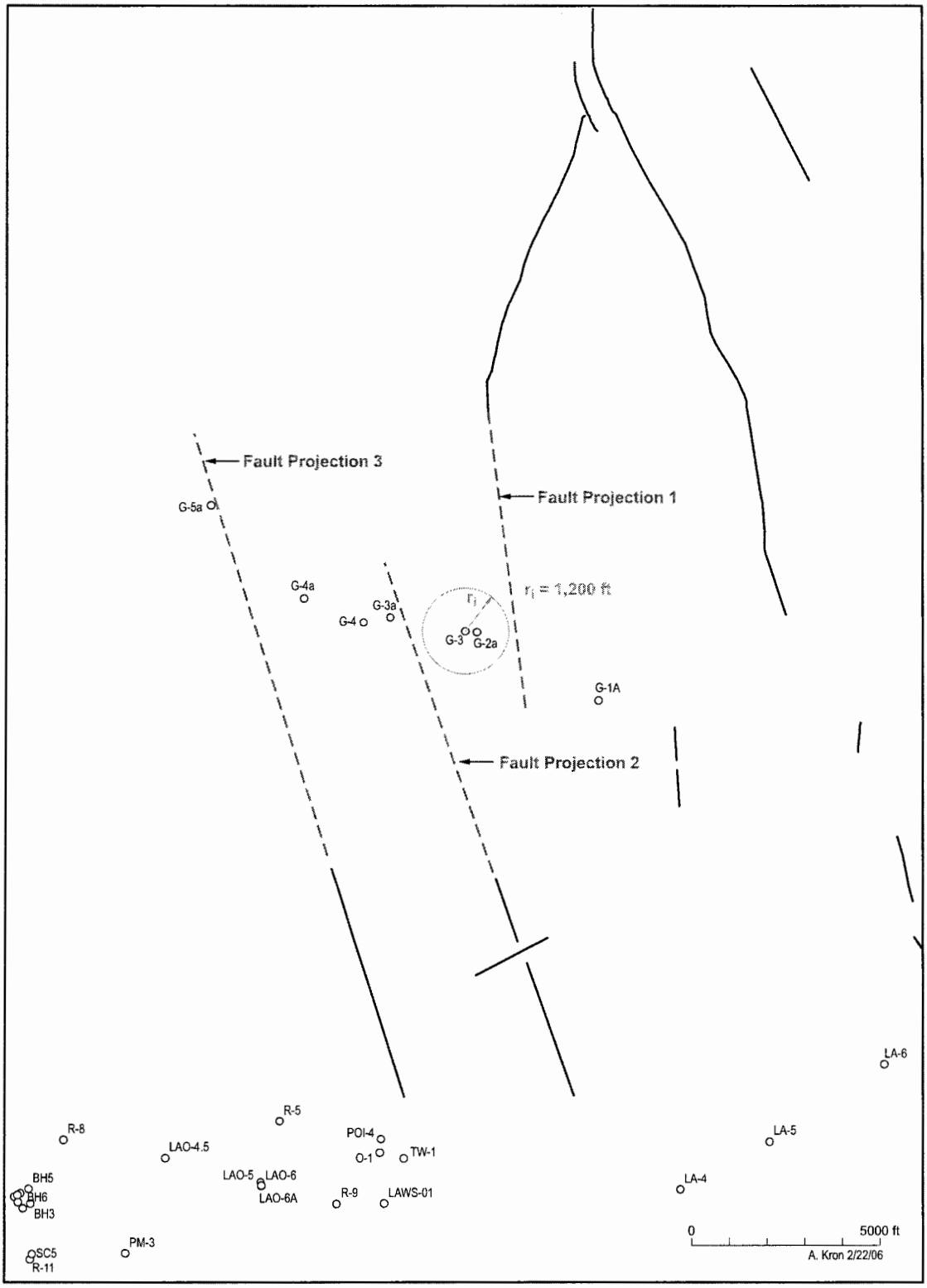

Figure 23. Possible locations of barrier boundaries identified from aquifer tests and fault projections associated with mapped faults (modified after Dethier, 2003)

As previously noted, we know that an image well is located somewhere on a circle with $r_i \approx 1200$ ft as seen in Figure 23. If we combine this radial distance with other geologic information, we may identify the precise location of this image well. In addition, we may also identify several other potential boundary locations (and simultaneously associate them with known geological features). For example, if we project the Dethier mapped faults into Guaje Canyon, are they located near any of the Guaje wells? Recall that any potential boundary projection must be the perpendicular bisector of the line connecting the suspected image well and the production well that revealed the boundary effect. The first thing we notice is that several fault projections pass near wells G-3 and G-2a but these are located too far away. Several other fault projections pass near other Guaje wells as shown in Figure 23. But none of these fault projections meet our criteria either. We conclude that this lack of correlation means that the G-3 boundary effect most likely resulted from aquifer thinning between wells G-2a, G-3 and G-3a. This aquifer thinning is clearly shown in Figure 3 and is based on spinner logs from each replacement well.

There are actually several interesting fault projections shown in Figure 23. The first one is located about 1,200 ft east of well G-2a. But is it not the perpendicular bisector that we were seeking in Figure 22. Recall that we also identified multiple boundaries. In addition, Fault Projection 1 shown in Figure 23 passes between wells G-2a and G-1a. This is important because there was no pumping effect recorded in well G-1a during the 2005 aquifer test at G-2a. If this fault projection is actually associated with a fault (and we think it is), it explains why we did not see any drawdown at well G-1a in response to the 2005 aquifer test at G-2a. Two additional projections are also shown in Figure 23. Fault Projection 2 passes between wells G-3 and G-3a and may account for the poor hydraulic communication noted in the 2005 aquifer test at G-2a (see Figures 9 and 10). This same projection may also account for a continuation of this poor communication between wells G-2a and G-4a as shown Figure 12. Finally, Fault Projection 3 passes between wells G-4a and G-5a. This last projection may explain why there is such a dramatic reduction in K values between these latter two wells.

In summary, we conclude that the first barrier boundary detected in drawdown data recorded at well G-3 is most likely associated with aquifer thinning between wells G-2a and G-3 to the west. This boundary was the dominant boundary detected in both the 1998 and 2005 G-2a aquifer tests. We also conclude that a second barrier boundary is probably associated with a buried fault located about 1200 ft east of well G-2a. This buried fault is oriented approximately north-south in Guaje Canyon. Two additional fault projections may also extend into the Guaje well field as shown in Figure 23. These projections correspond to fault extensions that were previously mapped by Dethier (2003).

Boundary Effects in 1998 Aquifer Tests at Wells G-4a and G-5a

According to Figures 16 and 17, barrier boundary effects were present in the G-4a aquifer test. These data show that boundary effects were present in well G-4a but are not obvious in well G-4. It is also apparent that these effects are smaller than at wells G-2a and G-3a seen earlier. In fact, these boundary effects appear to diminish toward the west because drawdown values associated with different boundaries are systematically smaller in the respective aquifer tests as we move to the west (i.e., in wells G-2a, G-3a, and G-4a). The corresponding T values also decline toward the west in these same wells. This declining influence coincides with westward aquifer thinning that was noted earlier even though K values remain relatively constant. These observations may suggest that all boundary effects are only associated with aquifer thinning. According to Figure 3, however, changes in b between wells G-3a, G-4a, and G-5a are relatively small. Hence, we think that boundary effects in these latter wells may also be associated with Fault Projections 2 and/or 3 that are shown in Figure 23. Supporting evidence for Fault Projection 2 was previously shown in Figures 9(d) and 14(a). Additional evidence for Fault Projection 3 is shown below.

Barrier boundary effects are also in the G-5a test according to Figure 19. These effects appear after about 450 min according to Figures 19(a) and 19(b). They also appear after $t/t' = 8$ in Figure 19(c), and corresponds to about 400 min into recovery. These boundary effects continue a diminishing trend toward the west that was noted above. The corresponding T values decline sharply from those previously noted in the other Guaje replacement wells. This sharp decline is also reflected in the corresponding K values from this well as seen in Table 10. These observations are consistent with the earlier suggestion that barrier boundary effects result from a buried fault located between wells G-4a and G-5a (i.e., Fault Projection 3 in Figure 23). Aquifer thinning toward the west contributes toward the observed boundary effects in wells G-2a, G-3a, and G-4a but not in G-5a. In fact, this contribution from aquifer thinning is probably declining toward the west as noted above. We also suspect that the thin, interbedded nature of the sediments in the high-production zone below Guaje Canyon is a primary cause for the barrier boundary effects observed in this sequence of aquifer tests. These effects are also supplemented by several buried faults (i.e., Fault Projections 1, 2, and 3) as seen in Figure 23.

VIII. SUMMARY AND CONCLUSIONS

The sequential aquifer tests in the Guaje Canyon well field are significant for several reasons. First, this test sequence recorded drawdown and recovery data that can be used to evaluate important aquifer parameters, including T, K, b, S, and S_s. These tests are supplemented by critically important spinner logs that accurately define thickness variations in high-yielding aquifer units within the regional aquifer. Hence, these high-yielding units are located above the first significant Miocene basalt flows in the eastern portions of the Guaje well field. But they are clearly interbedded with the basalts as we move toward the west. These complex unit relationships are directly analogous to those in the regional aquifer located in the central portions of the Pajarito Plateau. At the same time, however, these unit comparisons are also in stark contrast because the regional aquifer below Guaje Canyon behaves like a confined aquifer rather than a leaky or phreatic one. In other words, this aquifer does not exhibit the leaky-aquifer characteristics that are prevalent near municipal water supply wells PM-2, PM-4, and PM-5 (McLin, 2005a, 2006). In all fairness, however, we note that in those tests the apparent leaky-aquifer behavior took 2-5 days to appear in observation wells. In contrast, severe boundary effects appeared in most Guaje wells after several hundred minutes. Second, the replacement well spinner logs reveal a highly stratified aquifer below Guaje Canyon that dramatically thins toward the west. Finally, these tests have revealed multiple boundary effects. The first boundary effect is associated with westward thinning of the stratified aquifer while additional boundary effects may correspond to several projections of Dethier (2003) mapped faults into the Guaje Canyon well field. The first projection is located about 1200 ft east of well G-2a. The second projection passes between wells G-3 and G-3a, and a third passes between wells G-4a and G-5a. Other projections are possible but are not shown in Figure 23; however, these other projections are located too far away and do not affect water levels in Guaje wells. The full implications of these finding are still being evaluated. However, they suggest a very different hydrogeologic picture from that previously revealed in the central plateau region.

The following general conclusions for the Guaje Canyon well field can be summarized.

1. The specific capacity (Q/s) values at well G-2a increased between 1998 and 2005 as reported in Table 12. This improvement reflects a continuation in well development over time. Smaller changes were seen in other Guaje wells; however, these changes showed both small increases and decreases in Q/s values. This observation is important because it suggests that T values from the 2005 test at well G-2a are more representative than similar values from the 1998 test. These aquifer parameters are summarized in Table 11. These results also suggest that the 1998 aquifer tests at wells G-3a, G-4a, and G-5a are also representative since Q/s values have

not changed significantly over time in these wells. Hence, aquifer parameter values for these latter wells are summarized in Table 10.

2. Analyses of drawdown and recovery data from individual aquifer tests in the Guaje well field yield important estimates for aquifer transmissivity (T) and storage coefficient (S) as summarized in Tables 10 and 11. These analyses say that the regional aquifer below Guaje Canyon behaves like a traditional confined (or Theis) aquifer. In addition, these results favorably compare to T values obtained from specific capacity analyses as seen in Table 7. However, the combined Theis analyses for pumping and observation well pairs provided the best overall average estimates for individual T and S values. Hence, at well pairs G-2a and G-3, the best estimates are from Table 11 and showed that $T = 3700$ ft^2/day, $S = 0.0020$, and $b = 435$ ft. However, in wells G-3a, G-4a, and G-5a, the best estimates come from Table 10. Hence, at well G-3a, the best estimates suggested that $T = 2000$ ft^2/day, $S = 0.00077$, and $b = 261$ ft. At well G-4a, the best estimates indicated that $T = 1680$ ft^2/day, $S = 0.00011$, and $b = 245$ ft. Finally, at well G-5a, the best estimates indicated that $T = 700$ ft^2/day, $S = 0.00030$, and $b = 325$ ft.

3. These aquifer test results are strongly correlated to individual spinner logs that were obtained from each new Guaje replacement well (see Appendix A). Detailed analyses of these data are shown in Figures 4 and 5, and suggest that the high-yielding units within the regional aquifer below Guaje Canyon are located in the upper portions of each well screen. These high-H zones generally correspond to piedmont-derived fluvial sediments that have an eastern or northern source area. As seen in Figure 3, these units thicken toward the east below Guaje Canyon but are intermingled with Miocene basalts toward the west. The fine silty sands located below the basalts have relatively low-yielding water wells that are typical for the Tesuque Formation (Santa Fe Group). In many respects, these spinner logs are the most valuable data from the Guaje well field because they precisely locate alternating high and low-yielding water units that are sandwiched together to form the regional aquifer below Guaje Cannon. In addition, these logs also demonstrate that the screen length in each well is not a good representation for aquifer thickness as seen in Figure 3.

4. These sequential aquifer tests have clearly identified a dramatic reduction in T values between well G-2a on the east and well G-5a on the west. This dramatic change in T is strongly correlated to an equally dramatic thinning of the high-yielding aquifer units between wells G-2a and G-3a that were shown in Figure 3. These changes in T values are also related to the presence of several fault projections shown in Figure 23. This characterization is completely new and comes as a surprise. These findings will hopefully shed insight on future exploration for other high-yielding water well locations.

5. Barrier boundary effects were observed in most wells during the sequential aquifer tests described here. However, distances to individual boundaries could not be uniquely determined. These effects appear to diminish toward the west along with T values, and suggest that they are primarily associated with aquifer thinning.

6. Results from both the 1998 and 2005 aquifer tests at well G-2a clearly identified multiple barrier boundary effects. These boundaries were confirmed by drawdown data recorded in several observation wells. The first boundary was associated with aquifer thinning between wells G-2a, G-3, and G-3a. This first boundary was also confirmed in the G-3a aquifer test using drawdown data recorded at G-3. A second boundary probably corresponds to a geometrically projected normal fault that was previously mapped by Dethier (2003) and terminates about 6,000 ft to the north. The projection of this mapped fault into the buried alluvium in Guaje Canyon is shown in Figure 23 (i.e., Fault Projection 1), and suggests that

this north-south oriented barrier boundary is about 1,200 ft east of G-2a. Other projections (i.e., Fault Projections 2 and 3 shown in Figure 23) are also possible and are supported by water level responses in several observation wells. Hence, water levels in G-1a showed no response to pumping at G-2a. However, water levels in wells G-3a and G-4a responded to G-2a pumping while G-5a did not. Furthermore, there is a dramatic reduction in *K* values between wells G-4a and G-5a that can not be explained by aquifer thinning. These observations support the conclusion that Fault Projection 2 may be a leaky boundary but that Fault Projection 3 reflects a strong discontinuity in *K* values.

7. Well G-1a was monitored as an observation well during the 2005 aquifer test at G-2a because the pump had been temporally removed from this well (recall that there are no access tubes in G-1a so a pressure transducer can not usually be installed). The fact that no analyzable response was recorded here is significant for several reasons. First, it limits the maximum radius of eastward pumping influence from well G-2a to about 3,000 ft (i.e., more than the distance between wells G-2a and G-3a where there was drawdown but less than the distance between wells G-2a and G-1a where there was no drawdown). The westward radius, however, extends almost 4800 ft from wells G-2a toward G-4a as seen in Figure 12(b). Hence, the radius of influence at G-2a is asymmetrical and points up-gradient (i.e., toward the west). Second, the lack of drawdown at well G-1a in response to G-2a pumping suggests that a barrier boundary is located between these wells. Recall that a Dethier mapped fault was projected into Guaje Canyon. This projection is located approximately 1200 ft east of G-2a and is between these two wells.

8. The 2005 aquifer test at well G-2a was preceded by almost 80 days of recovery because there was no pumping at wells G-1a, G-2a, G-3a, and G-4a during this period. Drawdown was recorded in wells G-2a, G-3, G-3a, and G-4a during this test. However, data from G-4a were not analyzed because of the poor hydraulic communication between these wells. These observations imply that Fault Projection 2 in Figure 23 is leaky and only partially off-sets high-*K* zones in the regional aquifer between wells G-2a and G-3a.

9. Step-drawdown tests were conducted at each new Guaje replacement well. Analyses of these test data are summarized in Figure 8 (well G-2a), Figure 15 (well G-3a), Figure 18 (well G-4a), and Figure 20 (well G-5a). These data are important in setting optimal water production rates in individual wells so that energy costs associated with pumping water over the lifetime of each well can be minimized. These optimal rates were summarized in Table 9, and favorably compare to normal production rates.

IX. ACKNOWLEDGEMENTS

This work was supported by the Pathways Protection Program within the Environmental Stewardship Division at Los Alamos National Laboratory. Special thanks are extended to Mr. Timothy Glasco, Deputy Utility Manager, Mr. Wayne Witten, Water System Superintendent, and Mr. Daryl Hastings, Water System Operator, all with the Department of Public Utilities, County of Los Alamos, for their support and cooperation in conducting the 2005 aquifer test at well G-2a. This manuscript also benefited greatly from comments and suggestions provided by David Broxton, Elizabeth Keating, Ardyth Simmons, and Velimir Vesselinov of Los Alamos National Laboratory; and David Schafer of Schafer and Associates, Inc., North Oaks, Minnesota, for their invaluable discussions and critical reviews of this report.

X. REFERENCES

ASTM, 2004. Standard Test Method (Analytical Procedures) for Determining the Efficiency of a Production Well in a Confined Aquifer from a Constant Rate Pumping Test. Designation D6034-96. American Society for Testing and Materials International, West Conshotocken, PA (USA).

Bear, J., 1979. *Hydraulics of Groundwater*. McGraw-Hill, New York, p. 569.

Bouwer, H., 1978. *Groundwater Hydrology*. McGraw-Hill, New York, p. 480.

Bradbury, K.R., and E.R. Rothschild, 1985, A Computerized Technique for Estimating Hydraulic Conductivity of Aquifers from Specific-Capacity Data. Ground Water, vol. 23, no. 2, pp. 240–246.

Broxton, D.E., and S.L. Reneau, 1996. Buried Early Pleistocene Landscapes Beneath the Pajarito Plateau, Northern New Mexico. New Mexico Geological Society, 47th Field Conference Guidebook to Jemez Mountains, New Mexico Bureau of Mines, Socorro, NM, pp. 325–334.

Broxton, D.E., and D.T. Vaniman, 2005. Geologic Framework of a Groundwater System on the Margin of a Rift Basin, Pajarito Plateau, North-Central New Mexico. Vadose Zone Journal, vol. 4, no. 3, pp. 522–550.

Collins, K.A., A.M. Simmons, B.A. Robinson, and C.L. Nylander (editors), 2006. Los Alamos National Laboratory's Hydrogeologic Studies of the Pajarito Plateau: A Synthesis of Hydrogeologic Work Plan Activities, 1998–2004. Los Alamos National Laboratory report, LA-14263-MS, Los Alamos, NM.

Conover, C.S., C.V. Theis, and R.L. Griggs, 1963. Geology and Hydrology of the Valle Grande and Valle Toledo, Sandoval County, New Mexico. USGS Water Supply Paper 1619-Y, 37 p., US Government Printing Office, Washington, D.C.

Cooper, H.H., and C.E. Jacob, 1946. A Generalized Graphical Method for Evaluating Formation Constants and Summarizing Well-Field History. Transactions, American Geophysical Union, vol. 27, pp. 526-534.

Cushman, R.L., 1965. An Evaluation of Aquifer and Well Characteristics of Municipal Well Fields in Los Alamos and Guaje Canyon near Los Alamos, New Mexico. USGS Water Supply Paper 1809-D, 50 p., US Government Printing Office, Washington, D.C.

Dethier, D.P., 2003. Geologic Map of the Puye Quadrangle, Los Alamos, Rio Arriba, Sandoval, and Santa Fe Counties, New Mexico. Miscellaneous Field Studies Map MF-2419 (version 1), USGS, Denver, Colorado (available on-line as a PDF file at http://pubs.usgs.gov/mf/2003/mf-2419).

Driscoll, F.G., 1986. *Groundwater and Wells*, Johnson Division, St. Paul, Minnesota.

Fetter, C.W., 1994. *Applied Hydrology* (3rd edition), Prentice-Hall, New Jersey, 691 p.

Griggs, R.L., 1964. Geology and Ground-Water Resources of the Los Alamos Area, New Mexico; USGS, Water Supply Report 1753, 107 p., US Government Printing Office, Washington, D.C.

Koch, R.J., and D.B. Rogers, 2003. Water Supply at Los Alamos, 1998-2001. Los Alamos National Laboratory report, LA-13985-PR, Los Alamos, NM.

Kruseman, G.P., and N.A. de Ridder, 1976. Analysis and Evaluation of Pumping Test Data. Bulletin 11, International Institute for Land Reclamation and Improvement, Wageningen, The Netherlands.

McLin, S.G., 2005a. Analysis of the PM-2 Aquifer Test Using Multiple Observation Wells. Los Alamos National Laboratory report, LA-14225-MS, Los Alamos, NM.

McLin, S.G., 2005b. Estimating Transmissivity from Specific Capacity using Matlab. Ground Water, vol. 43, no. 4, p. 611–614.

McLin, S.G., 2006. Analysis of the PM-4 Aquifer Test Using Multiple Observation Wells. Los Alamos National Laboratory report, LA-14252-MS, Los Alamos, NM.

Moench, A.F., 1997. Flow to a Well of Finite Diameter in a Homogeneous, Anisotropic, Water Table Aquifer. Water Resources Research, vol. 33, no. 6, pp. 1397–1407.

Neuman, S.P., 1974. Effect of Partial Penetration on Flow in Unconfined Aquifers Considering Delayed Gravity Response. Water Resources Research, vol. 10, no. 2, pp. 303–312.

Purtymun, W.D., 1984. Hydrologic Characteristics of the Main Aquifer in the Los Alamos Area: Development of Ground Water Supplies. Los Alamos National Laboratory Report, LA-9957-MS, Los Alamos, NM.

Purtymun, W.D., 1995. Geologic and Hydrologic Records of Observation Wells, Test Holes, Test Wells, Supply Wells, Springs, and Surface Water Stations in the Los Alamos Area. Los Alamos National Laboratory report, LA-12883-MS, Los Alamos, NM.

Purtymun, W.D., and A.K. Stoker, 1988. Water Supply at Los Alamos: Current Status of Wells and Future Water Supply. Los Alamos National Laboratory report LA-11332-MS, Los Alamos, NM.

Purtymun, W.D., and S. Johansen, 1974. General Geohydrology of the Pajarito Plateau. New Mexico Geological Society, 25th Field Conference Guidebook to Ghost Ranch. New Mexico Bureau of Mines, Socorro, NM, pp. 347–349.

Reneau, S.L., and D.P. Dethier, 1996. Pliocene and Quaternary History of the Rio Grande, White Rock Canyon and Vicinity, New Mexico. New Mexico Geological Society, 47th Field Conference Guidebook to Jemez Mountains, New Mexico Bureau of Mines, Socorro, NM, pp. 317–324.

Rosco-Moss Company, 1990. *Handbook of Ground Water Development*. John Wiley and Sons, New York, pp. 493.

Schafer, D.C., 1979. Casing Storage can Affect Pumping Test Data. Johnson Driller's Journal, Jan-Feb 1979.

Shomaker, J., 1999. Well report: Construction Details And Testing, Guaje Replacement Wells GR-1, GR-2, GR-3, and GR-4, Santa Fe County, New Mexico. Private consulting report to Los Alamos National Laboratory, John Shomaker and Associates, Inc., Albuquerque, NM.

Theis, C.V., 1935. The Relation Between the Lowering of the Piezometric Surface and the Rate and Duration of Discharge of a Well Using Groundwater Storage. American Geophysical Union Transactions, vol. 16, pp. 519–524.

Theis, C.V., 1963. Estimating the Transmissivity of a Water Table Aquifer from the Specific Capacity of a Well. U.S. Geological Survey, Water Supply Paper 1536-I, pp. 332–336, US Government Printing Office, Washington, D.C.

Theis, C.V., and C.S. Conover, 1962. Pumping tests in the Los Alamos Canyon Well Field near Los Alamos, New Mexico. U.S. Geological Survey, Water Supply Paper 1619-I, p. 24, US Government Printing Office, Washington, D.C.

Thiem, G., 1906. Hydrologische Methoden, Ph.D. dissertation, Royal Technical University, Stuttgart (now the University of Stuttgart); published by J.M. Gebhardt, Leipzig, Germany, 65 p. (in German).

Walton, W.C., 1970, *Groundwater Resource Evaluation*, McGraw-Hill Book Company, New York, 664 p.

WoldeGabriel, G., R.G. Warren, S. Chipera, and E. Keating, 2005. Geological characteristics of the Guaje Canyon well field in the Pajarito Plateau of the Espanola Basin, Rio Grande rift. Los Alamos National Laboratory Report LA-11332-MS, Los Alamos, NM.

APPENDIX A. WELL COMPLETION DIAGRAMS AND LOCATION DATA

Table A-1
Coordinate locations and elevations[a] of individual wells

Well	X-Coordinate[b]	Y-Coordinate[c]	Elevation[d]	Distance from G-2a[e]	from G-3a[e]	from G-4a[e]	from G-5a[e]
G-1a	514997	1784291	6014	3718	6013	8374	11633
G-2a	511730	1786066	6140	0	2359	4744	7917
G-3	511432	1786156	6139	311	2050	4434	7610
G-3a	509417	1786532	6212	2359	0	2385	5669
G-4	508705	1786390	6229	3042	726	1743	5169
G-4a	507087	1787039	6299	4744	2385	0	3528
G-5a	504633	1789574	6416	7917	5669	3528	0

[a] Locations and elevations of brass survey pins in concrete well pads.

[b] X, or Easting, coordinate using New Mexico State Plane coordinate system (ft).

[c] Y, or Northing, coordinate using New Mexico State Plane coordinate system (ft).

[d] Elevation above mean sea level (ft).

[e] Distance (ft) from G-2a, G-3a, G-4a, or G-5a to each well computed as follows: $r = \mathrm{sqrt}[(x_1-x_2)^2+(y_1-y_2)^2]$, where $(x_1, y_1) = (x, y)$ well coordinate and $(x_2, y_2) = (x, y)$ coordinate of well G-2a, G-3a, G-4a, or G-5a, respectively.

Data Source: Purtymun (1995) and Chavez-Grieves (1998).

Table A-2
Well completion data for Guaje Canyon wells

Well Name	G-1a	G-2a	G-3	G-3a	G-4a	G-5a
Conductor Casing						
Hole Diameter (inches)	unk[a]	48	unk[a]	48	48	48
Casing Diameter (inches)	unk[a]	38	unk[a]	38	38	38
Depth (ft bgs)	unk[a]	33	unk[a]	33	33	33
Wellhead Protection Surface Casing						
Hole Diameter (inches)	unk[a]	34	unk[a]	34	34	34
Casing Diameter (inches)	unk[a]	28	unk[a]	28	28	28
Depth (ft bgs)	unk[a]	490	unk[a]	515	581	680
Final Well Casing and Screen						
Hole Diameter (inches)	20	26	20	26	26	26
Casing Diameter (inches)	12	16	12	16	16	16
Screen Diameter (inches)	10	16	10	16	16	16
Filter Pack Thickness (inches)	5	5	5	5	5	5
Screen Slot Size Openning (inches)	0.050	0.050	0.050	0.050	0.050	0.050
Borehole Depth (ft bgs)	1,519	2,030	1,792	2,030	2,030	2,030
Casing and Screen Depth (ft bgs)	1,513	2,000	1,785	2,000	2,000	2,000
Top of Screen (ft bgs)	272	565	695	589	655	765
Bottom of Screen (ft bgs)	1,513	1,980	1,785	1,980	1,980	1,980
Total Screen Length (ft)	563[b]	1,415	400[b]	1,391	1,325	1,215
Gauge Line for Transducer Access						
Number of Gauge Lines	0	2	0	2	2	2
Gauge Line Diameter (inches)	NA[c]	2	NA[c]	2	2	2
Gauge Line Entrance into Casing (ft bgs)	NA[c]	645	NA[c]	670	735	845
Other Information						
Reference Figure Number	A-1	A-2	A-3	A-4	A-5	A-6
Year Completed	1954	1998	1951	1998	1998	1998

[a] Unknown

[b] Alternating casing and screen

[c] Not Applicable

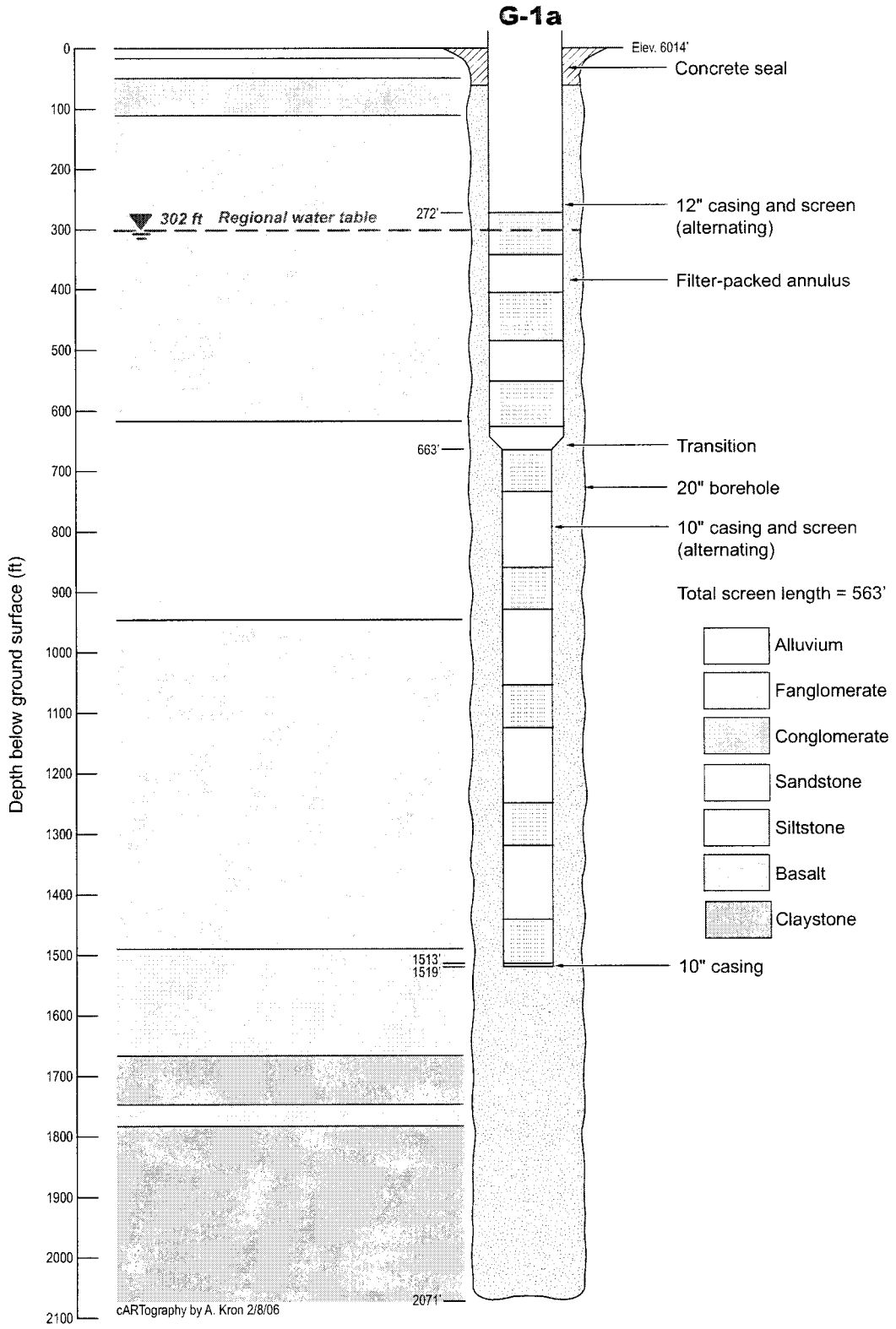

Figure A-1. Well completion diagram for G-1a showing geologic units penetrated

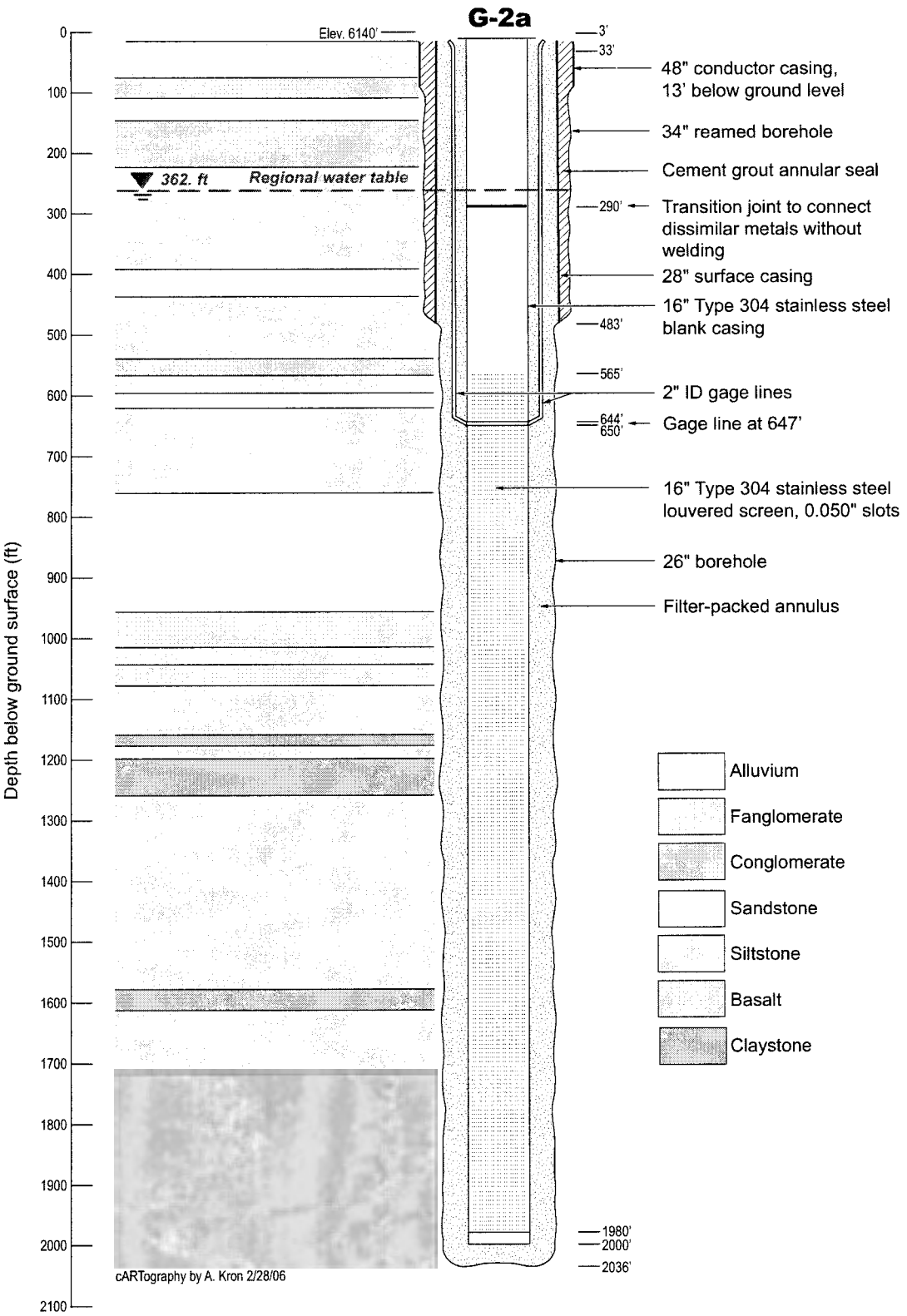

Figure A-2. Well completion diagram for G-2a showing geologic units penetrated

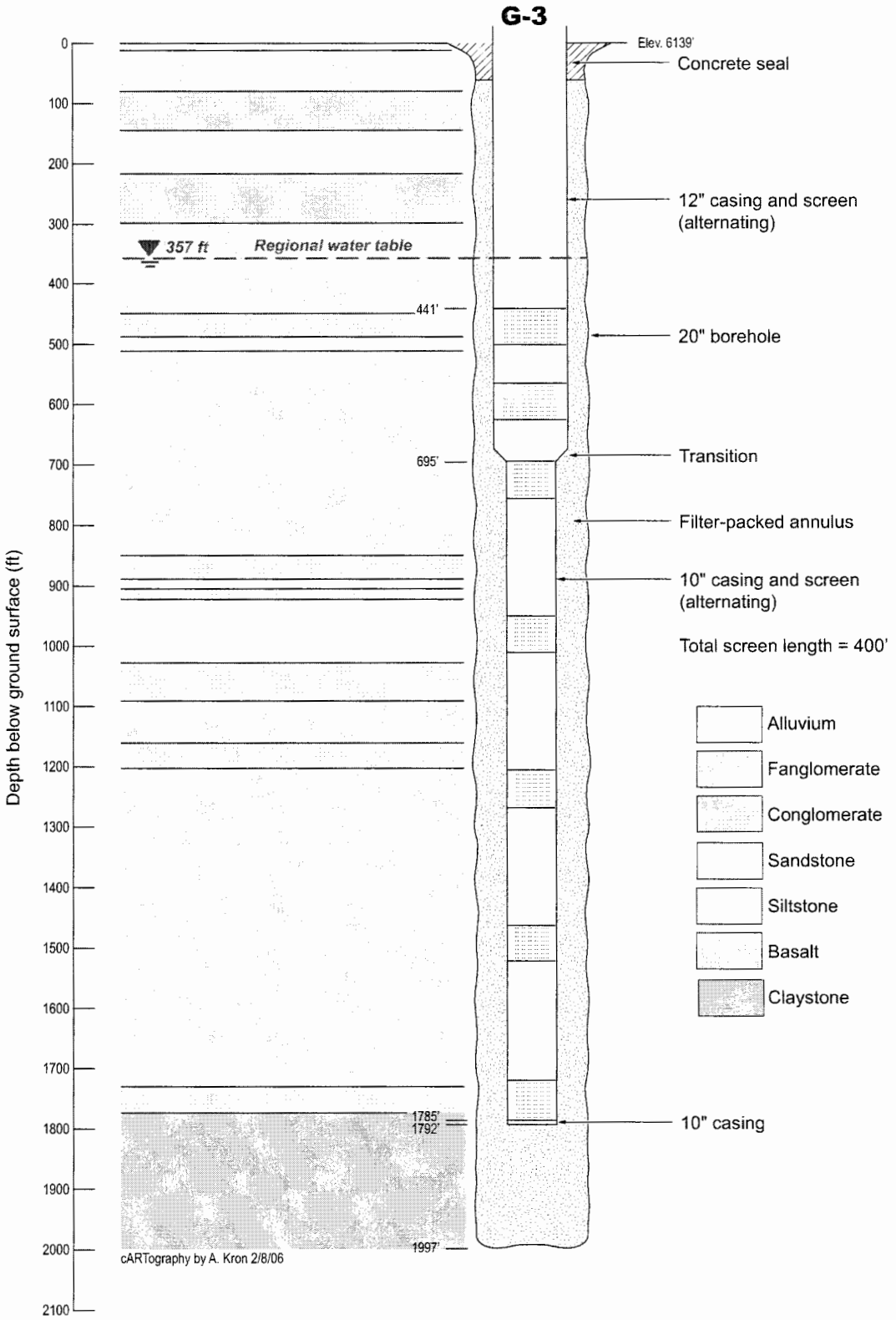

Figure A-3. Well completion diagram for G-3 showing geologic units penetrated

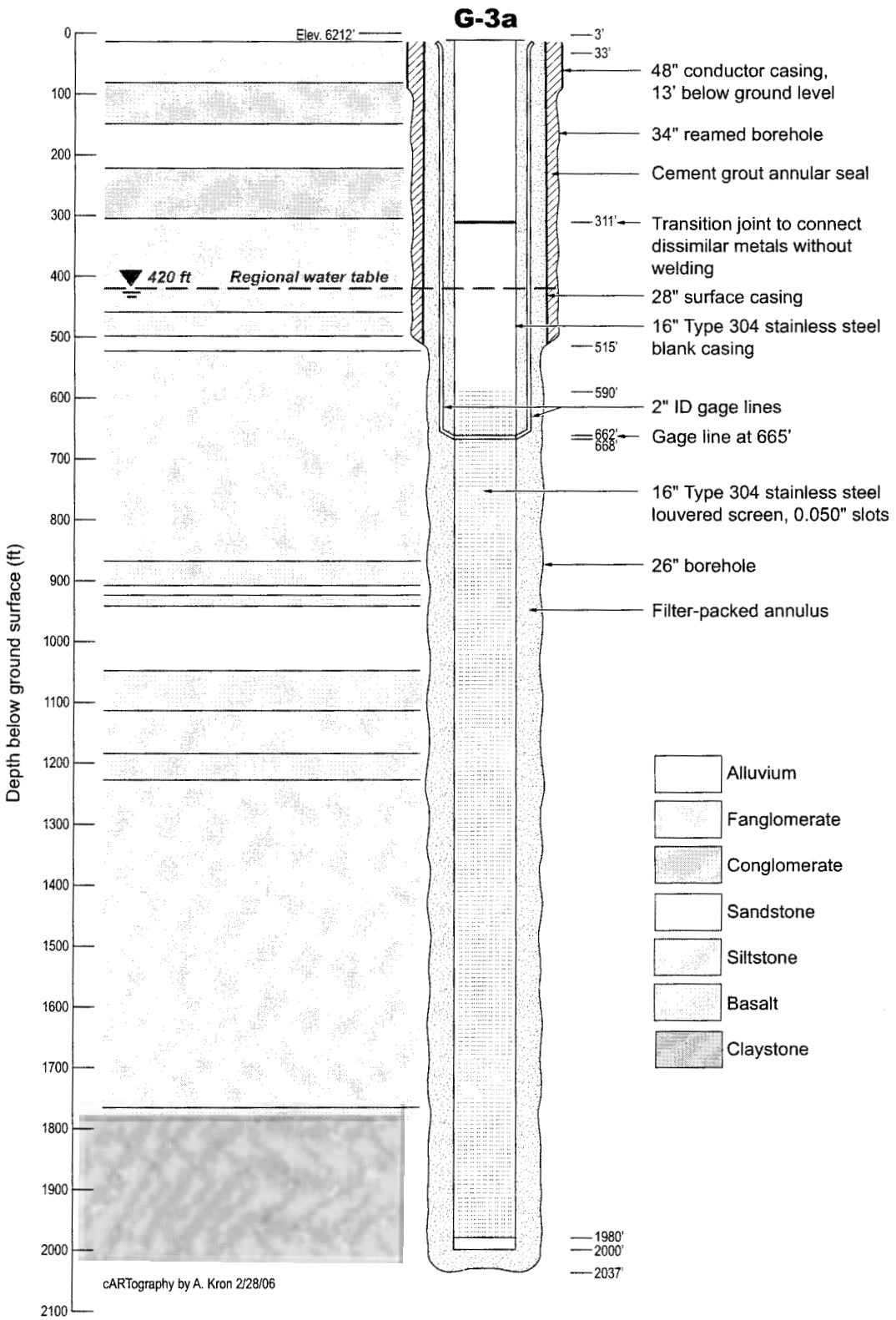

Figure A-4. Well completion diagram for G-3a showing geologic units penetrated

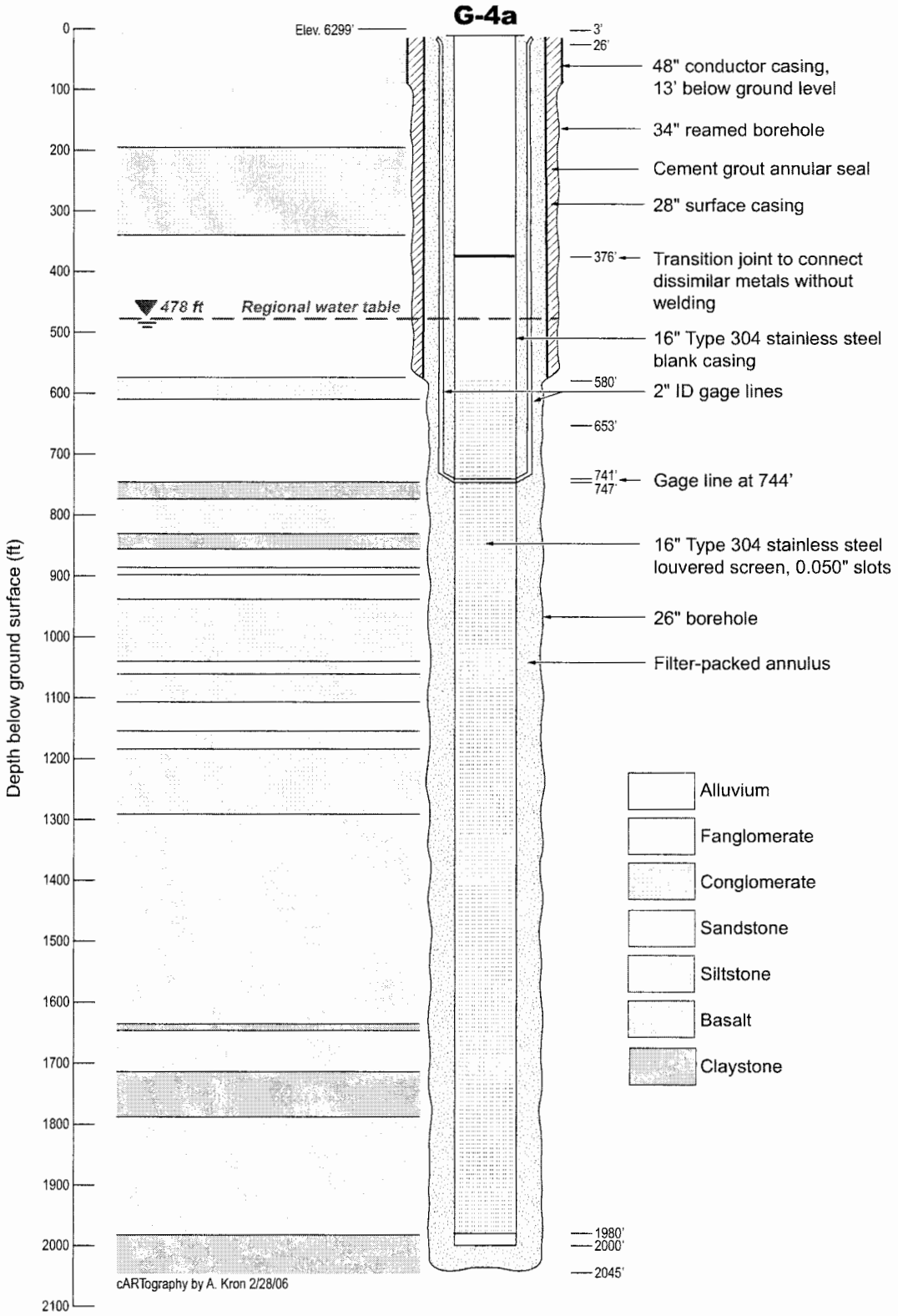

Figure A-5. Well completion diagram for G-4a showing geologic units penetrated

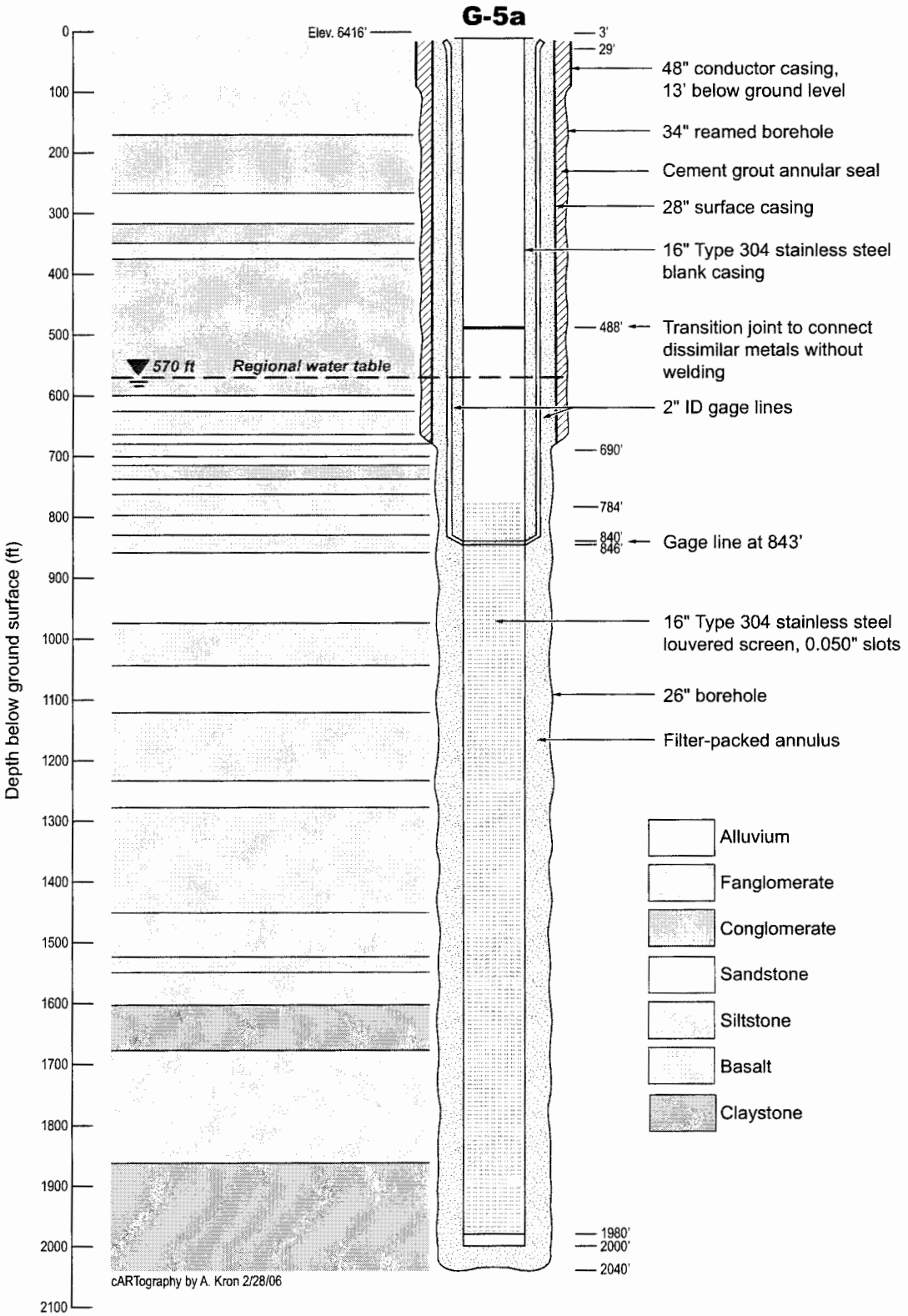

Figure A-6. Well completion diagram for G-5a showing geologic units penetrated

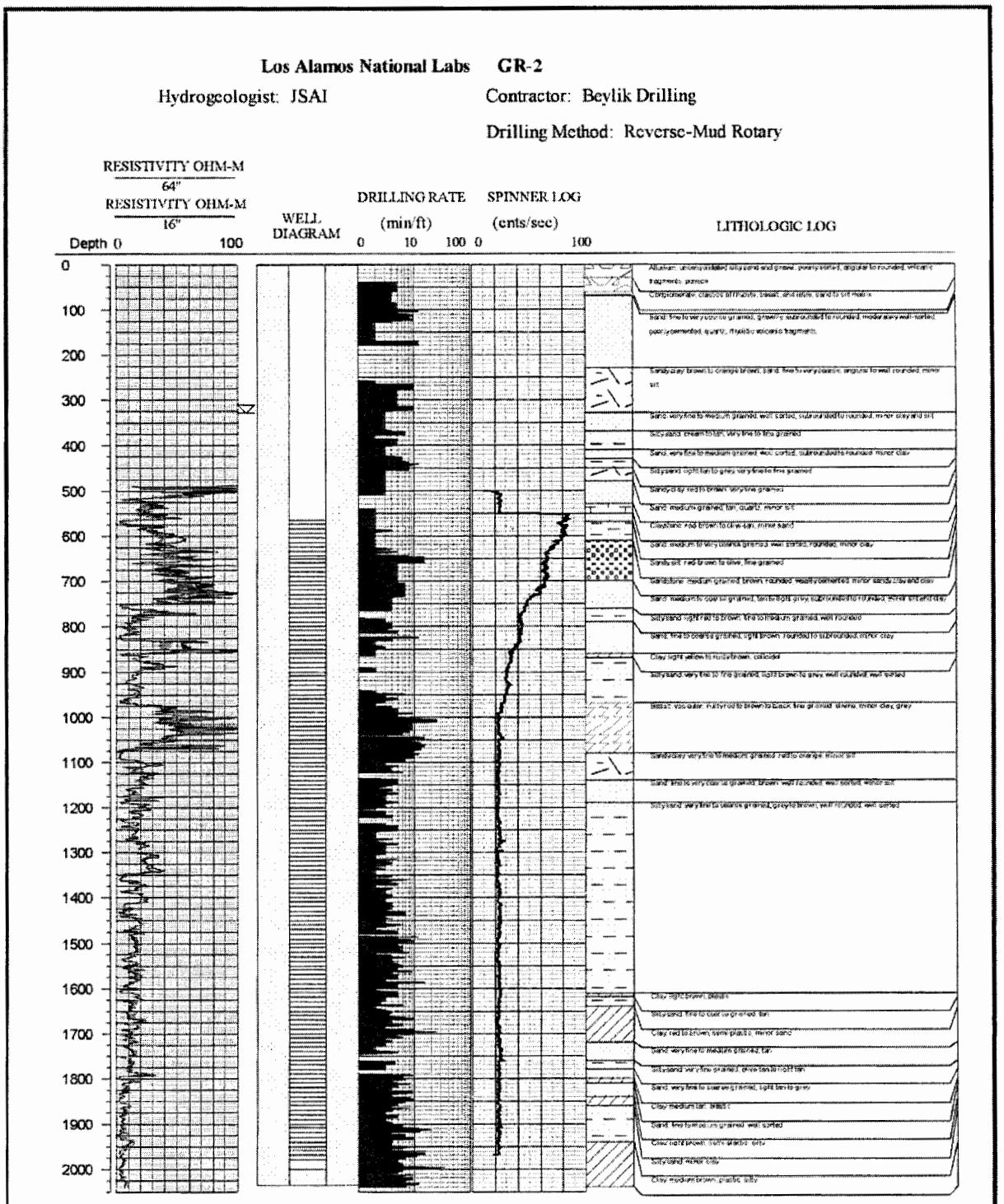

Figure A-7. Original geophysical and spinner logs for well G-2a

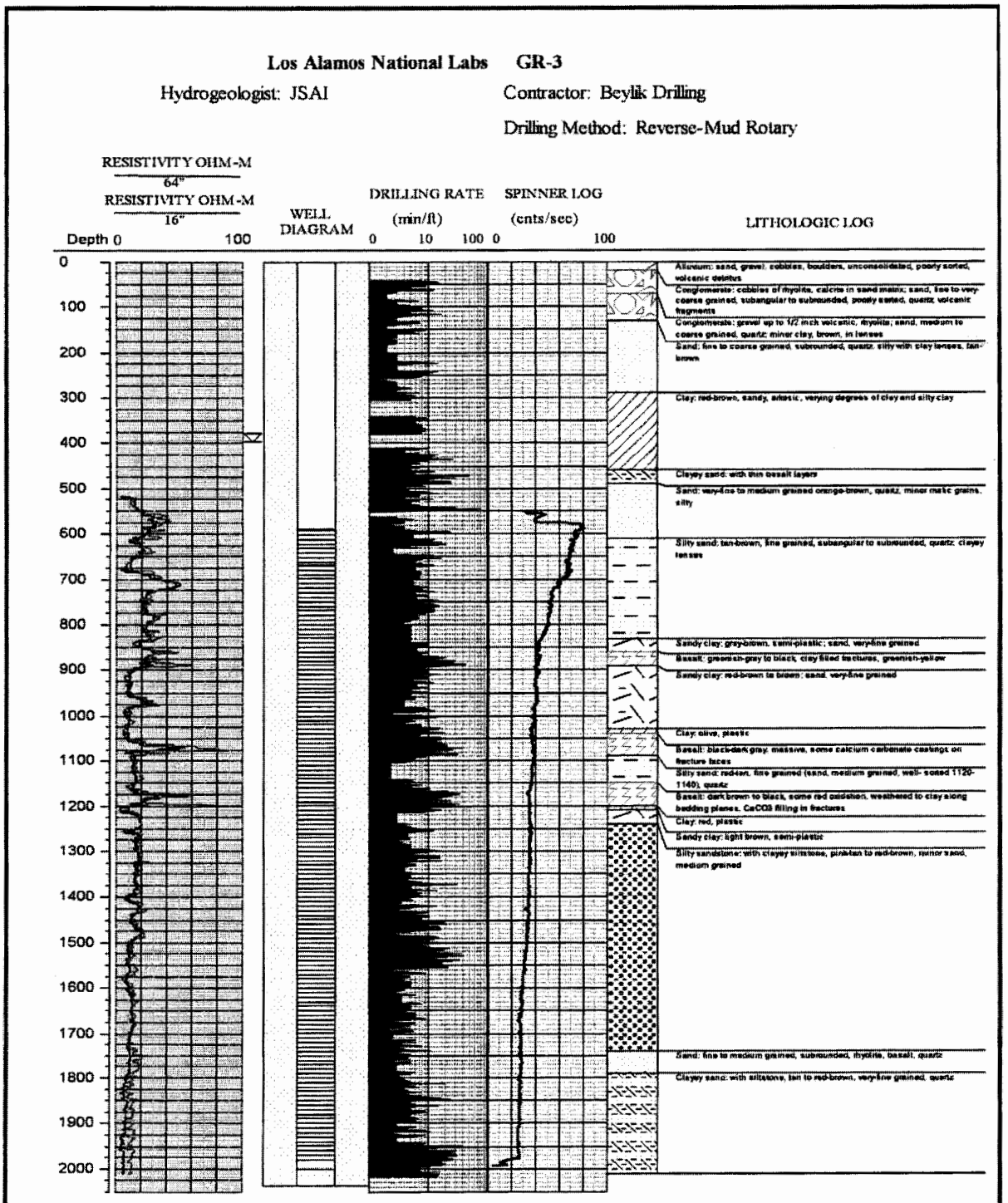

Figure 5. Presentation of resistivity log, location of perforated interval, drilling time, borehole velocity, and lithology, GR-3.

JOHN SHOMAKER & ASSOCIATES, INC.

Figure A-8. Original geophysical and spinner logs for well G-3a

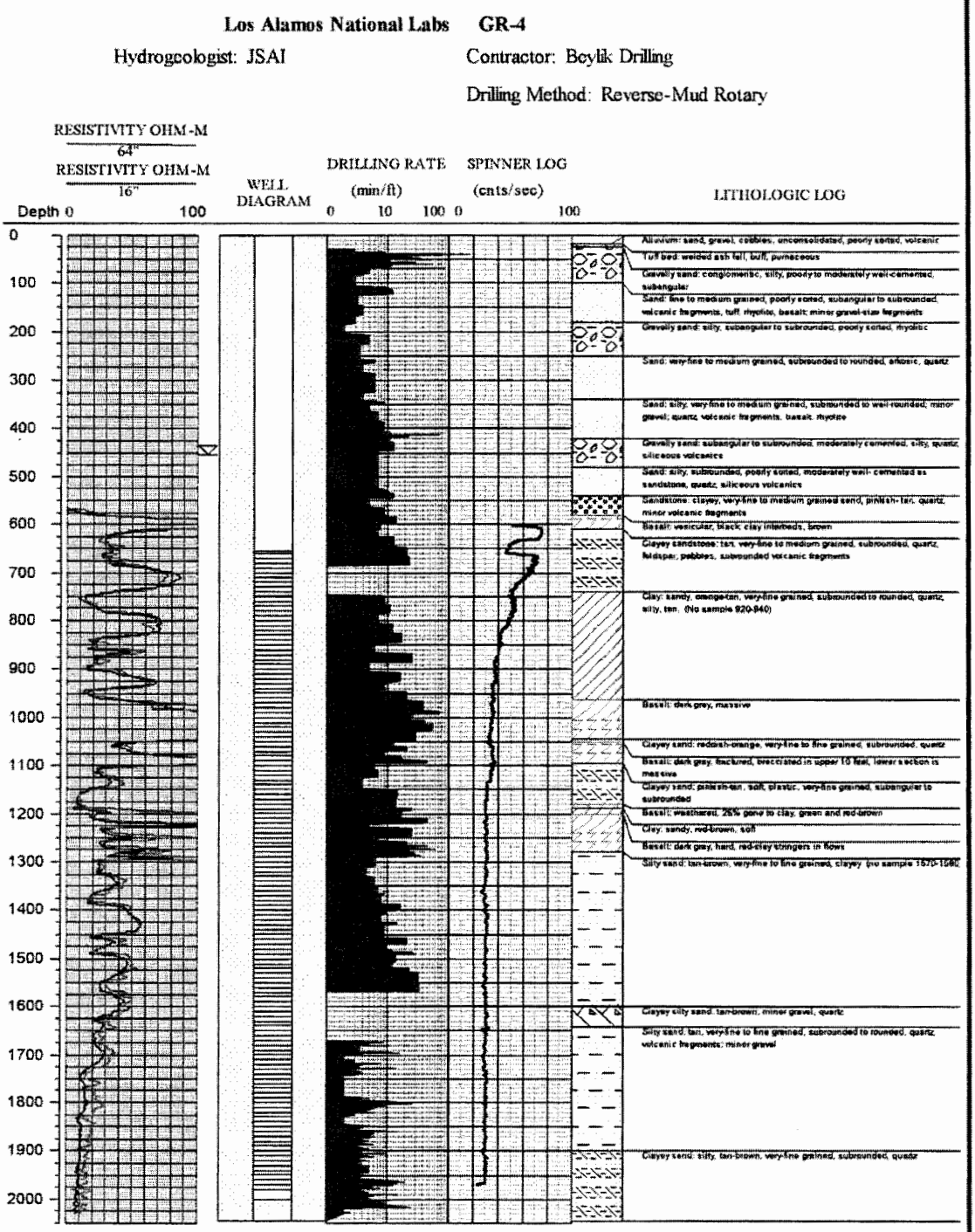

Figure 6. Presentation of resistivity log, location of perforated interval, drilling time, borehole velocity, and lithology, GR-4.

JOHN SHOMAKER & ASSOCIATES, INC.

Figure A-9. Original geophysical and spinner logs for well G-4a

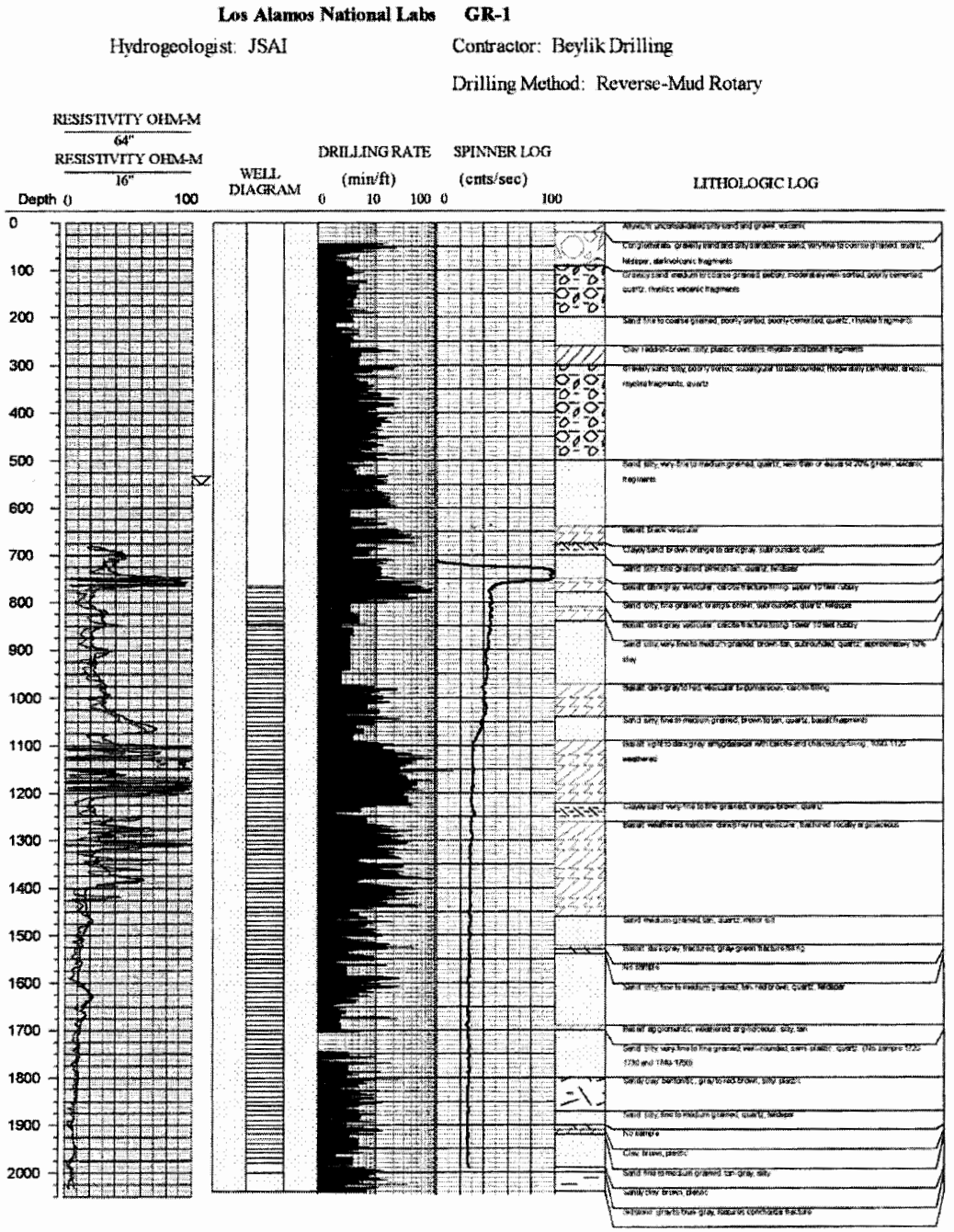

Figure 3. Presentation of resistivity log, location of perforated interval, drilling time, borehole velocity, and lithology, GR-1.

JOHN SHOMAKER & ASSOCIATES, INC.

Figure A-10. Original geophysical and spinner logs for well G-5a

APPENDIX B. DESCRIPTION OF DATA FILES ON CD-ROM

Table B-1 lists data files that are contained on the CD-ROM located on the inside back cover of this report. These drawdown and recovery data were collected from numerous wells during the aquifer test described in the report. Table B-1 describes the naming convention used to identify these data files. Each data file contains important data in tab-delimited, text format. The file name tells which well the data came from. For example, G2a-p1998.txt contains drawdown (or pumping) data from the 1998 aquifer test at well G-2a. The first column in this file contains elapsed time (days) since pumping began; the second column contains drawdown (ft). Other data files contain simple recovery data (i.e. G2a-r1998.txt); however, all files are structured identically (i.e., time in column one is time since recovery began and recovery in column two). Some files contain both drawdown and residual recovery data (i.e., G2a-pr2005.txt from the 2005 aquifer test at well G-2a). These data are different from individual drawdown or recovery data files. These differences are explained in the report. All of the data in individual files from the same aquifer test were simultaneously recorded at the same time.

Table B-1
Data files contained on the CD-ROM included with this report

File Name on CD-ROM	Well	See Figure	Remarks
G2a-p1998.txt	G-2a	6a, 7b	Drawdown data from G-2a while G-2a pumped.
G2a-pr-1998.txt	G-2a	6c	Drawdown and recovery data from G-2a.
G2a-r-1998.txt	G-2a	6b	Simple recovery data from G-2a.
G2a-StepTest-1998.txt	G-2a	8a	Step-drawdown test from G-2a.
G3-p1998-G2a.txt	G-3	7a, 7b	Drawdown data from G-3 while G-2a pumped.
G3-pr1998-G2a.txt	G-3	none	Drawdown and recovery data from G-3.
G3-r1998-G2a.txt	G-3	none	Simple recovery data from G-3.
G3a-p1998.txt	G-3a	13a, 14b	Drawdown data from G-3a while G-3a pumped.
G3a-pr-1998.txt	G-3a	13c	Drawdown and recovery data from G-3a.
G3a-r-1998.txt	G-3a	13b	Simple recovery data from G-3a.
G3a-StepTest-1998.txt	G-3a	15a	Step-drawdown test from G-3a.
G3-p1998-G2a.txt	G-3	14a, 14b	Drawdown data from G-3 while G-3a pumped.
G4a-p1998.txt	G-4a	16a, 17b	Drawdown data from G-4a while G-4a pumped.
G4a-pr-1998.txt	G-4a	16c	Drawdown and recovery data from G-4a.
G4a-r-1998.txt	G-4a	16b	Simple recovery data from G-4a.
G4a-StepTest-1998.txt	G-4a	18a	Step-drawdown test from G-4a.
G4-p1998-G4a.txt	G-4	17a, 17b	Drawdown in G-4 while G-4a pumped.
G3-p1998-G4a.txt	G-3	none	Drawdown in G-3 while G-4a pumped.
G5a-p1998.txt	G-5a	19a	Drawdown data from G-5a while G-5a pumped.
G5a-pr-1998.txt	G-5a	19c	Drawdown and recovery data from G-5a.
G5a-r-1998.txt	G-5a	19b	Simple recovery data from G-5a.
G5a-StepTest-1998.txt	G-5a	20a	Step-drawdown test from G-5a.
G2a-p2005.txt	G-2a	9a, 10b	Drawdown data from G-2a while G-2a pumped.
G2a-pr2005.txt	G-2a	9b	Drawdown and recovery data from G-2a.
G3a-p2005-G2a.txt	G3a	9d, 10c, 10d	Drawdown data from G-3a while G-2a pumped.
G3-p2005-G2a.txt	G-3	9c, 10b, 10c, 10d	Drawdown data from G-3 while G-2a pumped.

This page intentionally left blank.

APPENDIX C. GEOLOGIC MAP OF THE PUYE QUADRANGLE, LOS ALAMOS, RIO ARRIBA, SANDOVAL, AND SANTA FE COUNTIES

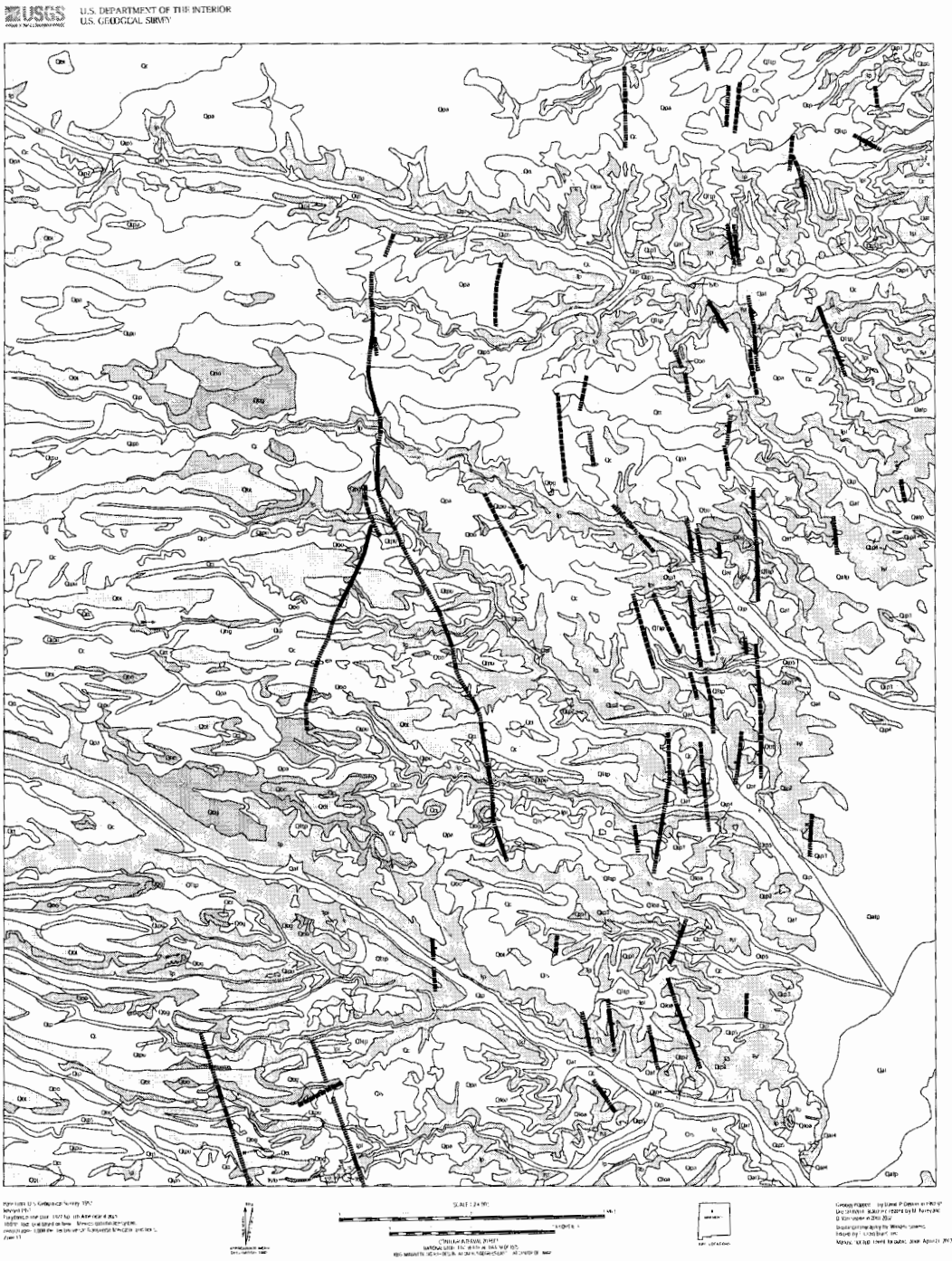

GEOLOGIC MAP OF THE PUYE QUADRANGLE, LOS ALAMOS, RIO ARRIBA, SANDOVAL, AND SANTA FE COUNTIES, NEW MEXICO

By
David P. Dethier
2003